UNIVERSITÀ POLITECNICA DELLE MARCHE
FACULTY OF ENGINEERING

Master's degree in Biomedical Engineering

ASSESSMENT OF DRIVER'S THERMAL COMFORT THROUGH FACIAL THERMAL INFRARED IMAGING

Supervisor:
Prof. Eng. Laura Burattini

Candidate:
Katyana Campanella

Co-supervisor:
Prof. Arcangelo Merla

Co-supervisor:
Doc. Eng. Lorenza Mancini

A.A. 2019 /2020

Summary

List of figures

List of tables

ABSTRACT

Among the principal causes of road accidents, that provoke thousands of deaths every year, there are driver's drowsiness and distraction. In order to reduce the risks of accidents caused by these two psychophysiological conditions, this study has the purpose to develop a model able to predict the thermal comfort requirements of the subject inside a vehicle, exploiting thermal facial infrared imaging, in such a way to obtain the automatization of the heating ventilation air conditioner (HVAC) system functioning.
Nowadays, thermal infrared images, the result of the application of infrared (IR) thermography imaging technique, are widely spread to obtain a detailed representation of a scene's temperature. Indeed, this technology provides relevant information about the radiant energy spontaneously emitted from the body and can be used to extract temperature data through the inverse of Stephen–Boltzmann law. The potential of this technique consists of the total non-harmfulness and non-invasiveness, being a technology that does not require any type of contact and of energy irradiation. Another its advantage is the preservation of the user's privacy.
In this study, infrared thermography has been applied to monitor driver's facial temperature variations inside a vehicle where the settings of the HVAC system were changed into too hot and/ or, after a certain period, to too cold temperatures.
The facial temperature patterns, extracted by an IR thermo-camera, have been studied, analyzed, and then compared in time with the individual's thermal sensations expressed during the experiments in order to be able to recognize a possible relationship, that would allow a complete automatized functioning of the air conditioner system to the individual's thermal requirements. In this way, thermal comfort would be ensured continuously to the vehicle's occupants, gaining a better driving experience. Moreover, good thermal conditions reduce the fatigue and driver stress. Another important effect is the reduction in energy consumption provided by the automatic control and adaptation of the operation of HVAC systems.
However, thermal comfort, defined by the American society of Heating, Refrigerating and Air Conditioning Engineers (ASHRAE) as the condition of mind that expresses satisfaction with thermal environment, is a complex cognitive process strictly dependent on individual's physical, physiological and psychological condition, and for this reason, it cannot be summarized into a unique standard valid for all the individuals [1]. Indeed, as specified in this work, each psychophysiological state reflects into a particular facial thermal map, that is the result of the thermoregulatory mechanisms regulated by the hypothalamus to maintain homeostasis in response to both external temperature changes and physiological emotional changes due to external stimuli.
Thus, in this study, three different approaches were described and discussed: the explorative phase, the control theory phase, and the linear regression phase. All these approaches had the common purpose to acquire some knowledge about the thermal data, to extract a relationship between the cutaneous temperature variations and the related thermal perceptions of the subjects and tries to create a model capable to accurately predict the subject's thermal sensation. The data available to train the models refer to 7 experiment's sessions.
In the first explorative phase have been implemented 10 different tests based on the nose tip thermal data of the experiment session 4. Specifically, these tests were based on the nose tip signal, its derivative and some its transformations, and then were compared with the thermal sensation expressed by the subject through a vote. From this phase, it has been highlighted the strong correlation among the derivative of the temperature signal and the self-reported thermal comfort index. Moreover, the presence of a delay between the two signals has been observed. Indeed, through the tests performed, it resulted that the subject becomes aware about a temperature change after few minutes that the cutaneous temperature variations occurred.
In the second phase of control system theory, transfer functions have been computed, for each experiment session, as the ratio of the Fourier transform of the recorded thermal sensation and the Fourier transform of the nose tip thermal signature.
However, no similar pattern among the transfer functions of all the experiment sessions has been found because each individual, in each experiment sessions, reacted to the thermal variations with different frequency and intensity.

In the third linear regression model phase, have been computed three different linear models based respectively on nose tip thermal data, glabella thermal data, and both of them, and the relative thermal sensations. Before to create these models, it was applied a shift to the thermal sensations, in order to reach the greatest correlation among the two vectors inside an interval of 7 minutes.
From this approach, it was underlined the strong linear correlation between both the nose tip and glabella temperature variations and the relative thermal perception, although the presence of a mean delay of about 4 minutes for both the facial regions. Thus, it was evidenced that the subject's thermal comfort could be easily predicted through the facial thermal signature relative to the nose tip and glabella regions acquired through an infrared thermo camera, in a linear way, by applying a short delay.
However, this study focuses and analyzes the thermal data referred to nose tip and glabella regions, acquired into steady state conditions where all the interferences due to the metabolic rate, psychophysical state of the individual have been neglected. Moreover, also interferences due to geometry of the car, solar intensity and reflective fluctuations are not considered.
In fact, this work, being a first approach to this issue, idealizes the real circumstances into the vehicular environment, but in future studies all the other influencing factors would be taken into account in order to provide a more accurate analysis.

CHAPTER 1

1.1. INTRODUCTION

Nowadays, an effect of the globalization is the substantially rising in the mobility. Indeed, the people, to date, spend a lot of time inside a vehicle [2] [3]. According to a report of 2016 published by the institute CSA research, a European driver spends, an average, 4 years and 1 month in a car, during his life [4]. While the American Automobile Association Foundation for Traffic Safety has reported that U.S. drivers spend medially more than 12 days driving each year. For this reason, it is fundamental to convert the cabin ambient into the most comfortable one in order to reach a better driving experience and to avoid, or at least reduce, the risk of road accidents.

Driving performance can be affected and influenced by several factors, such as fatigue, drowsiness, stress and distractions that provoke a decrease of attention, of reaction time, of situational awareness and compromise the safety of all vehicle's occupants.

Suboptimal level of cognitive functioning (e.g., inattention, drowsiness) is a key cause of road accidents and poor driving performance, as declared by the American Automobile Association (AAA) Foundation for Traffic Safety in 2018 [5].

In fact, among the main causes affecting a driver's performance, drowsiness and distraction, played an important role. Specifically, distracted driving has provoked, according to the latest estimation by the National Highway Traffic Safety Administration (NHTSA), in the USA, more than 2800 deaths and approximately 400,000 people injures, in 2018 [6].

Driver drowsiness is considered, for drivers at all ages, as a major risk of driving accidents worldwide, likely responsible for 10–30% of all road traffic accidents, including also the fatal ones. According to the data published by the NHTSA, drowsiness caused 17% of all fatal crashes in recent years. And, as reported by Automobile Club Italia (ACI), this percentage corresponds to a fifth of all the car accidents [7] [8] [9] [10].

Thus, it would be advantageous to implement and install a device inside a car that, by the constant monitoring of driver's state, can autonomously adapt the functioning of heating ventilation air conditioner (HVAC) system in order to avoid the decrease of his attention. In particular, the driver's psychophysiological state can be defined studying his facial thermographic signal. Thus, for example, if the drowsiness state is detected, the HVAC system could adapt its functioning releasing cold area and providing as result the increase of subject's awareness. Moreover, the automatic system adaptation can avoid the distraction of the driver for its set, and consequently can reduce the risk of road accidents.

Therefore, the current study presents novel methods to evaluate and predict the driver's thermal comfort sensations, exploiting his facial thermal signature, in order to obtain a real time automatization of the HVAC system, based on subject's real thermal requirements. In this way, comfortable and healthy vehicular climate could be continuously ensured. As consequence, not only the reduction of driver's stress is recorded, but also the good visibility, by avoiding the fogging phenomenon, is guaranteed, contributing to safer driving experience [3] [11].

Thermal signature has been acquired through an infrared (IR) thermo-camera, and then through the processing of these data, the thermal comfort has been estimated.

Specifically, the CHAPTER 2 presents a general overview of IR thermography, while in the CHAPTER 3 a complete description of thermal comfort is provided. Then, the aim of this study is reported in the CHAPTER 4. While the CHAPTER 5 describes the experimental setup and data acquisition, the three performed approaches and all the methods implemented. CHAPTER 6 and CHAPTER 7 report the obtained results and the relative discussions. Finally, in CHAPTER 8 all the conclusions and the limits of this works have been reported.

CHAPTER 2

2.1. INFRARED THERMOGRAPHY GENERAL OVERVIEW

The term "Thermography" derives from the union of two Greek words: *"thermos"*, that means heat and *"graph"*, that means to write, so literally writing of heat. Thermography can be defined as the science of heat, which makes the invisible visible to the human eye. Indeed, heat is not a quantity that we can see, but we can only feel sensation about it. So, thermography makes visible heat distribution of the target area [12].

Today Infrared thermography or Thermal Infrared (TIR) imaging is a fast method of investigation to acquire valuable information about object's temperature, useful for a targeted diagnosis and control about target condition at a glance, allowing observation through a special instrument, about thermal energy emitted by every object, as well as by human skin, in form of electromagnetic waves.
Generally, when we are interested into a general evaluation of the health status, both of an electrical and biological system, temperature values are the first to be inspected, since they are good indicators of illness [13] [14]. Moreover, infrared (IR) thermography potential is not limited to provide images about the heat distribution over an area, but through these it is possible to evaluate the thermal distribution of a body without the presence of contact sensors that can alter the psychophysiological state of an individual [15]. In particular, it directly records radiating energy released from the body, and temperature is only a measure that is strictly related with this emitted radiation [16].

2.2. WHAT IR THERMOGRAPHY IS?

2.2.1. ELECTROMAGNETIC SPECTRUM

The electromagnetic spectrum is the set of all electromagnetic waves that exist in nature, characterized by their frequency and the related wavelength. According to their energy content, the electromagnetic spectrum is subdivided into several bands, but only a small portion, the visible spectrum, can be perceived by the naked human eye. Visible spectrum is included into a range of wavelengths between 380-740 nm.
From radiations with the longest wavelengths, lowest frequencies, and lowest energy content to radiations with highest energy content, highest frequencies and lowest wavelengths, we can find radio waves, microwaves, infrared rays, visible light, ultraviolet radiation, x-rays, and gamma rays, as depicted in Figure 1.

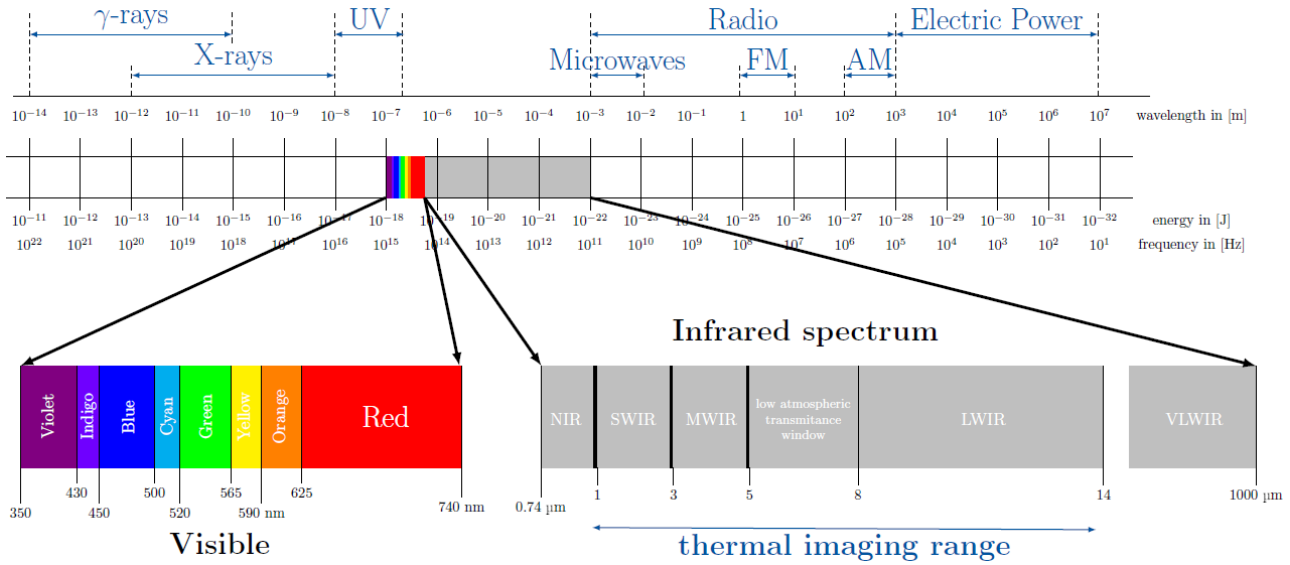

Figure 1. Subdivision of electromagnetic spectrum

However, being unable to see beyond the visible spectrum, the discovery of all the other bands of the electromagnetic field has represented a great step in the history of science and in biomedical applications: for instance, x rays (0.01 – 10 nm) provided the possibility of investigating hard tissues without any superficial cutaneous cut. Similarly, ultrasound radiation (10 – 100 nm) allowed the detection of internal organs and soft tissues, as well as the visualization of dynamic phenomena, such as the aperture of mitral valve. Infrared radiation (740 – 10^6 nm) allowed the acquisition and processing of thermal information through non-contact measuring devices and, unlike the previous mentioned imaging techniques, it does not require irradiation of the target [17].
The infrared spectral band lies close to the narrow visible range, and it is characterized by a wider range of wavelengths. According to the ISO 20473 IR range is subdivided into different bands: the near infrared (NIR), spectral region closest to visible range, which ranges from 0.74 to 0.9 μm, the short wavelength infrared (SWIR), which extends from 0.9 to 3 μm, the mid wavelength infrared (MWIR), which ranges from 3 to 5 μm, the long wavelength infrared (LWIR), which ranges from 8 to 14 μm, and the very long wavelength infrared (VLWIR) which ranges from 14 to 1000 μm. Nevertheless, thermography exploits only the range included between 0.9 and 14 μm. This range, called thermal imaging range, is also characterized by a lower energy and frequency content with respect to the visible field [17].

2.2.2. HISTORICAL NOTES

Infrared thermal radiation existence beyond the visible range was discovered by W. Herschel in the 1800 [18]. Herschel performed experiments to study the spectrum of sunlight using a prism and a thermometer. Through the use of the prism, he separated the visible light into each color band from which it is composed, and for each color he measured the relative temperature, recording a rise of temperature, and consequently a heat production, proportional with the increase of the wavelength. However, he recorded the highest temperature outside the visible range, into “dark light”, the portion of the electromagnetic spectrum that is invisible to the naked eye [19], providing the first evidence of infrared form of light existence. Their similar behavior has suggested that the infrared radiation follows the same optical properties and principles of the visible light, based on reflection, absorption, and transmission [16] [18].
Despite of its discover dates back to 1800, first IR thermal applications started to be widely used since the early 1960 in different areas [16]. In particular, its first diffusion, occurred in the United States and had mainly military purposes, such as investigation and supervision during night, when insufficient light reduces the visibility [18] [19] [20].

2.2.3. PHYSICAL PRINCIPLE

In order to understand how infrared electromagnetic waves generate thermal images and how they provide us temperature information, a review of optic laws and physical principles exploited by IR radiation, is provided [16]. In particular, since IR radiation source corresponds to the heat energy held by an object, we will focus on the laws of thermodynamics, based on heat and temperature exchange [16].

Heat transmission can occur through three modalities: conduction, convection, and irradiation.
This last one is involved in the infrared thermography; whose aim is to detect radiation emitted from an object.

In fact, all objects are composed by particles that are in random motion. These particles contain a proper kinetic heat, sometimes referred to as true heat. Specifically, objects kept at a temperature above absolute zero Kelvin (-273.14 ° C) contain this random motion, which leads to particles colliding, changing their energy state and leading to the release IR electromagnetic radiation [19].
Since all objects on our planet, including the human body, have a temperature above the absolute zero, they all emit radiation in the IR range through atmosphere [14]. This thermal energy can be captured only by

thermal sensors, which detect IR radiation [21] [22] [23]. Thus, for this purpose, thermo cameras with small detectors, sensible to IR wavelengths, are employed.

It is important to note that the IR cameras measure irradiance and that the temperature is only a secondary measure derived from the IR radiation emitted. The outgoing radiation, that IR thermal system detects, is the radiation that comes from the object regardless of the heat source that originated it and it is a linear combination of the absorbed radiation from the object itself, radiation coming from reflection of heat source, and the radiation coming from transmission from the heat source. So, the Total Radiation (W) acquired by the IR camera can be expressed as:

$$W = \alpha W + \rho W + \tau W \quad (1)$$

where W total energy is the sum of absorption (α), reflection (ρ) and transmission (τ) contribution energy. These coefficients range from 0 (worst performance) to 1 (best performance).
A fundamental concept is the perfect black body, because it describes how the temperature of an object can be related to its radiant properties. Blackbody, capable to absorb all the radiation, is described by values of ρ and τ equal to 0 and α value equals to 1. It is an object that completely absorbs all the electromagnetic radiation that it receives at every wavelength and radiates energy at a maximum potential rate per unit area and unit wavelength at any given temperature, feature called spectral radiant emittance. For this reason it is also considered an ideal radiator [19]. The radiative properties of a blackbody are function of both temperature and wavelength, as mathematically described by Plank's law. They are described by a series of bell-shaped curves, (T and λ dependent), as shown in Figure 2.

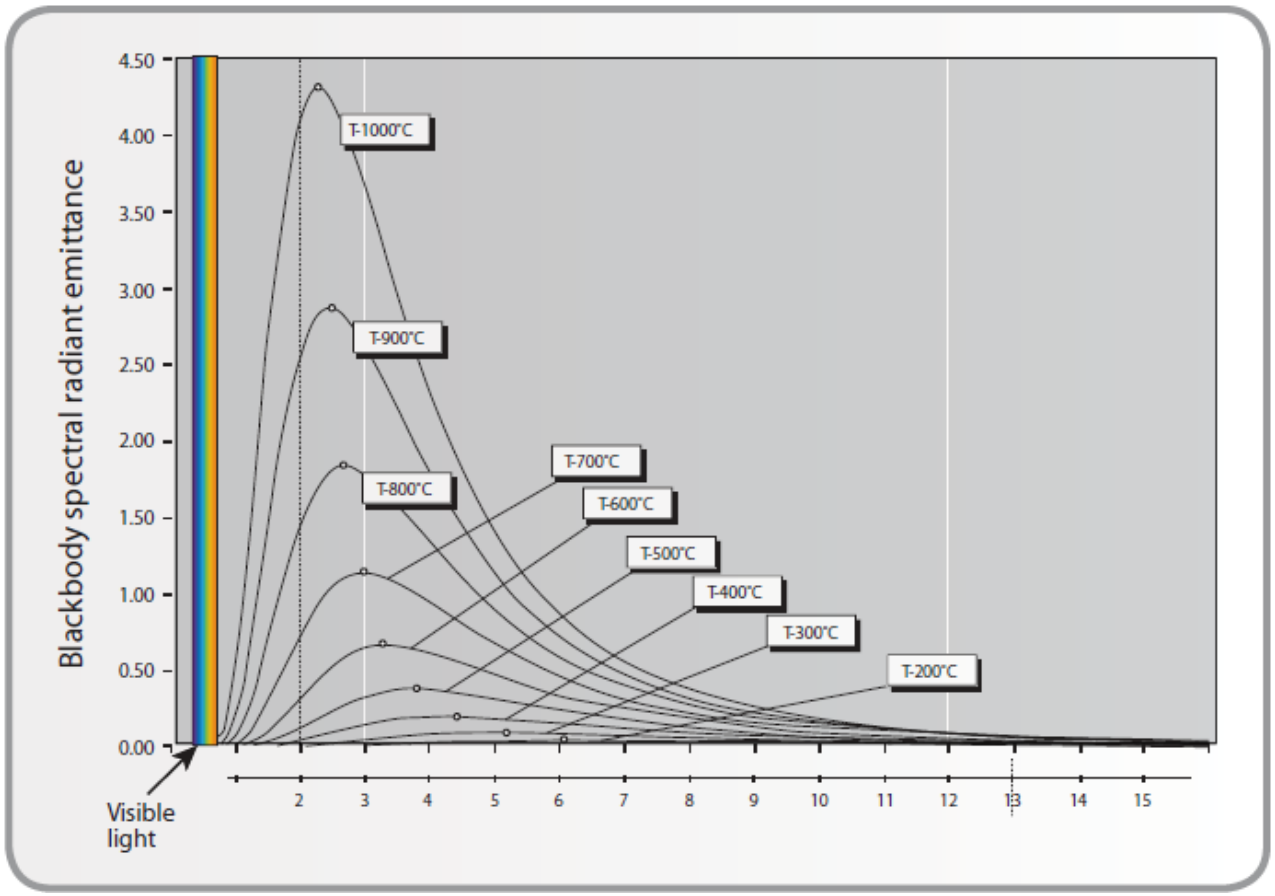

Figure 2. Illustration of Planck's law

Peaks of these bell-shaped curves represent the maximum IR radiation intensity at a particular λ_{max}, that can be computed through Wien's displacement law:

$$\lambda_{max} = \frac{2898}{T} \quad (2)$$

The maximum intensity reached at the peak decreases with temperature.

Moreover, in a blackbody the absorption coefficient α equals to emissivity value ε, that describes the ability to radiate thermal energy, in relation to its real temperature. So, based on Kirkoff's law, as α value, also ε value is 1, because a blackbody, being a perfect radiator, has not any reflective and transmitted component.

Therefore, the concept of blackbody is fundamental because it provides a direct relationship between IR radiation and object's temperature, as demonstrated by Stephen–Boltzmann law:

$$W = \varepsilon \sigma T^4 \quad (3)$$

Where ε = 1, the Stefan-Boltzmann's constant is $\sigma = 5.67 \times 10^{-8}$ W/m^2 K^4, and T is the blackbody's temperature measured in Kelvin.
Black body is an ideal material with best properties of perfect absorber and perfect emitter. Real objects do not have these perfect qualities. For this reason, the black body was used as a reference material in order to obtain for all the target materials radiative properties that are coherent among them since are normalized with respect the perfect emitter [24]. In particular, the emissivity coefficient ε of an object is defined as the ratio between the object's emitted energy (W_{obj}), and the emitted energy from a black body (W_{bb}) at the same temperature:

$$\varepsilon = \frac{W_{obj}}{W_{bb}} \quad (4)$$

So, emissivity value indicates how efficient our heat radiator is and it is determined mainly by the object material and its surface structure. ε is a dimensionless unit of measure and it varies between 0 and 1. Specifically, greater is emissivity value, more real lecture of the object's temperature by the thermal camera is obtained, because this means that the radiant energy detected depends above all by proper object's heat (absorption or emissivity value) and it has less dependence on reflective and transmitted energy contributions.
According to Stephen–Boltzmann law formula (2), the radiant energy W relative to a more general object, different from a blackbody, will be the same energy relative to a blackbody reduced by ε value of the inspected object. Then, through the inverse Stephen–Boltzmann formula, it is possible to obtain the value of the target object temperature, knowing value of W that was directly measured by the thermo camera and ε value, set in the camera, taken by appropriate tables based on object of interest [22]. Otherwise, also to confirm these tabulated ε values, is possible to directly measure the emissivity comparing the radiation emitted by the sample material and that emitted by a blackbody at the same temperature.
Moreover, emissivity value allows also to distinguish two different types of materials: grey bodies, whit ε < 1 and equal for all the λ, and selective radiators, whose emittance is highly dependent on different λ [22]. Generally, all the objects are considered as grey bodies. This assumption holds because sensors used for thermographic measurements work in a narrow wavelengths range, where emissivity value can be considered constant. Consequently, we can assert that thermal sensors are the most important part of the thermo cameras, which are involved into the detection of radiant energy.
However, not all the radiation captured by thermal sensors of the infrared thermo camera comes from the target object, but it is the result of three different radioactive sources (Figure 3): target object, surrounding environment interactions (reflection, transmission, attenuation, etc.), and atmosphere [17].

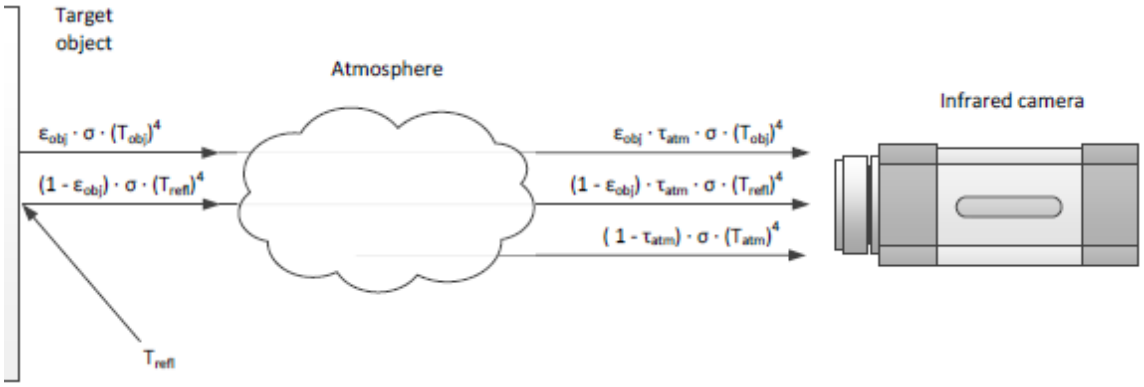

Figure 3. Total radiation received by the infrared camera. Atmospheric, reflective, transmitted energy components, other the proper radiant energy of the object.

So, the total radiation energy acquired is the sum of three contribution energies, that are attenuated by the atmosphere present between the target object and the device used to capture the radiation:
Emission from the target object: $W_{obj} = \varepsilon_{obj}\, \tau_{atm}\, \sigma\, (T_{obj})^4$;
Reflected emission from the ambient sources: $W_{amb} = (1 - \varepsilon_{obj})\, \tau_{atm}\, \sigma\, (T_{refl})^4$;
Emission from the atmosphere: $W_{atm} = (1 - \tau_{atm})\, \sigma\, (T_{atm})^4$.
So, the total radiation (W_{tot}) received by the IR camera results:

$$W_{tot} = W_{obj} + W_{amb} + W_{atm} = \varepsilon_{obj}\, \tau_{atm} \sigma (T_{obj})^4 + (1 - \varepsilon_{obj}) \tau_{atm} \sigma (T_{refl})^4 + (1 - \tau_{atm}) \sigma (T_{atm})^4 \quad (5)$$

And the temperature of an object can be computed through formula (6), setting in the camera parameters as object's emissivity (ε_{obj}), transmittance of atmosphere (τ_{atm}), reflected temperature (T_{refl}) and atmospheric/ambient temperature (T_{atm}).

$$T_{obj} = \sqrt[4]{\frac{W_{tot} - (1 - \varepsilon_{obj}) \tau_{atm} \sigma (T_{refl})^4 - (1 - \tau_{atm}) \sigma (T_{atm})^4}{\varepsilon_{obj}\, \tau_{atm} \sigma}} \quad (6)$$

Thus, atmosphere affects the measurement of examined object's temperature and provokes a radiation attenuation. The attenuation results in a lower measured apparent object's temperature, that becomes much lower increasing the distance, and it is due to absorption, scattering, reflection, refraction and transmission phenomena that occurs between gases particles [17] [22] [25].
However, atmospheric attenuation is not the same for the entire IR range, as visible in Figure 4, but there are two atmospheric windows, where its low influence can be observed, and they are mid wave (MW) window (2 – 5 µm), and long wave (LW) window (8 – 14 µm). In particular, LW window is less affected by atmosphere, because it acts as a high pass filter.

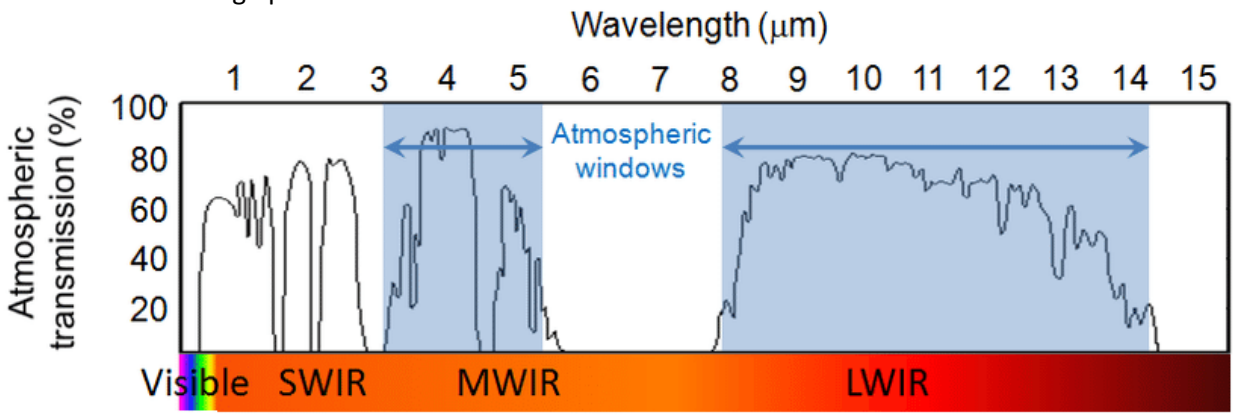

Figure 4. Atmospheric transmission spectrum showing two mid-infrared windows at 3-5 and 8-14 µm wavelengths. The area above the curve shows the attenuation due to the atmosphere.

2.2.4. DEVICE COMPONENTS AND THEIR EVOLUTION IN TIME

IR cameras are composed by three elements, as depicted in Figure 5 [17] [22]:

- lens
- detector
  - ❖ thermal microbolometer
  - ❖ quantum detector
    - ▪ cooler for the quantum detector
- software and electronics for processing and displaying the image.

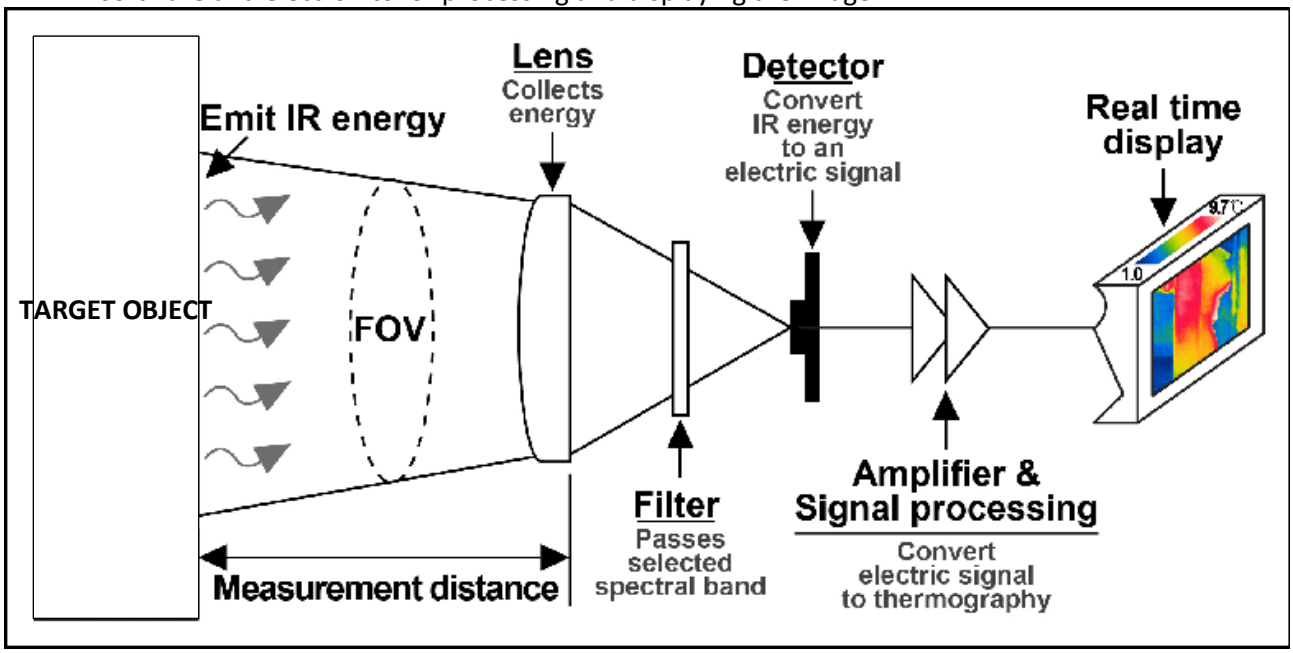

Figure 5. Simplified block diagram of an IR camera.

Infrared cameras are positioned at a certain distance from the target object in order to obtain a sufficiently large field of view to inspect the area of interest and to capture the emitted IR radiation.
Through the use of specialized lenses, cameras collect IR radiation and focus and align it on infrared detectors, in order to obtain a thermal image, that is the correct reflection of the object internal energy [21]. Due to the good mechanical properties, Si and Ge, are generally lens materials adopted, allowing a quite complete transmission of IR incident radiation (close to 100%) thanks also to the presence of antireflective coatings that cover the lens and avoid any radiant dispersion [22].

Since other types of radiation can also be captured by the lens, there is a filter behind it, which allows only the IR radiation to pass through, in order to prevent other types of radiation from causing distortions in the measurement. Then, IR radiation arrives on the detectors, devices involved into the conversion of the mechanical energy that they receive as input into an electrical energy, in form of voltage or current signal, by means of an A/D converter.
Several improvements in the IR imaging technology are achieved during the years and until today, there have been four different generations of IR camera detectors. They have gone through “scan to image” and “single-color focal plane array (FPA)”, and currently are moving towards large-format, multi-color 3rd and 4th generations, as shown in Figure 6 [18] [26] [27] [28].

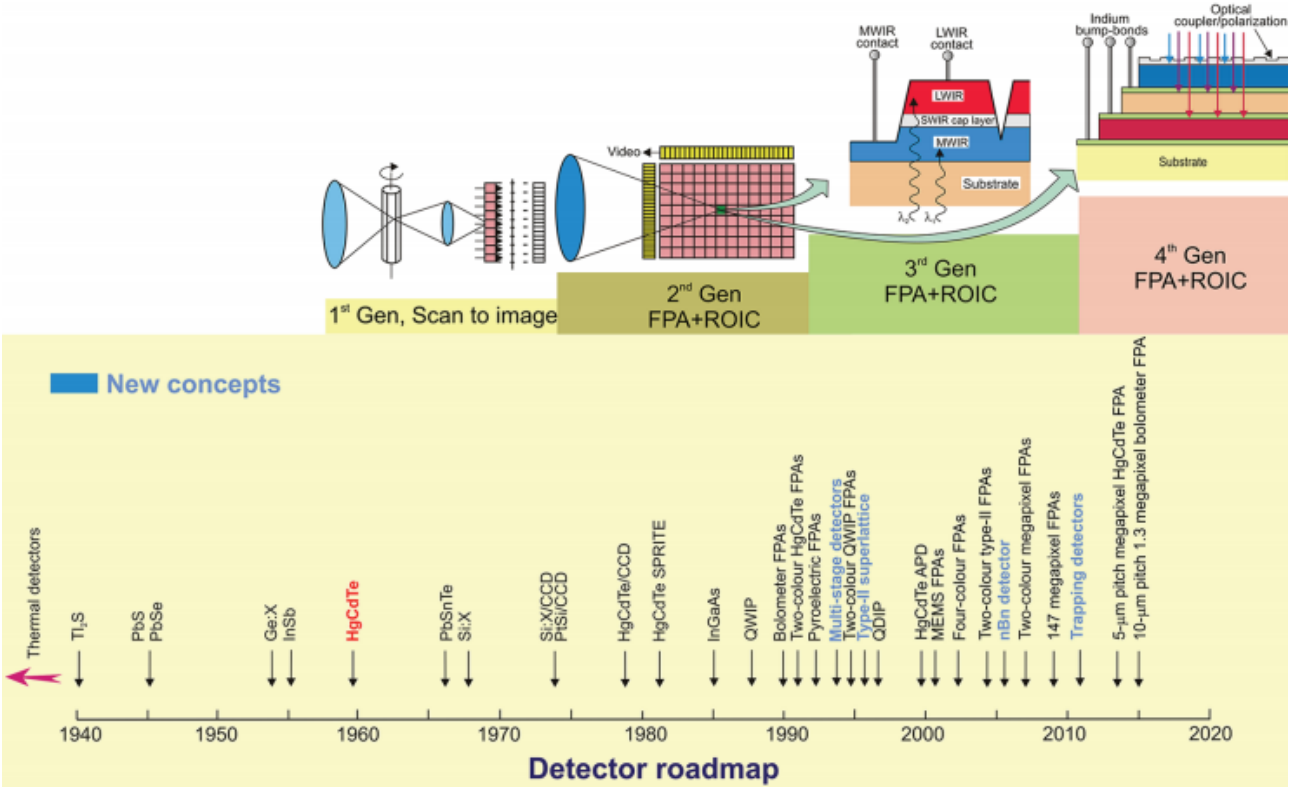

Figure 6. History of the development of IR detector systems. Four generation systems can be considered. First generation (scanning systems), second generation (staring systems with electronic scanning), third generation (staring systems with many pixels and two-color functionality), and fourth generation (staring systems with a very large number of pixels, multi-color functionality, and other on-chip functions, e.g., better radiation/pixel coupling, avalanche multiplication in pixels, and polarization/phase sensitivity).

First generation cameras include a single element or 1D small array detector and two scanning mirrors to create the thermal image [15] [18]. Their limit, exposed when applied to measure radiant energy of the human skin, is due to the presence of a single detector, because it was insufficient to measure large variations in temperature that occurs in different locations of the body, allowing an unreliable skin temperature (Tsk) measure since it can depend above all from small area of superficial veins [13].
Another limit was represented by saturation issues. Saturation indicates the limit of the highest irradiance that can be measured by a detector. In the 1st generation array saturation occurs in a short time because the presence of a single detector limits the amount of charges that the system can store, bringing the system to saturation [15].
To solve these saturation problems a second-generation cameras was supplied, staring systems, in which was increased the number of detectors organized in a large linear array or in two small 2-D arrays, coupled with a readout integrated circuits (ROIC) [15]. The result is a one-color image electronically scanned [27] [28].
The third and fourth current generation cameras have substantially enhanced the reliability and sensitivity of these IR systems through the use of large focal plane array detectors [15]. The term “focal plane array” (FPA) refers to an assemblage of individual detector picture elements (“pixels”) located at the focal plane of an imaging system and it refers principally to 2D arrays [18]. The total flux per unit of area (irradiance) that falls on each pixel, contributes to the generation of a signal, that depends on the flux, and on the product between the radiance of the source and the field of view. These pixels are very small (order of micrometer), and their size determines the sensitivity and resolution of the entire system. In addition to the size, also the number of these pixels (detectors), that range from 60˙000 to up 1˙000˙000, influences the resolution of the camera. Typical values of FPA spatial resolution can be 160x120 or for more modern system until 1280x1024 pixels.

In addition to the larger number of pixels, the higher thermal sensitivity and the better thermal resolution, these newest devices also include innovations that regard higher frame rates (> 25 Hz), increased acquisition frequency as well as multicolor functionality (two-color for 3rd generation, multicolor for 4th generation) and

other on−chip functions. Multicolor functionalities, new type of contrast, allow advanced color processing algorithms to further improve sensitivity compared to that of single-color devices, enabling a discrimination for absolute temperature and providing unique signatures of objects in the scene. The unit cell of integrated multicolor FPAs consists of several co−located detectors each sensitive to a different spectral band [13] [18].

To date, detectors are classified into two categories, which differ mainly in the material with which they are made of: Thermal (nonquantum) microbolometer FPA and Quantum FPA detectors. Even if it has not had significant impact, a third category of detectors, radiation field detectors, which respond directly to the radiation field, should be mentioned [28]. In the Table 1 are summarized all the characteristics for the two most important different types of detector [18] [21] [22].

Table 1. Microbolometer and quantum detectors.

THERMAL MICROBOLOMETER	QUANTUM OR PHOTON DETECTORS
No cooling system	Cooling system down to cryogenic temperatures
Low sensitivity to IR spectrum, don't change with λ	High sensitivity to IR spectrum, change with λ
Slow response time (~ 12 ms)	Quick response time (~ 1 μs)
Dependent on radiation power	Depends on energy and intensity of IR incident radiation and on its spectrum
Metal or semiconductor materials (PZT, a-Si, VOx, PLZT, PST, PLT, PT, PZN, PSrT, BST, LBMO, BT, PVDF)	InSb, InGaAs, PtSi, HgCdTe, GaAs/AlGaAs for Quantum Well Infrared Photon (QWIP)
Low cost and compact camera	High cost
Broad IR spectral response	Narrow IR spectral response
Based on a change of resistance, voltage and current when heated by IR radiation. The thermal signal depends on the radiant power, but not on its spectral content, so it is wavelength independent.	Based on a change of electrons state in a crystal structure reacting with incident photons with sufficient energy. Detector can carry photocurrent, that is proportional to intensity of incident radiation.

Improvements also in materials for detector with better thermal sensitivity have been achieved.
The preferred materials, that allow highest performance are VOx and HgCdTe, respectively for thermal and quantum detector [15].

For what it concerns thermal detectors, such as microbolometer, thermocouples and bolometers, are cheaper and more accessible with respect to quantum detector since thermal detectors operate at a room temperature, where no cooling system is required, consequently the cost of the camera and of its maintenance is reduced [21]. So, these uncooled systems, due to their low cost, are very popular.
Radiant energy absorbed and focused onto the microbolometer film causes an increase of the element temperature and a variation of its electrical resistance, that are used to generate an electrical output. The element and absorbing film are insulated by a cavity from the substrate to maximize the temperature change by minimizing thermal leakage. This enables a small amount of radiant power to be detected [21].
Isolation of the array microbolometer elements prevent thermal leakage and introduce noise through fluctuations in heat exchange with other components in the camera [21]. In fact, these devices are considered quite noisy [18].
Moreover, both types of detectors are capable to provide a response curve that is sensible to a certain range of radiation wavelength, specifically MWIR and LWIR ranges as can be visible in the Figure 7 [13]. However, thermal detectors, differently from quantum ones, are generally sensitive to a wide range of infrared wavelengths. Thus, thermal effects are generally wavelength independent. Signal depends upon radiant power (or its rate of change), but not upon its spectral content and the photonic nature of the incident radiation [18].

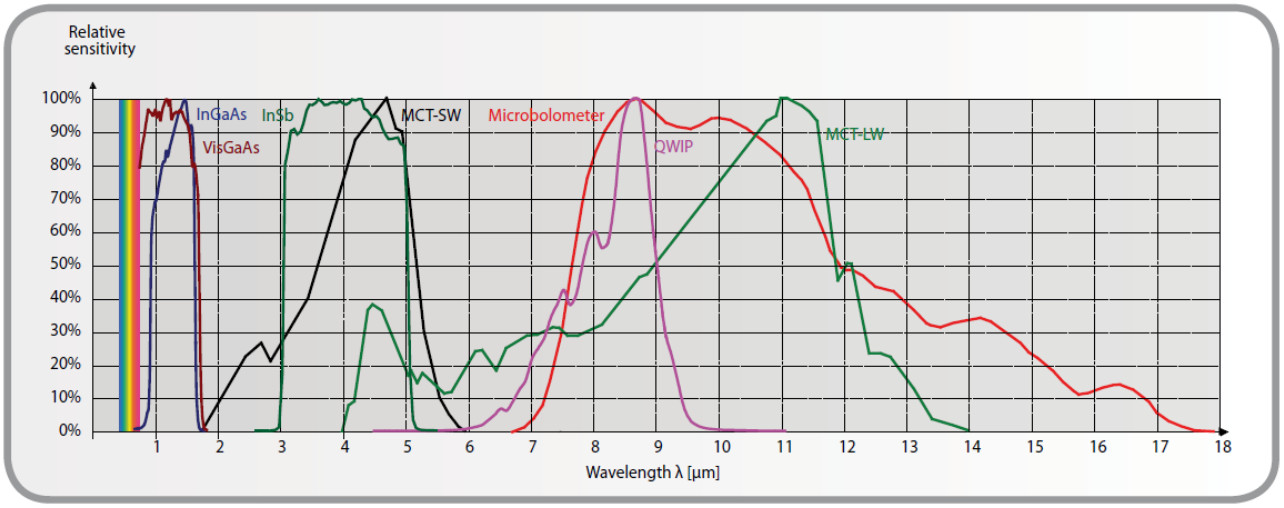

Figure 7. Response range and relative sensitivity of all different types of detectors.

On the contrary, quantum detectors require a cooling system, that can be provided through the use of liquid nitrogen or temperatures using liquid nitrogen or, in more versatile cameras, through the use of a small Stirling cycle refrigerator unit [21] [22]. This cryogenic cooling is necessary to prevent the thermal generation of charge carriers [18]. In addition, the presence of a Sterling cycle cooler, is the cause of the high cost of this cooled detector. Indeed, Sterling cycle cooler is the expensive component in the photon detector IR camera, and its maintenance influences the cost because it has a lifetime around only 10000 hours. Thereby, cooling requirements are the main obstacle to the widespread use of IR systems based of semiconductor photon detectors making them bulky, heavy, expensive and inconvenient to use [18].

In order to choose among different types of detectors, the situation where they will be applied, the target object's features, and characteristics of the detectors, as spectral sensitivity, cost, thermal sensitivity, resistance to highest temperature, image quality, noise, etc., must be considered to obtain optimal results [22].
Moreover, practical for the choice of the instrument with appropriate characteristics, in relation to the measure that we are interested in, it is important not to confuse thermography with radiometry; although both are based on measurements of radiation emitted by an object, they serve different purposes.
Thermography produces an IR map obtained by the IR radiation emitted by an object in the IR electromagnetic spectrum (0.9 – 14 µm) and detected by IR camera. The result is an image of that radiation, and it is the starting point to evaluate the relative temperature about the target object. So, the final aim of thermography is to quantify how hot an object and this information can be very useful because temperature can be an index that can predict illness.
Differently radiometry is focused on the measure of radiant electromagnetic energy released by an object associated in the IR spectrum [22].
Once the IR radiation, which is invisible to the naked human eye, is detected by sensors of IR sensing cameras, they cooperate with a computer software in order to interpret thermal maps obtained from the acquisition [29].

In the software processing phase the multistage calibration and correction process of all gain and offset of the detectors must be applied in order to obtain a more accurate thermographic map. Moreover, calibration consists into the compensation of error and noise due to external factors, as atmospheric attenuation, reflected ambient temperature, camera's ambient temperature, that can alter the accuracy of the interested signal's measurement [30]. For this reason, a correction algorithm must be applied by the IR camera software in order to obtain as result the temperature relative to the target object without any dependence on attenuations due to atmosphere and ambient surrounding. This process is called compensation [17] [22] [25].
Once the camera is properly calibrated, digital signals (voltage or current), are transformed into radiance values. In turn, the radiance values obtained are converted by electronics and specialized software into

temperature values, displaying on the monitor the thermal distributions and providing a temperature analysis with ± 1°C of precision. Conversion from radiance, radiative energy inside or emitted by an object, captured by an IR thermal camera, into temperature values can be performed knowing the emissivity of the target object, (and setting it in the camera) and exploiting the Stefan-Boltzmann equation. Infact, recalling to the Stefan-Boltzmann equation (2), due to the strong positive relationship that exists between an object's true kinetic temperature (reflective of the energy state of the object) and the amount of radiant flux radiated from the object (i.e., from a blackbody), the radiant energy can be used to distantly estimate the object's true kinetic temperature [19]. Infrared thermography testing uses the corresponding relationship between thermal radiation and temperature to compute the thermal map [30].
In order to obtain a useful thermal map some processing steps must be applied to the digital raw signal. These steps include filtration, thinning and binarization that allow to reduce noise and remove background information, segmentation, useful to select only the interested area for the registration, and thermal image computations [21] [22] [30].

The result is a thermogram, or thermal map, a detailed representation of a scene's temperature, which depicts the variations of the temperature across a target scene [13] [19] [22] [31]. These thermal images are a spatial two-dimensional (2-D) map of the 3-D temperature distribution of the target, being a qualitative determination mean of surface temperature [21] [29].
Thus, IR thermography provides a false color depiction of a target and supplies a visual rendering of the energy emitted, transmitted, and reflected by an object and its environment [17] [19] [29].
IR thermography systems produce both qualitative and quantitative representations of temperature patterns, showing thermal variations, that can be indicative of different state, as abnormality.

2.2.5. ADVANTAGES AND LIMITATIONS

IR thermography is an imaging technique that has had big success, due to its considerable number of advantages, allowing its diffusion worldwide. It is a non-destructive technique, that does not require any type of preparation before the inspection, and it is considered a passive technique because it detects passively the IR radiation spontaneously emitted by an object's surface. Moreover, it is a non-contact screening procedure that allows to record radiation at distance from the source of heat. Contactless feature, other for its hygienic properties that ensure no contamination of examined piece, is a good advantage for systems that estimate in real time object temperature through detection of IR emission above all in case of extremely hot objects or dangerous products, such as acids. Also for environments, as airports, where a lot of screening of infections are performed, above all during pandemics periods, when contact is not recommended, measures are however safely acquired, keeping the user out of danger [17] [25]. Not less important is its high-speed data capture with high sensitivity and spatial resolution, that allows to provide 2D thermal images in real time, enabling to record transient thermal events, and to acquire information from fast moving targets and from fast changing thermal patterns [17] [22] [32]. Regarding its performance, low cost, high accuracy of its recording, good precision in thermal quantification, real time monitoring of ROI, high-resolution of uncooled focal plane array detectors, coupled with high-speed computers running sophisticated image analysis software able to capture 200 frames per second with a sensitivity of 0.009 ° C, are, by now, just essential features that characterize IR systems [17] [29] [33].
However, IRT has also some disadvantages. It is highly dependent on working conditions, such as the surrounding temperature, airflow or humidity. Therefore, when IRT is used in controlled environments with stable settings, with a minimal interference from external space, in order to obtain more reliable measurements and minimize noise and errors, current standard protocols must be applied [17] [29]. On the contrary, its application in dynamic environment results more complex because the presence of many external factors that cannot be controlled, as transient phenomena, and the absence of protocols to follow. Moreover, IRT is also highly dependent by the choice of sensors and type of detectors and material, material characteristics, (as number of sensors, FOP dimensions, etc.) and experimental setup [17].

2.2.6. IR THERMOGRAPHY APPLICATIONS

TIR has a very wide range of applications, ranging from biomedical and no biomedical field [13] [25] [34].
Among the no biomedical field applications there are building inspection, structural damage detection, global monitoring of environmental pollution and climate changes, long time prognoses of agriculture crop yield, chemical process monitoring, driving assistance, assessment in electrical field, Fourier transform IR spectroscopy, IR astronomy, and military purposes [34].

Regarding the biomedical applications, IRT is applied above all for diagnostic purposes. It allows a more general evaluation of health subject status, through fever screening and wound assessment, but also a more specific assessment, as cancer detection, infection, eye disease through corneal temperature measurement, diabetes, diagnosis of rheumatologic diseases, ischemic monitoring and vascular disease [14] [17] [18] [25] [30] [34]. TIR imaging measures allow to describe the objective evidence of the patient health status because radiation from human skin, temperature, and in particular, heat pattern changes, are a direct reflection of the biological activity on the body [19] [34]. In fact, it is considered as an indicator of illness, because a change in temperature generally is related to some pathological conditions. Also when some changes in physiological conditions of the human body occur, the whole body or local heat balance is destroyed or affected, so the clinical manifestation is that the tissue temperature increases or decreases [30]. Thus, the study of the heat exchange processes of the body from the deeper tissues to the skin and, subsequently, to the environment can provide information on pathology. Heat transfer processes occurs through the skin, that is the largest human organ that helps to maintain the body's thermal equilibrium with the environment. For this reason it is important to focus on the cutaneous temperature, rather than body temperature [29].

TIR APPLICATION TO HUMAN BODY
Thermal IR imaging is largely applied into clinical field as contactless and non-invasive method to record cutaneous temperature accurately. It can be exploited to evaluate the health status of the subject, to assess his psychophysiological state, to obtain information of autonomic nervous system (ANS) activity. For example, it can be applied to record the level of engagement of the subject while performing an action. Human skin is a good emitter, that allows us to obtain reliable information on its radiative properties and consequently on its relative temperature. In fact, human skin is characterized by an emissivity value, closer to the blackbody one, about 0.98. Having higher ε value for an object is an advantage because it means that it has higher radiative properties, and a more accurate temperature estimation can be performed.
Moreover, experiments showed that biological tissues and human skin, whose physiological temperature ranges from 35°C to 41°C, emits a continuous spectrum of radiant energy essentially in the range of 2–20 μm wavelengths, and specifically into the MWIR (2 – 5 μm) and LWIR (8 – 14 μm) ranges, since these are the regions of the greatest IR radiation intensity. Consequently, IR thermography in clinical field often operates in these two ranges [25]. Among the two, LWIR range is referred as the thermal infrared range, and it is the most inspected for its primary use in the infrared thermal imaging, because in this window there is a less attenuation due to atmosphere and lies the intensity average peak at 9–10 μm [14] [19] [22] [25].
These human features allowed to determine noninvasively skin temperature and investigate skin microcirculation, essential factors into diagnostic systems, through infrared cameras [13] [34]. Thus, IR thermography application into medical field has a great positive influence because it, differently from other medical imaging approaches, provides useful information that describe properties, condition and quality of tested objects exploiting the safe characteristics of the electromagnetic field that does not damage in any way the internal tissue and surface [17] [30] [32].Thermography non-harmfulness and safety guarantee the reliability and effectiveness of its application because it is limited to detect passively the IR radiation spontaneously emitted by human skin without involving harmful ionizing radiation such as X-rays, computed tomography, MRI, etc., venous access or other invasive procedures, that by hitting the surface of interest can result dangerous [29] [32] [33].
Moreover, no-contact feature of thermal systems is relevant above all in medical field in situation where the patient is not collaborative, as in the case of children, and allows a thermal registration, free from any alteration of patient's psychophysiological state [25] [29] [30].

Then, it can be used as a support to other scanning techniques 2D as X-rays and 3D as CT and MRI, to perform standard anatomical investigations allowing possible a correlation between areas of the target [21].
IRT devices are considered user-friendly for recording skin surface temperature because their ease of use, for absence of pain, and its capacity to record a great number of adjacent temperature measurements for different purposes [13] [17]. Indeed, through the use of IRT systems, measures of vital signs can be automatically extracted, as heart rate (HR) and respiration rate (RR). According to the task of the measurement, different region of interest (ROI), are investigated. However, the preferred ROI, from which the thermal signal is extracted, is the facial region. Among the reasons of this preference, the presence of blood vessels with a high density, from which temperature variations are more evident, through vasodilatation and vasoconstriction, is the most important. Moreover, this area is quite free and generally, there is not any type of occlusion, due to external object as clothes, scarf and bracelets, etc., that can alter the measurements during daily actions. However, for facial thermal assessment, an issue is represented by difficult face detection, in case of occlusions due to rotation [32]. In this case, some algorithms for the face frontalization, can be applied, but a loss of signal cannot be recovered. Specifically, in thermal camera system is implemented a face frontalization algorithm that allows to reconstruct face shape wrapping each Delaunay triangulation into a frontal reference shape [35] [36] [37] [38] [39] [40]. Also, the presence of beard provokes inaccuracies in the measurements because, like hair, beard is a heat insulator [32]. In particular, ROIs of the face are focalized on nose, forehead periorbital region, cheeks and chin.

2.2.6.1. APPLICATION FOR THE EVALUATION OF THE SUBJECT PSYCOPHYSIOLOGICAL STATE

Thermal signature is an ecological alternative to other standard techniques, as galvanic skin response (GSR) and electroencephalography (EEG) measurements, to assess psychophysiological subject's state. TIR imaging provides information about physiological processes in real time [15] [21].
In fact, IR imaging allows to infer the peripheral autonomic nervous system activity through the modulation of the cutaneous temperature, which is a known expression of the psycho-physiological state of the subject. Indeed, experienced emotions, including stress or fatigue, can produce changes in skin temperature [6].
Subsequently to external stimuli, physiological emotional changes occur that provoke the activation of peripheral ANS, whose role is to respond to these changes in order to maintain the state of equilibrium. Through the antagonist function of the sympathetic and parasympathetic branches of ANS, are triggered some physiological modulations, such as changes in heart rate, respiration rate, blood pressure, blood flow and muscular activity, resulting into a change in cutaneous temperature [41] [42].
Thus, each psychophysiological state triggers a certain ANS activity, that produces a thermal facial configuration. In this way, analyzing thermal cutaneous pattern is possible to estimate the psychophysiological subject's state.
For example, drowsiness is described by a reduction of blood flow and by a change in facial thermal patterns, resulting in a decreased temperature until to 0.54°C in correspondence of supratrochlear arteries. Temperature decrease in drowsiness state results although with less evidence also in other facial arteries [7]. Moreover, compared to a wakeful state, drowsiness condition is characterized also by an evident decrease of respiration rate of about 3.5 breaths per minute (bpm) and by an increase of its standard deviation (SD) of 0.7 bpm [43].
On the contrary, anxiety sensation, sexual arousal and love emotions, result in an increase of temperature in periorbital and forehead region, due to the blood perfusion [44] [45].
Moreover, in order to automatically recognize different emotions, some emotion analysis classifiers are implemented. Classifiers, as support vector machine (SVM), k-nearest-neighbors (kNN) classifier, binary decision tree (BDT), or Linear discriminant analysis (LDA), can be trained on a thermal images database, which includes several annotated emotions [35] [46]. Otherwise, emotion classifiers can be trained analyzing changes in HR, HRV, RR, blood pressure parameters, extracted from thermal map when fearful, anxious, angry, stressful and relaxed subject's state are simulated [35] [46] [47] [48]. Specifically, breathing signal, easily detected from thermal images by analyzing nostril temperature change, is a salient physiological signal that responds to behavioral, emotional and cognitive challenges. Monitoring dynamic thermal activity in specific area, as nostril, allows to quantify both duration and relative depth of each breath cycle. These

parameters, respiratory rate and depth of breath cycle, are the first values influenced by a variation of emotional condition. For example, during stress condition, when workload increases, changes in respiratory rate and tidal volume, as well as in blood pressure, are recorded. Thus, emotions are strictly correlated with physiological changes, controlled by autonomic nervous system and the human physiology can explain how a psychophysiological condition can be represented by thermal variations [49] [50] [51] [52].

2.2.6.2. PHYSIOLOGY

Specifically, the radiance of a specific object, that represents the direct measure of IR imaging, is an exponential function of the surface temperature, which, in turn, is an indicator of the level of blood perfusion in the skin [21]. Blood perfusion, in turn, is a factor that examines physiological changes and responses, due to an alteration of normal state and homeostasis condition [21].
So, regional variations in body surface temperature, recorded into thermal map image, reflect information contained by the microcirculatory dynamics of the skin surface [53]. In particular, also small vascular changes can cause large changes in skin surface temperature [33].
These variations in blood flow, correspond to different regulating mechanisms that try to return into a normal state in response to a particular event that has changed its basal behavior [13]. Strictly related to blood flow variations is the activation of the autonomic nervous system which controls vasoconstriction and vasodilatation of the capillary vessels to maintain homeostasis [13] [16].
Changes in skin temperature are the results of several mechanisms triggered by the thermoregulatory center in the hypothalamus in order to maintain homeostasis in response to hot or cold stress conditions.
Temperature information of external and internal environment was sensed by specific sensory receptors, called thermoreceptors, that can be differentiated in two types: cold and warm thermoreceptors. Cold receptors are more numerous with respect warm ones, for this reason, generally all the people are more sensitive to cold stress. Cold receptors detect a decrease below the basal core temperature (~37°C), while warm receptors detect an increase above the basal temperature, perceiving hot sensation from 37°C to 45°C. Both thermoreceptors are located uniformly around the hair roots and under skin surface along the subcutaneous layers, and they can be identified as free nerve endings receptors type. They are involved into sending this thermal sensation to the hypothalamus into the forebrain, through Aδ sensory afferent neurons. These myelinated fibers are characterized by a relatively small axon diameter of 1-5 μm, that allows the conduction of information to the CNS with an average velocity of 5-30 m/s. In addition, they can be classified as tonic receptors, because they slowly adapt between 20 °C and 40 °C, to constant stimuli. Once this information arrives at the hypothalamus, it promotes some thermoregulation processes in order to maintain constant core body temperature. These processes consist of changes of respiration rate, heart rate, metabolic rate, activation of adrenal, sweat and thyroid glands, activation of skeletal muscles provoking shivering and constriction or vasodilatation of smooth muscles in arterioles. Moreover, variations in blood flow correspond to different regulating mechanisms, that try to return into a normal state in response to a particular event, that has changed its basal behavior [13]. Strictly related to blood flow variations, there is the activation of the autonomic nervous system which controls vasoconstriction and vasodilatation of the capillary vessels to maintain homeostasis [13] [16]. Thus, these physiological responses are directly linked with external temperature variations. In particular, the thermoregulatory control of blood flow provokes vasodilatation during heat stress condition, that in turn promotes an increase of blood flow to the skin surface where the excess of internal heat will be dissipated through irradiation. So, in correspondence of skin surface an increase of cutaneous temperature can be detected, while at the same time the core body temperature decreases reaching the equilibrium. On the contrary, during cold stress conditions, capillaries vasoconstriction is activated resulting into a decrease of the blood flow to limit heat loss, a local superficial temperature decrease, and an increase of core body temperature [54] [55] [56] [57].

A constant core body temperature is vital to preserve homeostasis, and it is controlled by the hypothalamus, which balances production of heat with heat loss [21]. In order to maintain normal thermoregulation, the peripheral nervous system, controls the skin blood flow in a uniform and symmetrical manner, resulting in a right/left thermal pattern that is also symmetrical [33].

Heat is generated by metabolism and by the contraction of muscles, and it is transported throughout the body by the circulation of blood. A small area in the anterior of the hypothalamus detects an increase in blood temperature and sends neuronal signals to activate methods of heat loss such as vasodilatation, perspiration, exhalation, and a reduction in the metabolic rate, to maintain the equilibrium. While, when hypothalamus detects a decrease in blood temperature, it leads to activation of some mechanisms to reduce heat loss, as activation of blood vessels vasoconstriction [21].

2.2.6.2.1. FACE CONFIGURATION FOR EACH EMOTIONAL STATE

TIR imaging is involved into the detection of several emotions through the measure of facial cutaneous temperature and its topographic distribution, that is regulated by ANS, whose aim is to achieve thermal homeostasis in response to external stimuli and physiological emotional changes [44] [52].
Applied with these purposes, thermal images of the face can provide information about emotional excitations such as stress, fear, sexual arousal, surprise, anger, joy, embarrassment, mental stress, pain [20] [52]. Each physiological state of the subject is correlated with a different peripheral autonomic activity of the central nervous system, providing a specific face configuration [6] [52].
In particular, monotonous actions and rest conditions, where great amount of mental workload is not necessary, generate activation of parasympathetic nervous system, that causes vascular relaxation and a gradual rise in temperature occurs. On the contrary, stress conditions, situations where mental workload rises, provoke activation of sympathetic systems, and peripheral vascular vasoconstriction occurs, resulting in a temperature decrease [6] [52]. In this way emotional engagement can be monitored, classifying positive engagement with a rise in temperature, neutral condition by constant values, and negative ones described by an increase of stress and a decrease in temperature [52].
Stress detection is a widely diffused application. The infrared lock-in technique reflects the stress distribution of structural components by measuring the signal of temperature changes caused by load excitation, and then quickly and accurately locates the local stress mutation position and stress concentration of structural components, so as to realize the rapid detection of structural components damage. Moreover mental stress condition, is strictly related with a workload increase, and it can be identified by a temperature decrease on the nose tip, about 0.55°C, while forehead temperature remains relatively constant [44] [45]. Correlated to this, there is fatigue sensation, because it is considered as the result of accumulated stress [58].
Fearful situation instead provokes a decrease in temperature of 2°C on the fingertip, as result of the vasoconstriction. However other studies have observed that felling of fear causes a temperature drop over the whole face, but the largest temperature decrease occurs on the nose tip [44] [45].
However, several studies have been performed in order to detect a correlation between each emotional state and the effects that it provokes in each face region, as summarized in the Table 2, by I. Fernández-Cuevas et al [16] and by S. Ioannou, V. Gallese, and A. Merla [20] [44] in their studies:

Table 2. Skin thermal variations in the considered ROI across emotions.

	Emotions									
	Stress	Fear	Embarra-ssment	Startle	Sexual arousal	Anxiety	Joy	Pain	Guilt	Displea-sure (exercise)
Regions										
Nose	↓	↓			↑		↓		↓	
Cheeks				↓						↑
Periorbital				↑	↑	↑				
Supraorbital				↑		↑				
Forehead	↓↑	↓			↑	↑		↓		↑
Maxillary	↓	↓		↓				↓	↓	
Neck–carotid				↑						
Nose	↓									
Tail		↓						↓		
Fingers/palm		↓						↓		
Lips/mouth			↑		↑					

Consequently, IR imaging system provides, in indirect way, also information about sympathetic nervous systems, vascular system, musculoskeletal system, mental workload, emotional engagement, local inflammatory processes and endocrine and oncological conditions in real time, resulting a non-invasive complement to physiological data gathering [19] [31] [33].

2.2.6.2.2. APPLICATIONS FOR THERMAL COMFORT

IR thermography is applied to assess the thermal comfort in a closed environment. Differently from other techniques thermography exploits physiological information extracted directly from thermal image of individual occupants of the building. Thus, IRT can predict in real time the subjective thermal comfort considering physiological parameters that reflect the human thermal sensations. In addition, this technique allows to investigate how physiological parameters change and how they adapt to the external environment. Physiological signals, extracted by thermal maps, are essential for thermal comfort assessment, because the autonomic nervous system tends to adjust, through opposite mechanisms as vasodilatation and vasoconstriction, regulated by sympathetic and parasympathetic branches, temperature changes that occurs between the external environment and the body.
In particular, cold sensation provokes blood vessels vasoconstriction, while hot sensation vasodilatation of blood vessels, leading to temperature changes onto the human skin. For this reason, Tsk is a useful parameter used to estimate thermal comfort sensation [54] [56].
This assumption allowed the conversion of heating ventilation and air conditioning (HVAC) systems, from passive and user-empirical adapting devices, to an automated, user-centric and data-driven principle of operation that can simultaneously improve occupant satisfaction and well-being in indoor environments [54].
To date, there are three available methods to evaluate thermal comfort: the rational or heat-balance approach, adaptive approach and physiological based method.
While human physiology and human thermal comfort remain a complex issues, the measured temperature distributions on the body's surface can be a useful valuable indicator about thermal sensations [11].

In this study, we will apply IR thermography for thermal comfort purposes into a car space.

CHAPTER 3

3.1. WHAT THERMAL COMFORT IS?

3.1.1. DEFINITION

Thermal comfort is defined by The American Society of Heating, Refrigerating and Air-Conditioning Engineers (ASHRAE) as that condition of mind that expresses satisfaction with thermal environment [1] [56]**.** This condition describes an equilibrium between body and external ambient and presupposes that any driving impulse to correct the environment is not required [1].

Discomfort sensation is related to user's thermal dissatisfaction, caused by too warm or too cold body, or by unwanted heating or cooling of a certain part of the body. Cold discomfort is strongly related to the mean skin temperature, while warmth discomfort is strongly related to the skin sweating caused by sweat secretion [1].

Standards, provided by ASHRAE, determine appropriate thermal conditions, specifying thermal parameters that should result in thermal satisfaction for at least 80% of occupants in a space. These standards recommend different comfort temperature ranges according to the environmental conditions, consequently, also optimal temperatures differ on the surrounding conditions [1] [54]. However, these standards are suitable for static environments, with uniform thermal conditions, considered also unrealistic ones [1].

Moreover, thermal satisfaction is defined as a cognitive process, strictly dependent from each individual subject and his physical, physiological, psychological condition, bringing to a different opinion, from subjects belonging to same culture, about thermal comfort sensation related to the same ambient. These different opinions suggest that satisfaction with the thermal environment cannot be based only on a general absolute standard valid for all individuals, but, on the contrary, it is a complex subjective response linked to one's own metabolic activity and insulation of clothes worn [1].

The human body's perception of environmental thermal comfort is not solely dependent on temperature, but on a combination of six variables. Four of these variables are related to the external ambient (air temperature, air humidity, air velocity and mean radiant temperature), two variables are related to the subject (clothing insulation and metabolic activity) [1] [59]. Specifically, air temperature is the temperature of the air surrounding the body, air humidity is the amount of water in the air, air velocity is the speed of the air moving across the subject and mean radiant temperature refers to the uniform temperature in an imaginary empty ambient, where the radiant heat transfer from the human body is equal to the radiant heat transfer in the actual non-uniform enclosure. In addition, clothing insulation refers to the thermal insulation provided by different clothes types and metabolic rate refers to the energy released by the metabolism and is function of the muscular activity.

Ability to provide thermal comfort to the subject, who is staying in certain environment, is a crucial ambient feature, that not only increases the health and productivity of the subject, but also, influences the saving of energy consumption, fundamental to avoid carbon dioxide emission due to combustion of fossil fuels, and a consequent climate change [1].

In order to reduce energy consumption, models that predict the thermal comfort required by the subject according his physiological state and adapt the functioning of heating, ventilation and air conditioning (HVAC) systems, were implemented [60]. These HVAC systems must be employed with suitable sensors would vary with human comfort sensation and his real needs, other than with ambient temperature [59].

3.1.2. HVAC SYSTEMS

The Heating, Ventilation, and Air Conditioner systems are devices implemented into closed environments with the aim to adapt their functioning in order to obtain a thermally comfortable ambient, often using time-invariant fixed setpoints derived from thermal comfort standards, such as the ASHRAE Standard 55 "the Environmental Conditions for Human Occupancy" [56].
Relying on time-invariant measurements, that characterize the internal building, as room shape, room size, and construction material, HVAC systems are programmed to deliver a predetermined amount of heating/cooling, causing in the most of the cases an unsatisfactory and inefficient HVAC systems performance, as well as causing a waste energy consumption [54]. User's thermal unsatisfaction derives because in the programmed workload of HVAC systems is not considered also the contribution of the time variant features (both external and personal factors) that affect occupant's thermal sensation, which evolves over time [54] [60].

Since air conditioning systems goal is to provide satisfaction to almost 80% of occupants, HVAC system commonly focuses on the climatization of large portions of the building or single rooms, allowing an automation based on general sensory input without consider individual requirements of residents [11]. But since thermal comfort sensation is subjective, and it can differ for everyone, in order to obtain better performance it is necessary to adapt dynamically HVAC functioning to the subject and to his unique thermal requirement in every instant of time [54].
So, a smart air conditioner must be able to compensate large variations from person to person in terms of physiological and psychological satisfaction and find an optimal temperature for everyone in each space. Adapting the HVAC system functioning also to dynamic factors has several advantages: other than ensuring thermal comfort, it provides an increase of health and productivity of the subject, increases satisfaction and efficiency and influences the saving of energy consumption [59].

If quantifying the impact of static factors on thermal comfort may not be so difficult, it is different for what concern to try to quantify the dynamic factors' impact [56]. So the best way to estimate dynamic personal thermal preferences is to apply continuous monitoring of thermal comfort to capture variations over time [56].

To summarize, in order to obtain an optimal estimation of thermal comfort is necessary to include information from both building constant features, and time variant features of ambient and of people sensations in real time through occupants' feedback making possible to adjust the set point temperature [1] [60].

3.1.3. METHODS TO EVALUATE THERMAL COMFORT

Currently, there are three available methods to evaluate thermal comfort: the rational or heat-balance approach, adaptive approach and physiological based method. In order to obtain a reliable result, these methods are validated through the use of seven-point ASHRAE thermal sensation scale. This scale is useful to record the patient opinions about how hot or cold they felt, repeatedly during the experiment [60].
This scale, called also Bedford scale, ranges from -3, cold discomfort, to + 3, hot discomfort, with 0 neutral in the middle. Answered values ±1 and 0 define the comfortable condition, while values of ±2 and ±3 define uncomfortable ones [1] [59].

3.1.3.1. PREDICTED MEAN VOTE (PMV) AND PREDICTIVE PERCENTAGE OF DISSATISFIED (PPD)

The rational or heat-balance approach is the most widely used quantitative method to evaluate the indoor thermal comfort in climate chambers and with standardized, steady-state or laboratory conditions [34]. By a steady-state heat transfer model between the subject and his surrounding environment, this method

predicts a range of temperatures, which reflects the thermal comfort sensation felt by occupants. In this steady-state model both six factors related to external environment and to human subject are assumed as standard and constant values valid for all occupants: relative humidity of 50%, mean relative velocity lower than 0.15 m/s, mean radiant temperature equals to air temperature, metabolic rate of 1.2 met, and clothing attenuation, 0.9 clo in winter and 0.5 clo in summer [1] [54]. According to these values, the model computes an index, called "predicted mean vote" (PMV), that predicts the steady state comfort responses of a large group of people according the seven-point thermal sensation scale (from −3 for cold to 3 for hot), as depicted in Figure 8.

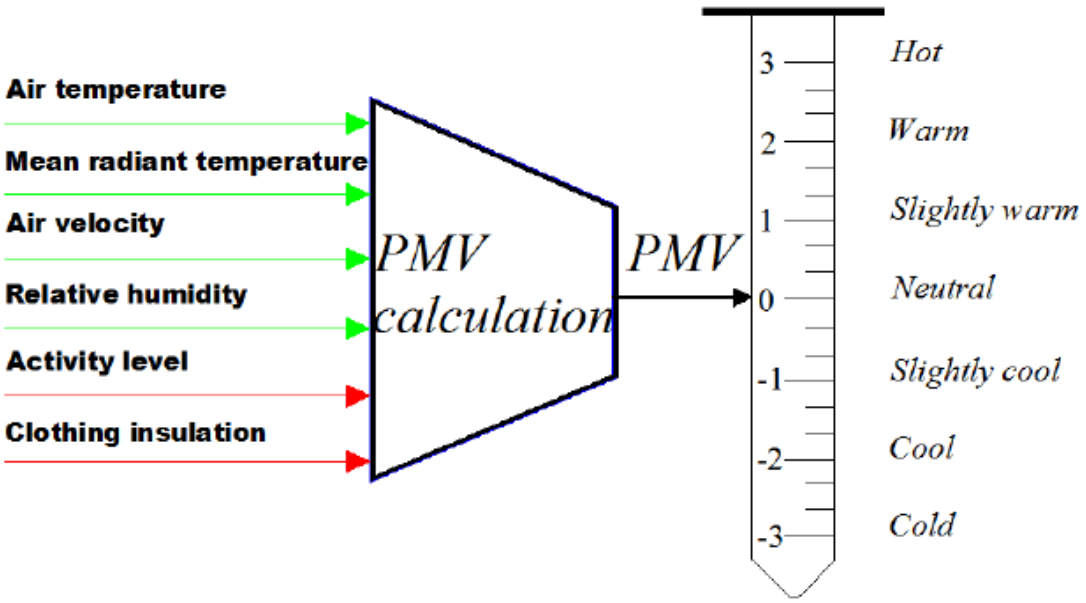

Figure 8. Factors that influence PMV computation and its scale values.

Related to PMV index, "Predicted Percentage of Dissatisfied'' (PPD) index, is computed too. PPD index describes the percentage of occupants dissatisfied with thermal condition at any time.
This model proposed by Fanger, computes PMV and PPD index according to the following equations:

$$PVM = [0.303 \exp\{-0.036M + 0.028\} * L] \quad (7)$$

$$PVM = a\,T + b\,P_V - c \quad (8)$$

$$PPD = 100 - 95\ exp\ [-(0.03353\ PMV^4 + 0.2179\ PMV^2)] \quad (9)$$

PMV index can be computed with two different formulas (7)(8). In equation (7), M indicates the metabolic heat production, and L is the thermal load on the body, defined as the difference between internal heat production and heat loss to the environment. In the formula (8) T represents the temperature (in Kelvin), P_V the pressure of water vapor, a, b, c coefficients related to environment's characteristics. As depicted in formula (9), PPD index is directly correlated to PMV index. Thus, it can be deduced that, even when the PMV index is 0, there are some individual cases of dissatisfaction with the level of temperature, due to some differences of approach in the evaluation of thermal comfort from one person to another. In particular, when PMV = 0, a minimum rate of dissatisfied of 5% exists [1].
In order to obtain a thermally acceptable environment, ASHRAE Standards 55 recommends maintaining values of PMV index within the range between −0.5 and 0.5 and PPD index values at less than 10% [1].

However, there are some limitations associated with this method. Since its dependency on the mean feedback of a group of people in climate chambers with laboratory settings, this method provides a generalized and stationary prediction of thermal comfort, that sometimes does not reflect real people needs. In fact, this method assumes same standardized parameters for all occupants in a same space, about their metabolic rate, and clothing. Moreover, to measure parameters such as the mean radiant temperature and

metabolic rate in the PMV model, expensive devices are required, making this method inapplicable in real operation settings.
On the contrary, methods able to provide a personalized comfort prediction based also on physiological responses and responses to transient situations, that more reflect living in real world situation, are required [1] [2].

3.1.3.2. ADAPTIVE METHODS

Qualitative adaptive methods are implemented in order to get more reliable information about the actual workplace comfort and the relevant (interacting) parameters. These adaptive methods have the purpose of analyzing the real acceptability of thermal environment, which strongly depends on the context, the behavior of occupants and their expectations. The adjustments have been summarized in three categories: behavior adaptation, physiological adaptation and psychological adaptation [1].
To understand occupants' requirement about thermal environment, user participation oriented and control loop are used to assess thermal comfort. This control loop starts with thermal votes received from occupants in the analyzed room, that are used directly to adjust the HVAC settings or model the comfort state using different statistical methods.
At each cycle, decision algorithms compute the comfortable setpoint based on the environmental conditions and the actual thermal votes collected during this period.
Direct thermal comfort feedback from the occupants through surveys allows to adapt continuously model and HVAC systems to real thermal needs of each occupants [54]. However, surveys can be both an advantage and a limitation. An advantage because allows to train the model with respect to physiological demand of the subject, through his feedback. Moreover, through user's answers we can indirectly obtain information about subject's physiological processes. While it represents a limitation because asking continuously occupants about their state of comfort, became impractical and less informative with the increase of the frequency [56].
As alternative to the questionnaires, the users can adjust themselves the room's temperature turning a switch, until desired results are achieved, and they felt thermally "neutral" [60].
Since this method is strictly related to periodic occupant's feedback, used as the ground truth to rectify the comfort prediction or to directly determine the new temperature setpoint, it can produce some errors because the frequency of feedback and its reliability tends to decrease with time as the novelty and excitement of the system fades away. Moreover, in this case behavioral adaptation, as wear heavier clothing, or close a window, is not considered in the current voting methods [54].

3.1.3.3. METHOD BASED ON PHYSIOLOGICAL SIGNALS

The third method consists into a mathematical model of thermal comfort, based on physiological parameters recorded directly from individual occupants of the building, and on their feedback, making possible estimation of an occupant's probability of discomfort [56] [60].
It allows to reduce or ultimately eliminate the need for continuous feedback for training of personal comfort models, since physiological responses could be used to learn personal comfort requirements. Indeed, continuously detecting human physiological responses (e.g., vasodilation, increased respiration, heart rate, skin temperature) is fundamental to understand people's thermal comfort level under different conditions, because a change of these physiological response is directly correlated with thermal discomfort sensation.
In fact, human body is a thermodynamic machine that exchanges heat with external environment and tries to maintain an internal homeostasis through several processes, (as respiration, shivering, etc.) to counteract external thermal loads. The body's heat balance equation, formula (10), describes a thermal balance between the heat produced by metabolism (M) and by muscular activity (W), the heat lost from the body through sweat evaporation (E), conduction (C), convection (K), and net radiation (R) and the heat stored into the body (S).

$$M - W = E + R + C + K + S \tag{10}$$

According to the two laws of thermodynamics, the same amount of heat generated internally of the body or assimilated must be delivered outside, in order to maintain equilibrium and homeostasis. A representation of all mechanisms involved in the heat balance equation and heat exchange between the subject and the external environment is depicted in Figure 9.

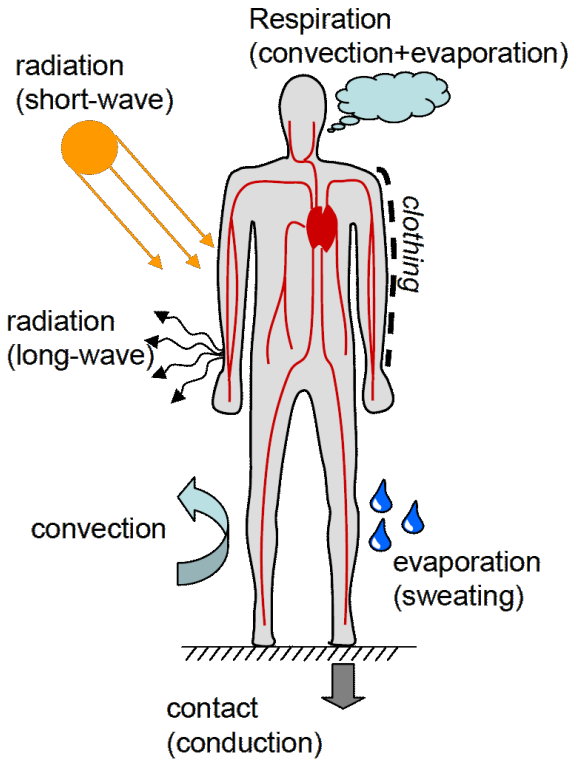

Figure 9. All the mechanisms involved into the heat exchange among the subject and the external environment.

Moreover, this balance, as depicted in Figure 10, is influenced by environmental parameters like air temperature, mean radiant temperature, relative air velocity, relative humidity, presence of radiant close surfaces, individual parameters like activity level or metabolic rate, human skin emissivity, and finally, by clothing thermal resistance. Since the presence of this great number of factors that influence the homeostasis condition, it is necessary to evaluate and control very precisely the experimental conditions and the quantization of the thermal skin variability. Tsk is strictly dependent on climatic environment, cognitive stimuli, physical activity, acclimatization as well as on emotional and psychological state of the subjects, their short and long-term medical histories [1] [56].

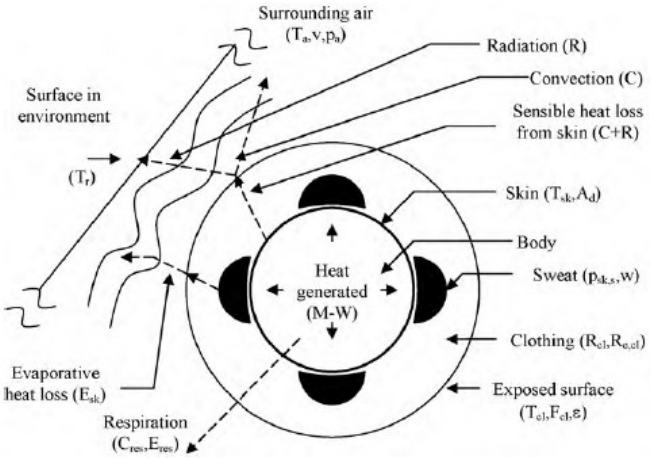

Figure 10. Factors that affect human heat balance equation.

Thus, all the mechanisms involved into the maintenance of thermal comfort form the thermoregulation process. There are two types of thermoregulation: behavioral thermoregulation that controls actions as active movement and adjustment of clothing and autonomic thermoregulation, controlled by the hypothalamus**.** Autonomic thermoregulation continuously tends to reach thermal equilibrium, through several heat exchanges with external environment, triggered by the thermoregulatory center in the hypothalamus. Hypothalamus receives thermal information referred to both external and internal body temperature from thermoreceptors, and in order to maintain a core body temperature around 37°C, provokes sweat secretion, shivering, changes in the metabolic rate, vasodilatation or vasoconstriction, etc., as depicted in Figure 11. If external temperature drops or rises, the body immediately reacts, but when temperature regulation mechanisms and heat exchanges are not enough to maintain homeostasis, discomfort state occurs [56].

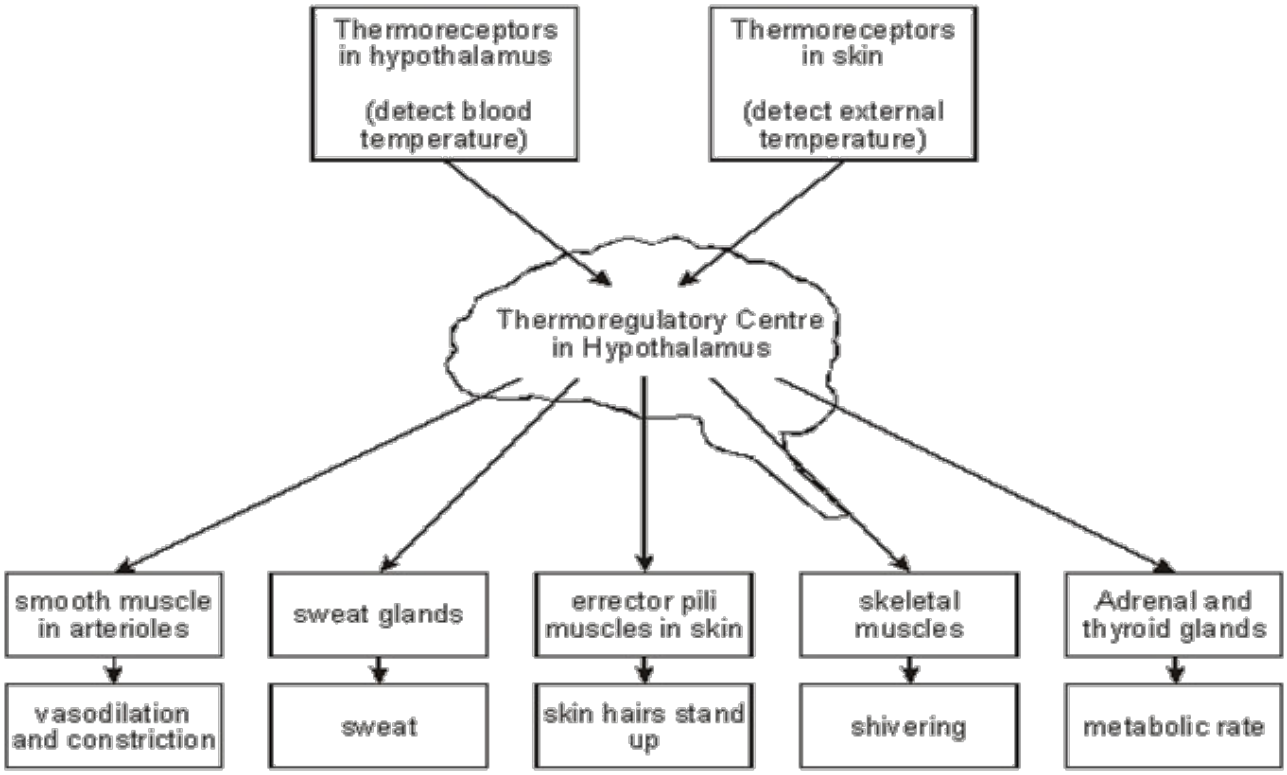

Figure 11. Thermoregulatory center in the hypothalamus.

In particular, thermal discomfort starts when the body heat cannot be dissipated to the surrounding environment, as when the ambient temperature is higher than the body temperature [1].
There are 2 types of thermal discomfort, that differentiate from the cause, cold and hot discomfort. Cold discomfort is strongly related with the low mean skin temperature, while hot discomfort is related to skin wittedness caused by sweat secretion.
In cold environments, for example, the body generates heat by movement (shivering); on the other hand, in too hot environments, cooling of the surface of the skin is achieved by evaporation. In general, there is a constant effort to keep the temperature of the body at the acceptable levels, which involves the continuous cooperation of the body with its environment. This task is performed by metabolic rate, that is associated with the activity that a person is performing at a specific time [1].
The total metabolic rate of work produced within the human body is dissipated to the environment through skin surface and the human body, that tries to maintain its core temperature at around 37 °C. So, as the Tsk also the blood flow is affected by thermal stress. Indeed, thermoregulation system, alters heat exchange with the environment by modifying the skin blood flow through cutaneous arterioles and veins vasoconstriction or vasodilatation. Specifically, during heat stress, vasodilation increases the flow of blood to the skin surface to dissipate excess internal heat, and vice versa, vasoconstriction decreases the blood flow to limit heat loss

during cold stress [1] [56]. Thus, in cold stress condition, mechanisms of temperature generation are activated, as shivering, vasoconstriction, increase of heart rate, increase of blood pressure, stimulation of thyroxin release, thyroid gland, which provokes an increase of the metabolic rate, and subsequently the body temperature increases. On the contrary, in hot stress conditions, temperature reduction mechanisms are activated, as transpiration and sweat evaporation, reduction in the heart rate and blood pressure, inhibition if thyroxin release, reduction in the metabolic rate and heat production. These processes reduce the body temperature.

Measuring variations of biological signals allows to develop personalized comfort thermal models improving the prediction accuracy, [54] [61]. The most informative and useful biological signals useful to estimate human thermal and comfort sensation are the measured heart rate, heart rate variability, respiration rate, and body temperature. The last one directly reflects the sympathetic activity of autonomic nervous system, that, when affected by heat stress, tries to compensate thermal discomfort, through vasodilation and vasoconstriction of the blood vessels causing a variation of Tsk [54] [60].
Common devices involved into the Tsk measurements are resistive temperature detectors (RTDs), thermocouples, thermistors, thermopiles based on integrated circuits, infrared thermometers, and the most modern infrared thermal cameras [59].
Contact thermocouples and contact thermometers provide measures of skin temperature with high accuracy, low-cost, and easy installation. However, they are very intrusive devices since they should be directly attached to the skin surface. This drawback limits its application onto laboratory settings because it is not possible to equip each occupant with the thermocouples in the operational residential or office environment without interfering with their activities. For this reason, contactless technologies, as infrared one, are preferred. An example is the infrared thermometer, a low-cost temperature sensor able to provide a non-contact measurement of Tsk. In order to get temperature measurements of the forehead, cheekbones, nose, and ear region, sensors must be placed close to the skin facial surface, at few centimeters from it. Many studies have solved this problem installing thermal sensors on an eyeglass [54] [60].
Applying infrared thermography is the best alternative to interpret human thermal comfort in indoor environments. This technique allows to predict subject's level of discomfort analyzing human average facial temperature and other physiological signals obtained by thermographic maps [54] [60]. Facial region usually is the target area preferred for the investigation and evaluation of cerebral thermoregulation through temperature measurements, because it has a high density of capillary vessels, and for the facility to monitor it [11] [27]. Moreover, thermal cameras have several advantages:

- the capability to non-intrusively capture infrared signals emitted from the human body,
- compact size, ease of installation, and preservation of occupants' privacy [54].
- a contactless real time automated investigation of temperature skin for each building occupant, [54] [60].

Thus, thermal infrared cameras application has solved the thermal modeling problem in an non-invasive way [60].
Moreover, in order to provide a complete assessment of the state of thermal comfort, they can be used in combination with other conventional sensors that measure room temperature, humidity and air velocity [11].

CHAPTER 4

4.1. AIM

The aim of this study is to exploit the thermal signals acquired by IR thermography for the estimation of the individual's thermal comfort in order to automatize HVAC system functioning to the individual's thermal requirements in a given environment. Indeed, to date, the HVAC system functioning is based only on time invariant factors referred to the ambient, as size, type, construction material, presence of windows, etc., and does not provide a thermal comfort that can be considered satisfactory by the user. Therefore, an automatization of the system based on dynamic factors, proper of subject's needs, expressed by the pattern of the thermal facial signature acquired, would allow to continuously provide a fulfilling thermal comfort.
In addition, providing a model able to adapt HVAC functioning, that respects the real needs of the occupant, plays an important role in building sustainability since it can reduces substantially energy consumption and provides more effective and satisfactory results [1] [60].
In fact, energy consumption is a critical issue that affects the whole world and contributes to climate change, that is a consequence of the combustion of fossil fuels and the carbon dioxide emissions. One half of the total energy consumption is associated with HVAC systems, whose purpose is to provide a thermal comfort in a given environment [56] [1] [60]. This percentage represents a significant amount of energy consumed on a daily basis simply to provide physical thermal comfort, and for which any possible reduction can have a significant impact on the total amount of energy used [60].
Thus, in order to quantify the individual thermal comfort and consequently optimize energy consumption, infrared thermal system is the preferred technology utilized in this field, because TIR provides real-time information about occupants' thermal comfort in non-obtrusive e non-invasive way [56].

4.2. APPLICATION IR THERMOGRAPHY IN VEHICLES

Specifically, this study focuses on the issue of automatization of HVAC systems inside a vehicle studying all thermal variations of the facial thermal signature in response to climatic variations inside a vehicle compartment. Thus, the aim is to provide a model capable to predict the driver's thermal comfort sensations relying on the thermal facial signature.
Air conditioning plays an important role also in the automotive sector. The automatic control and adaptation of the operation of HVAC systems to provide thermal comfort inside vehicles is a critical issue that is gaining much interest due to the increased time spent by people inside vehicles and due to the rising of mobility. Moreover, automated HVAC systems adaptation according to the real necessities of the user, allows to keep the cabin climate at a healthy and comfortable temperature with the result of a reduction in energy consumption. Reduction in energy consumption is important, not only to avoid waste energy consumption, but also to avoid impairment of battery power efficiency of most modern electric vehicles. Thus, local climatization that focuses on the individual needs rather than on the entire cabin enclosure parameters, offers a great potential for energy reduction and for an increase of driving range efficiency [11]. In addition, a thermally comfortable vehicular environment reduces driver's fatigue and stress resulting in a better driving experience and consequently, also the safety of all the occupants is improved [3] [59] [61] [62] [63].

CHAPTER 5

5.1. MATERIAL AND METHOD

In this section all the experimental procedures applied for data acquisition were accurately described, as well as all the hardware and software utilized in the experiment. Moreover, a complete description of the dataset, and of all the analysis and methods with which the data have been analyzed, was provided.

5.1.1. EXPERIMENTAL SETUP FOR DATA ACQUISITION

Experiments have been performed inside a vehicle, Volkswagen Tiguan, equipped with thermal and visual cameras, temperature and humidity sensors, a touch display for the recording of driver's thermal status assessment and two blackbodies at 37°C and 42°C, located next to the headrest of driver's seat.
Both the cameras are located in front of the driver's seat above the steering wheel in order to continuously capture the front side of face. FLIR A615 with a FOV 45° is the IR thermo camera used, it has a precision of ± 2°C and a resolution of 640 × 480 pixel [64]. Visible camera is RealSense D415, characterized by a FOV of 64°, and a resolution of 1920 x 1080 pixels [65]. Ambient temperature and humidity have been monitored with two Xiaomi sensors [66], mounted on the air vents.
During the entire duration of the experiment the HVAC system has been kept power on, ensuring to maintain closed the air vents and directed on the driver's face. All the car windows were kept closed, while the external ambient weather conditions were variable, according to the day of acquisition.
The process of the entire experiment has been described in Figure 12. The initial phase of the experiment consists of a period of subject's acclimatization inside the vehicle for about 5 minutes, during which the HVAC system, kept on, has reached the set temperature of 23 °C. Then, it was set to the lowest possible temperature deliver, at 16°C, to simulate the cold stress, or to the highest temperature possible to deliver, at 30 °C, to simulate the hot stress, and keeping the temperature at that level for about 15 minutes, the time required to lower or rise the temperature by a considerable difference in degrees.
Subsequently, the air conditioner system has been reset to 23 °C and kept at that temperature for about 5 minutes. After this re-acclimatation the system has been set on the reverse stress situation compared to the previous one applied, thus, on highest or lowest temperature for about other 15 minutes. The last phase consists of a phase of about 5 minutes in which the system has been set on 25 °C.

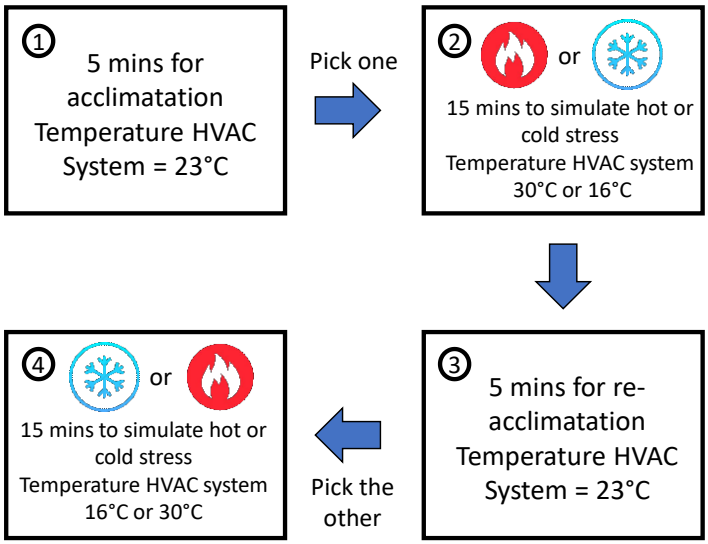

Figure 12. Experiment description.

For the entire duration of the test, approximately every 50 seconds, or whenever the subject perceived a change in his thermal state, the subject was asked to express his state about thermal comfort in terms of a vote according to the ASHRAE scale.

5.1.2. DATA

For data collection and experiment execution three healthy adult participants have been recruited. Before the start of the experimental trials, the participants were adequately informed about the protocol of the study, and they signed an informed consent form outlining the methods and the purposes of the experimentation. For each subject, several recordings are performed, obtaining a dataset of 7 different sessions, from which one session has been excluded. Thus, the final dataset utilized for this study includes six recordings performed on three different subjects, specifically, two recordings for each participant.
Data acquisition for each experiment session has been performed with a different sample frequency. Specifically, a sampling frequency of 5Hz has been used for the first experiment session, a sampling frequency of 2 Hz for the second experiment session, and a sampling frequency of 6 Hz for the other sessions. Each experiment session has been characterized by a different time duration; however, the overall mean time duration is about 58 minutes.
Facial temperature measurements were monitored during the overall experiments and were extracted by using an IR thermal camera FLIR A615. Specifically, the dataset includes thermal data about two facial regions, nose tip and forehead region, considered interesting and relevant signals because thermal signals relative to these two ROIs, generally are not covered or disrupted by obtrusive objects, reflecting the cutaneous thermal behavior of the body in response to the variation of the temperature inside the vehicle, during both hot and cold extreme stress conditions.
At the same time, signals in which are reported subject's thermal sensation have been analyzed.
Both signals have been analyzed and processed in Matlab R2019b, in order to extract relevant features.

From data of 68 landmarks were extracted the intensity values relative to the two ROIs, used in this study, at each frame. Moreover, vectors data relative to the time of the experiment, to the temperature, to the humidity inside the car, and a vector in which were recorded the subject's thermal sensation during the overall duration of the experiment, complete the dataset.

This study has been subdivided into three sections: the first one consists of the exploration and the analysis of the data and the study and exploration of the state of the art regarding thermal acquisition into a vehicle. Then, the other two phases consist of the analysis of the data, and the investigation of the issue, in order to create a predictive model, and it was performed following two different approaches: the system control theory and the linear regression model.

Data pre-processing was common for all the phases and it has been included the removal of NaN values from thermal signature, the removal of correspondent time instant, the answers' removal relative to the part of the thermal signal in which it lacks information, the reconstruction of the answers' vector given by the subject during the experiment, and its resampling. Pre-processing is fundamental in order to obtain clear and manageable vectors for the further data analysis completed in the three sections.

5.1.3. THERMAL DATA ANALYSIS AND PROCESSING PHASE

After data acquisition by mean of IR thermo cameras, an image processing has been applied in order to extract relevant thermal ROI signature, fundamental to obtain relevant psychophysiological information [36]. The image processing includes four steps, as depicted in Figure 13:

1. Face detection
2. Facial landmark localization
3. ROI localization and tracking
4. Thermal ROI signature extraction

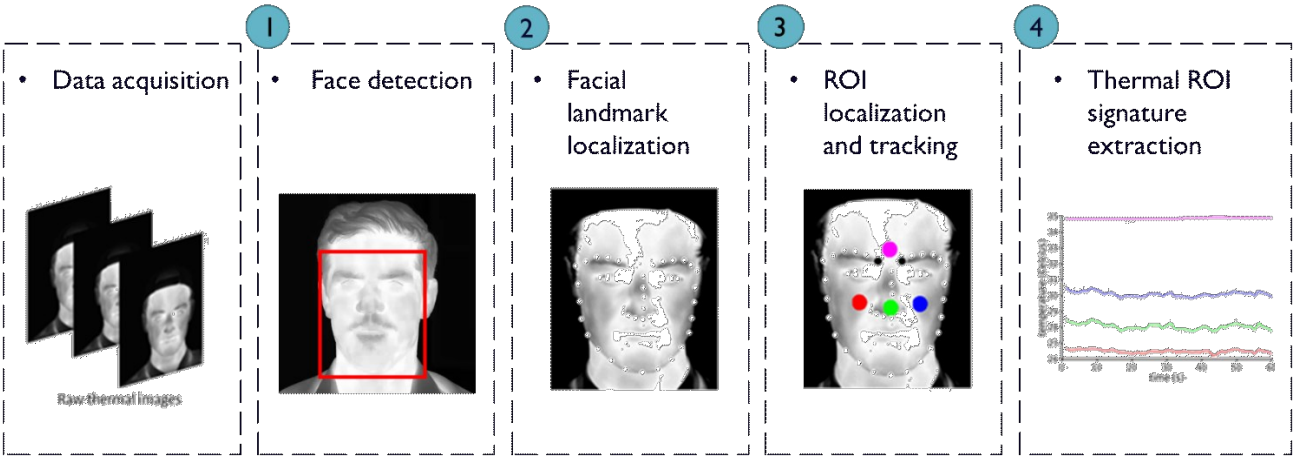

Figure 13. Thermal image processing.

Face detection in thermal images results more challenging with respect to apply it in the visible domain. Indeed, thermal images are characterized by low contrast, low details, blurred geometry, less spatial resolution, that can bring to lack textural information. For these reasons, the more spread and sophisticated face detection methods of the visible domain, that exploit color information, as well as geometry information, lack their potentiality if applied in the thermal domain [35] [37] [38].
Among the methods that perform face detection in thermal images there are:

- Thermal and visible domain co-registration: it exploits features of both visual and thermal images, integrates, and interpolates them yielding to better algorithm's performance. An optical calibration between the RGB and thermal cameras is required, in order to obtain at the same time information meaningful for both systems, through a proper mapping and a specific geometrical transformation from the visible imaging coordinate system to the thermal one. The process of correlation and focus alignment between the two processing systems is performed through a special checkerboard, by localizing the corners of a black and white squares [6] [39] [52] [67].
- Otsu's thresholding: exploits brightness, intensity of pixels, temperature distribution and some symmetric facial patterns to detect face and separate it from background. Indeed, facial region are characterized by a temperature distribution, and so also by a greater pixel intensity, with respect to the background [35] [37] [39] [68] [69] [70] [71] [72] .
- Data driven approach: it uses some machine-learning based algorithms that have already been successfully applied to face detection in the visible spectrum adapted for thermal images. Examples of these algorithms are HAAR CASCADE FEATURE face detector Viola-Jones algorithm (VJ), local binary pattern (LBP – VJ), histogram of oriented gradient trained with a support vector machine (HOG – SVM), scale invariant feature transform (SIFT-SVM). Automated classification using machine learning approach requires extensive amounts of manually annotated training data, for this reason several annotated thermal image databases are provided. Among them, that differentiate for the number of images, number of subject involved, types of images (thermal or both thermal and visible), image resolution, number of head pose, and number of images annotated, the database created by Kopaczka et all [39] is the preferred. It includes 90 subjects, 2500 fully annotated thermal images, high resolution (1024x768 pixels) images, wide range of head poses, manually placed and validated

landmarks for 68 facial points, high variation of expression and emotion, and the images are acquired with a neutral backdrop [37] [39] [46] [71] [72] [73] .

The output of face detection step is a bounding box that encircles the face region.
Then, the landmarks localization occurs, which consists of the identification in each video frame of X and Y coordinates of 68 landmarks that define facial key points, Figure 14. These algorithms provide an accurate and fast landmark localization exploiting feature based active appearance model or Deep alignment network. The algorithm's performance can be affected by occlusion (due to the presence of glasses, scarf, etc.) and orientation of head pose, (rotated face over a certain degree), and as consequence the algorithm is not able to assign a correct landmark position because of lack of the capability of face detection or for the missing data. To solve this issue a manual correction is performed.

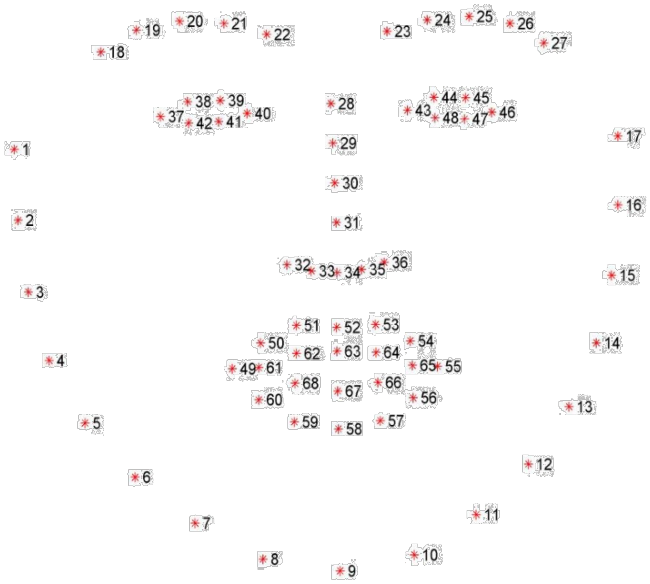

Figure 14. 68 facial landmark model.

Once the 68 landmarks have been detected, ROI can be easily defined, through simple algorithms that exploit landmarks' locations and their spatial relation as reference. In this way, ROI's coordinate are determined automatically [6] [35] [44] [74]. Typical facial ROIs investigated are nostril, nose tip, forehead, periorbital, maxillary, cheek, and chin regions. There are several methods to define different ROIs, through the use of landmarks coordinates, as depicted in Figure 15. For example, as described in Table 3, as suggested in the study of D. Cardone et al, [6], nostril regions can be identified by a circle whose center's coordinate are represented by landmark 33 and 35, respectively for right and left nostril, and with a diameter of 7 pixels. Glabella region instead is defined by a triangle whose vertices are represented by coordinate X, Y of landmarks 22, 23, 28.

Table 3. Geometrical features of some ROIs.

Region of Interest (ROI)	ROI Shape	ROI Position Relative to 68 Facial Landmark
ROI 1—Nose tip	Circle	$C = \left[\frac{x_{n-1}+x_{n+1}}{2}, \frac{y_{n-1}+y_{n+1}}{2}\right]$, d = 7 pixel [1]
ROI 2—Right nostril	Circle	$C = [x_{33}, y_{33}]$, d = 7 pixel [1]
ROI 3—Left nostril	Circle	$C = [x_{35}, y_{35}]$, d = 7 pixel [1]
ROI 4—Glabella	Polygon	Polyline ([P22, P23, P28]) [2]

[1] C = circle center; d = circle diameter; [2] Pn = n-th landmark; $n = 1, \ldots, 68$.

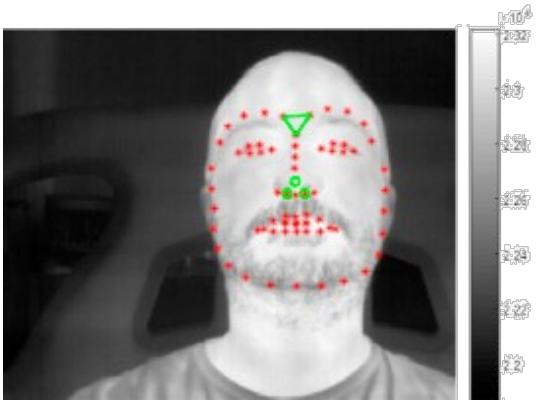

Figure 15. Example of glabella nose tip, and nostrils regions identified by landmarks coordinate.

Finally, temperature profiles have been extracted from each ROI. Temperature profiles refer to the mean of the pixels' intensity inside the ROI analyzed.

5.2. EXPLORATIVE PHASE

This first phase has the aim to get familiar with the data and to try to find a possible relationship between the variations of thermal nose tip data with the relative subject thermal comfort sensations expressed with a score among -3 to + 3 referred to ASHRAE scale reported in the vector in which are recorded the subject's thermal sensations.

In this explorative phase, the data analysis has been performed only for one experiment, the 4th one.

The performed pre-processing of nose tip thermal data consists of:

- Mean removal.
- Strong filtration through a third order low pass Butterworth filter with a cut-off frequency of 0.001Hz, and the function *filtfilt*.
- Derivative computation.
- Scaling of nose tip data and its derivative to ASHRAE scale, in which the filtered data have been divided for their norm and then multiplied by a factor 300.
- Quantization of the scaled signal in order to obtain a signal characterized only by values correspondent to the possible thermal sensations expressed in ASHRAE scale, -3, -2, -1, 0, 1, 2, 3. Specifically, quantization has been performed considering the amplitude range in which each sampled data falls. For example, as described in Table 4, if the amplitude of a sample of the scaled signals is included in the range [0.5 1.5], the sample value will be replaced with the integer sensation equal to 1.

Table 4. Quantization rules.

Signal limit	Sensation
> 2.5	3
[1.5 2.5]	2
[0.5 1.5]	1
[-0.5 0.5]	0
[-1.5 -0.5]	-1
[-2.5 -1.5]	-2
< 2.5	-3

Then, 10 tests to find the relation between scaled nose tip thermal data and subject's thermal sensations have been implemented. Specifically, for each test have been computed some signal transformations and then, the level of reliability of the prediction of the thermal sensation from the transformed signal has been evaluated considering for each recorded sensation provided by the subject the nearest in time sample of the transformed signal, and between them computing the correlation coefficient R, p-value, percentage of error (considering the number of wrong predicted sensation over the total number of predicted sensation) and the maximum error, i.e. how far is, in absolute value, the predicted sensation from the recorded one.

1. Prediction of sensations through quantized nose tip signal.

2. Prediction of sensations through quantized derivative of nose tip signal.

3. Prediction of sensations through quantized derivative of nose tip signal with a correction factor -2.

4. Prediction of sensations considering windows of quantized derivative of nose tip signal of length of 323 sample, corresponding to 51.73 s, the mean difference in time between two successive recorded events. In these windows have been analyzed the amplitude of the range and the slope of the curve. Sensations have been predicted making some considerations on range and slope of the curve. If the range in the analyzed window is greater in absolute value than a threshold 0.1, the quantization previously described is applied; while if the absolute value of the range in the analyzed window is <

0.1, the slope of the window is also considered. If the slope is positive, has been applied the previous quantization rules, modified by subtracting to each computed value -1. On the contrary, if the slope is negative, to the quantization has been added a factor +1. This test has been applied on both the derivative of the signal, as well as to the derivative with a correction factor -2.

5. Prediction of sensations through the mean value of quantized derivative in each window. Signal was divided into windows of 51.73 s, mean difference in time between two successive events. Then, in each window have been computed several features, subsequently used, as the mean value in this case.

6. Prediction of sensations through a signal composed by the weighted sum between the quantized nose tip signal and its derivative. The weighted factors were valorized for both as 0.5, but they have a different unit of measurement that allows the sum between the 2 signals, even if this summation would be considered physical incorrect.

7. Prediction of sensations through quantized derivative with a 2-minute delay.

8. Prediction of sensations through quantized derivative with a delay scrolling: each 10 minutes window a delay of 1 minute is applied.

9. Prediction of sensations though quantized derivative with a scrolling progressive delay every 15 minutes.

10. Prediction of sensations considering range of the weighted sum in windows of 3 minutes. Specifically, if between 2 successive 3 minutes windows there is a change in the slope of the weighted sum between nose tip temperature signal and its derivative, the values of the first window are extremized with a factor -1 or +1 according if the change of slope is, respectively, from decreasing to increasing, or the contrary.

Moreover, the same group of tests (from 4 to 10) referred to transformation of the derivative of nose tip signal using the corrected derivative of nose tip signal, the result of the previous test 3, was also computed.

5.3. CONTROL SYSTEM

The aim of this second section is to apply the theory of control systems and verify if it is possible to model our data with a transfer function.
According to the theory of control systems, a system can be defined as a set of several interacting parts whose behavior that connects them is investigated.

A control system is any physical system that establishes a relationship of correspondence, according to a predetermined law, between an input quantity and an output quantity, which constitutes the controlled quantity, even in the presence of disturbances. Moreover, it defines any set of objects which is interconnected to direct or force a system to desired specific values, or to perform a certain task.

Thus, a control system can be defined as a system, which provides the desired response by controlling the output, varying the input. Figure 16 shows the simple block diagram of a control system.

Figure 16. Control system block diagram.

In the specific case, nose tip thermal data represent the input signal, while the recorded events represent the output signal. Thus, we want to investigate if there is any mathematical law that regulates input and output, studying the variations in the input signal corresponding to the variations in the output one.
Before, to compute the transfer function that relates input and output, the system has been assumed to be a linear time invariant system (LTI).
Then, the transfer function (FdT), is defined as the ratio between the Laplace transform (TdL) of the output and the Laplace transform of the input signal, Figure 17.

Figure 17. Transfer function F(s) defined in Laplace domain.

TdL converts a function in the time domain into a correspondent function in the domain of the complex variable s, where $s = \sigma + j\,\omega$. Setting the real part σ of the complex variable *s* on zero, Fourier transform will be obtained, in function of $j\,\omega$. Thus, the Fourier transform is essentially the representation of f(t) in the frequency domain.
For this reason, to obtain the transfer function has been applied *fft* Matlab function, which computes the Fourier transform of the data given in input.

The aim is to discover if the transfer function that relates thermal data and thermal subject sensations is the same for all the experiments, in order to be able to assume that the transfer function found, if applied with new data, can be able to predict the thermal sensations.
For this reason, all the data referred to the 6 experiments, have been standardized and resampled into a common frequency, 6 Hz, in order to achieve significative results that can be compared to each other.
The data standardization or normalization has been computed in order to obtain signals with a property proper of a normal distribution with a null mean and a standard deviation equal to 1. Normalized vector Z has been computed as described in formula (11) for each element of the vector x to normalize:

$$Z = \frac{x_i - \mu}{\sigma} \tag{11}$$

Where x_i refers to element *i* of vector x, μ refers to the mean of vector x, and σ to the standard deviation of x.

Once all the data have been resampled and standardized, the mean value has been removed, and then, the Fourier transform has been computed for all the experiment sessions.

Then, to obtain the FdT, its mathematical definition, formula (12), has been applied for each experiment:

$$FdT = \frac{fft(output)}{fft(input)} \tag{12}$$

The result of the application of formula (12) is the transfer function of each experiment expressed in the frequency domain, composed by a real and an imaginary part. To visualize the real part, has been computed *abs (FdT),* and then it is plotted with respect to the relative frequency vector.
While, to visualize the imaginary part, that reflects the phase of the TdF, *angle (FdT)* has been applied, and plotted with respect the frequency vector.

5.4. LINEAR REGRESSION MODEL

The aim of this phase is to model the derivative of nose tip signal and the recorded sensations with a linear regression model. The inspiration to base the model on the derivative of the nose tip signals comes from the good correlation found between the derivative and events recorded.
Indeed, the time correspondence, between the time instants during which the answers are released and the time in which nose tip signal are recorded, has been found through an implemented function *correspondence.* The events have been resampled with segments characterized by the same number of samples found in the correspondent nose tip signal between two successive events. The same events resampling has been performed with a spline function.
The results obtained after events resampling are two vectors, nose tip and events, with the same length and number of samples and all the answers, about thermal sensations, relative to the part of nose tip signal characterized by NaN values, have been excluded. Then, both nose tip signal and resampled events have been filtered with a low pass filter with a cut off frequency of 0.001 Hz, and the derivative is computed, for all the experiments. Then, a shift among nose tip derivative and the event vectors has been applied to reach the maximum correlation. After the computation of the correlation between the derivative and the resampled events (both with spline and segments), these vectors result in a very strong correlation.
Thus, to perform the linear regression model, all the derivative as well as all the resampled events relative to all the experiments have been resampled to a common sample frequency (6 Hz) and concatenated in a unique vector, obtaining 2 new vectors, *derivative* and *events*.
Consequently, linear regression model has been implemented through the function *fitlm*, that applies the theory of the last square solutions into the matrix form. In this way, a regression line was computed attempting to model the known relationship between the two variables, derivative of nose tip signal and thermal comfort sensations, shifted, by fitting a linear equation to the observed and measured independent data. Specifically, the linear regression line was expressed, as shown in formula (13), in the form:

$$y = a_0 + a_1 \cdot x \tag{13}$$

Where y represents the dependent variable, a vector which includes all the thermal comfort sensations, that corresponds to what we want to predict implementing this model, and x represents the independent variable, the measured variable, i.e., a vector which includes all the derivative of nose tip signals after the shift in correspondence of the maximum correlation with the recorded events. Then, a_0 and a_1 represent respectively the intercept or bias (the value of y when x = 0) and the slope of the line, symbolized by the angular coefficient. a_0 and a_1 are the coefficients that have been estimated, so that the error is minimized. Expressing the regression line in matrix form formula (14) and its compression form formula (15), it has been obtained:

$$\begin{bmatrix} 1 & x_1 \\ 1 & x_2 \\ \vdots & \vdots \\ 1 & x_n \end{bmatrix} * \begin{bmatrix} a_0 \\ a_1 \end{bmatrix} = \begin{bmatrix} y_1 \\ y_2 \\ \vdots \\ y_n \end{bmatrix} \tag{14}$$

$$\mathbf{X * \phi = Y} \tag{15}$$

Then, the least square solution, that is the value estimation of the coefficients a_0 and a_1, included into the matrix ϕ, can be expresses as:

$$\boldsymbol{\phi = (X^T X)^{-1} X^T Y} \tag{16}$$

This method computes the best-fitting line for the observed data by minimizing the sum of the squares of the vertical deviations from each data point to the line (if a point lies on the fitted line exactly, then its vertical deviation is 0). In addition, since the deviations are first squared, then summed, there are no cancellations between positive and negative values.

The same procedure was also applied to thermal data relative to glabella region, and a linear regression model in which the independent values are represented by glabella thermal data was computed.
Then, a model based on both the derivative of nose tip and glabella data has been implemented, in which the independent values are x_1 and x_2, and the parameters to estimate become three, a_0, a_1, and a_2.

$$y = a_0 + a_1 \cdot x_1 + a_2 \cdot x_2 \quad (17)$$

Finally, residue analysis was computed for each implemented model to confirm the correctness of creating a linear model and to verify whether this model is reliable with a good predictive value and it was not modeled on any outliers that could have compromised its functionality.

5.4.1. ANALYSIS OF RESIDUALS

Through the analysis of residuals, the presence of any outliers was checked.
Moreover, examination of the residuals' behavior allows to investigate the validity of the linear assumption and investigate the existence of the linear relationship between the data.
The residuals represent the differences between the values observed in the dataset and the estimated values computed with the regression equation. In other words, the residuals indicate the variability of the data around the regression line.
Specifically, several conditions on residuals have been checked through some graphs and indexes:

- Normal distribution
- Non-correlation input independent variable with the error.
- Non-correlation output dependent variable with the error
- Linear distribution
- Absence of outliers that influences the regression line through indexes:
    - Leakage point, a measure of how much a given value of the independent variable deviates from its mean. It is an index included between 0 and 1.
    - Studentized residuals, a standardization in which leverage values are also considered. Values greater in absolute value than 3 are considered elevated.
    - Cook's distance, commonly used estimate of the influence of a data point when performing a least-squares regression analysis. Values greater than 1 are considered elevated.
- Absence of autocorrelation among residuals, through the Durbin -Watson coefficient. This index is included between 0 and 4. Values nearest to 2 indicate the absence of autocorrelation.

CHAPTER 6

6.1. RESULTS

For each studied phase are reported the result obtained, including the steps involved in the preprocessing phase. For this reason, also the result section is organized into three different subsections: results relative to the explorative phase, relative to the control theory, and to the regression line.

PREPROCESSING

The steps that have characterized the initial preprocessing are reported in the following images to describe how have been obtained the clean signals for the further analysis starting from the raw signals. Specifically, Figure 18 shows the starting raw nose tip signals and the relative recorded answers during the total duration of all the experiments. From this image, it is notable the different time duration that has characterized each experiment, the considerable absence of part of signals, due to the lowest contrast at highest temperature and the different frequency with which the answers have been released. The mean time duration of the experiments is 58 minutes, and the experiment 1 results the longest one with a duration of 75 minutes, while the shortest one is the experiment 5 with a duration of 44 minutes. Experiments 2, 5, 6, and 7 are characterized by an elevated number of NaN values, in which the system was unable to capture the signal. Experiment 4, instead, is characterized by a low number of NaN values, (133), that has allowed a complete investigation of the signal for the entire duration of the experiment.

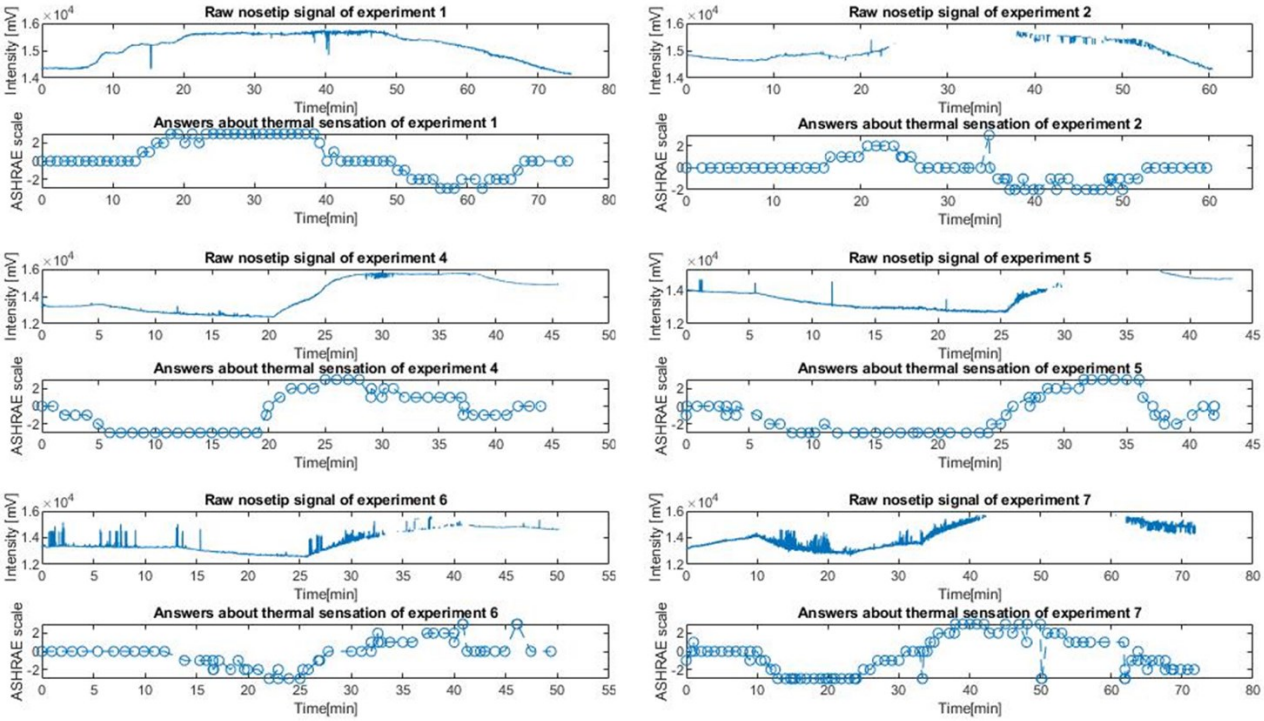

Figure 18. Raw nose tip signal and relative recorded answers of all experiments.

The successive steps consist of resampling of answers vector, with a progressive procedure that controls portion of the signal between 2 consecutive events at time. Then, after having been found the correspondent portion of the answers signal into the nose tip signal, the interested portion of events has been resampled with a line with the same number of samples that characterize the portion of the nose tip signal. In this way, have been obtained, two vectors with the same number of samples, equal length, and the answers relative to the portion of the nose tip signal in which are present NaN values have been excluded.

In the following Figure 19 have been depicted the nose tip signals and the relative answers resampled with this technique, relative to all the experiments.

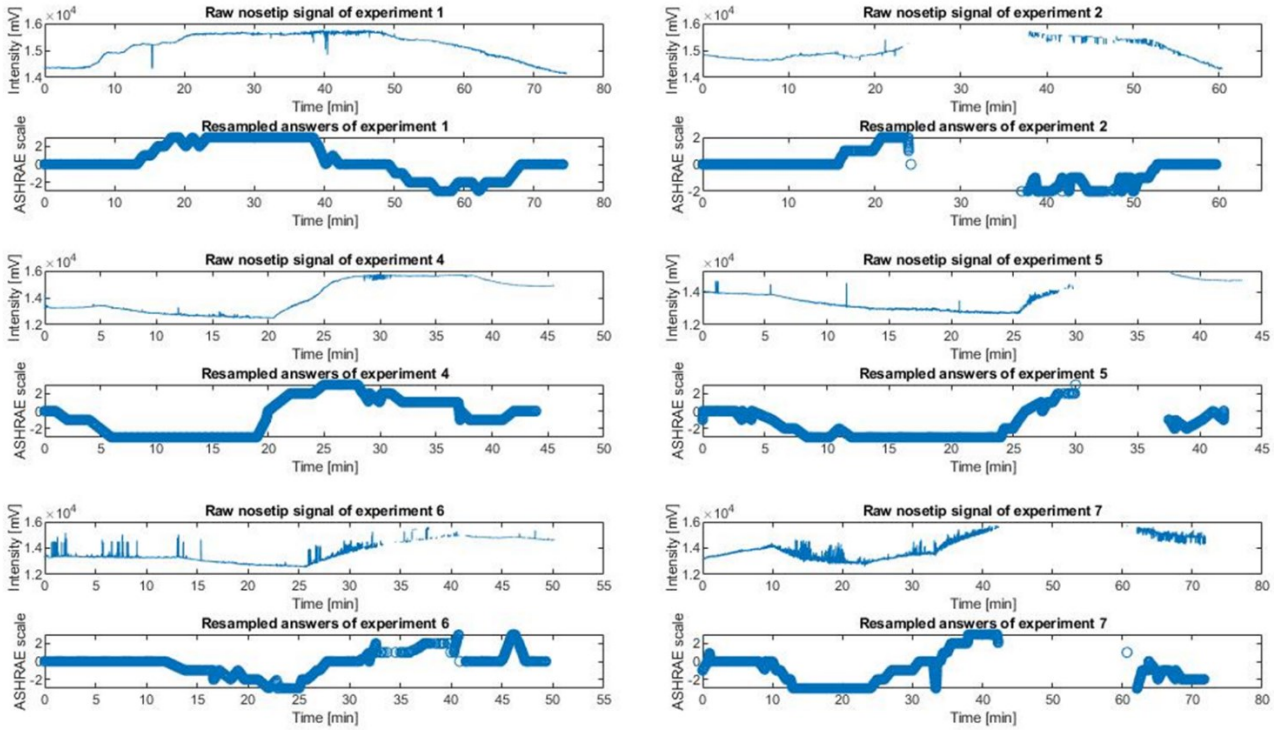

Figure 19. Raw nose tip signals and resampled answers relative to all the experiments.

Then, all the areas without signal have been removed from both signals, nose tip and answers, as well as from the relative time vectors, obtaining shorter signals in time duration, but with a significant content acquired with a constant sampling frequency, as shown in the following Figure 20. Thus, the effective time duration of the experiment is reduced, and its mean value corresponds to 47 minutes.

However, it is important to note that the parts of the signals insignificant, because characterized by NaN values, were removed in order to obtain cleared and homogeneous signals and for the ease of further analysis. Nevertheless, in this way, each information regarding the time of the physiological mechanisms has been corrupted. Thus, for the inaccuracy of these thermal data, it has not been possible to make considerations about the timing in which the physiological mechanisms were occurred.

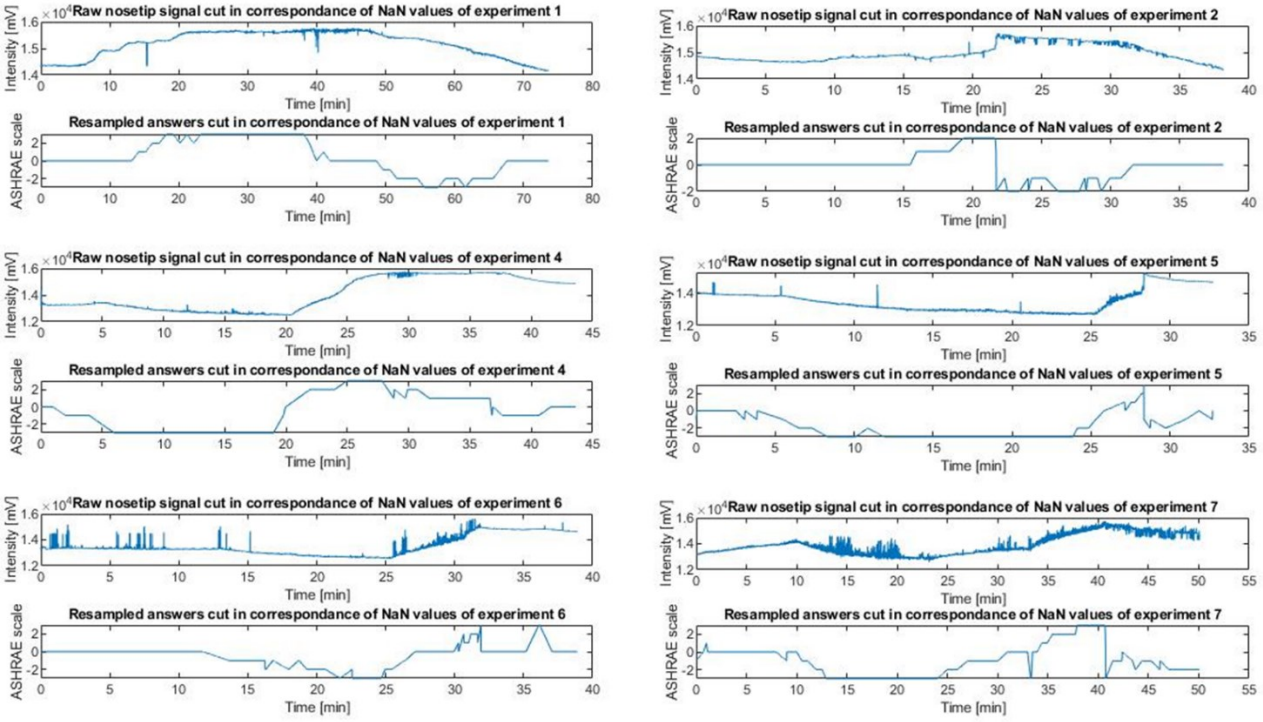

Figure 20. Nose tip and answers signals of all the experiments cut in correspondence of NaN values.

In the Table 5 are summarized all the features, previously showed, regarding all the experiments. Specifically, the sampling frequency, the initial total length of the experiment, the initial total length of the recorded answers, the number of NaN found in each nose tip vector and the total length of the vectors from which has been removed the insignificant part characterized by NaN values.

Table 5. Summary of all technical features that characterize the experiments.

Exp	Fs [Hz]	Time events [min]	Time nose tip data [min]	N° of NaN	Time nose tip data without NaN values [min]
1	5.12	74.14	74.60	172	74.04
2	2.12	59.70	60.35	2762	38.64
4	6.21	43.97	45.52	133	45.16
5	6.26	41.94	43.51	3516	34.17
6	6.23	49.36	50.11	3926	39.63
7	6.26	71.70	71.93	8155	50.22

Finally, in Figure 21 are depicted all the signals of nose tip and the relative answers of all the experiments after the filtration with a low pass filter Butterworth of the 3rd order with a cut off frequency of 0.001 Hz.

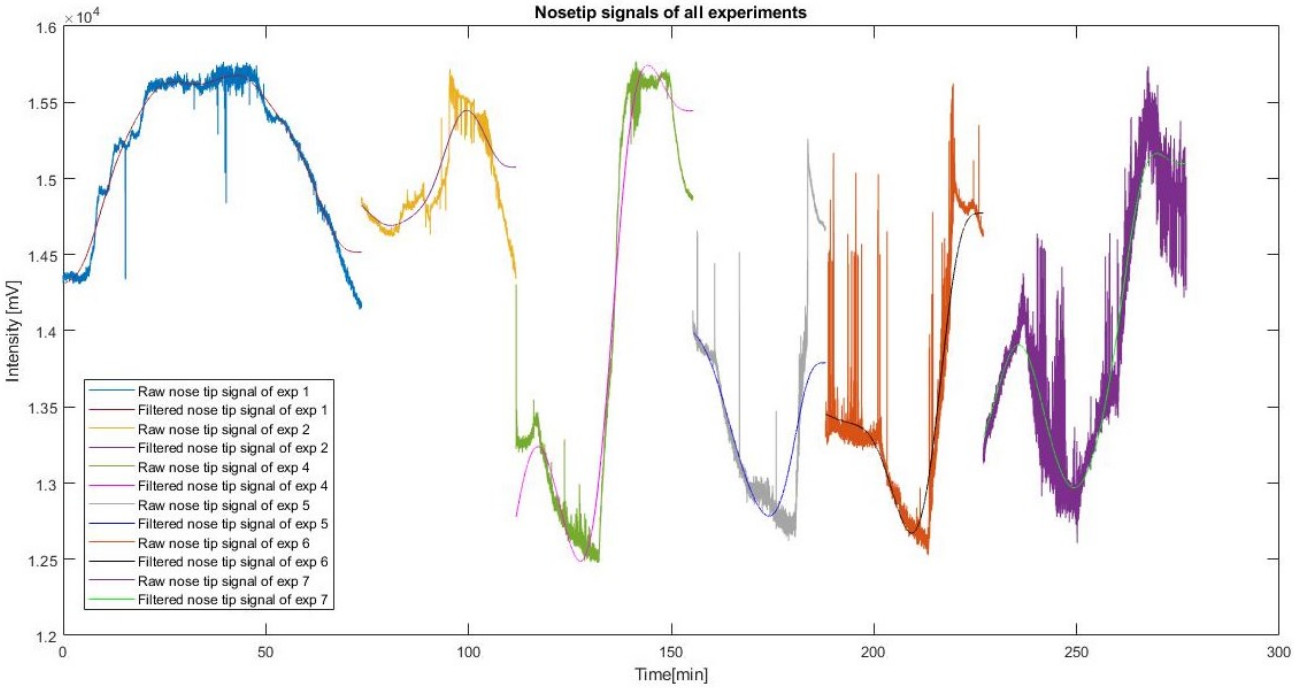

Figure 21. Raw nose tip signal and filtered nose tip signals of all experiments.

In Figure 22, both nose tip signal and its filtration were compared with the reconstructed answers about thermal sensation and the filtered answers.

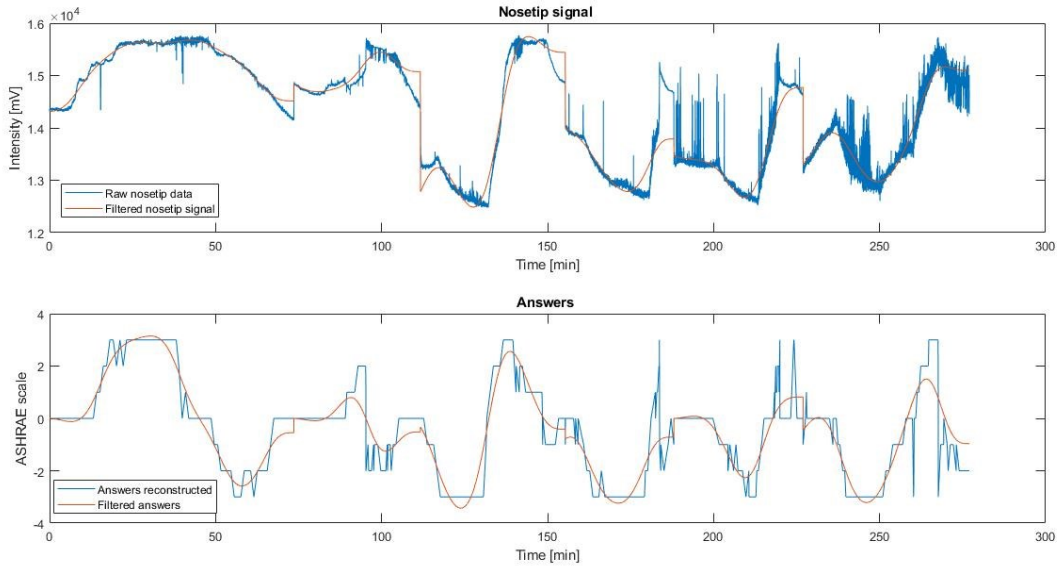

Figure 22. Nose tip signals and relative answers both filtered, referred to all the experiments concatenated into a single vector.

6.1.1. EXPLORATIVE PHASE

In this section the results relative to all the ten tests performed in the first explorative phase on the data relative to experiment 4, are reported. The level of performance of each test was evaluated through four indexes, the correlation coefficient, R and the relative p-value, the percentage of error and the maximum error detected.

6.1.1.1. TEST 1

The first test, that relies the prediction of thermal sensations on the quantized nose tip signal, has provided a good and significative correlation among the recorded answers and the predicted ones, (R = 0,67), a high percentage of error (84,31%) and the maximum error value of 4. Figure 23 shows the predicted answers relative to the thermal comfort sensations compared to those recorded.

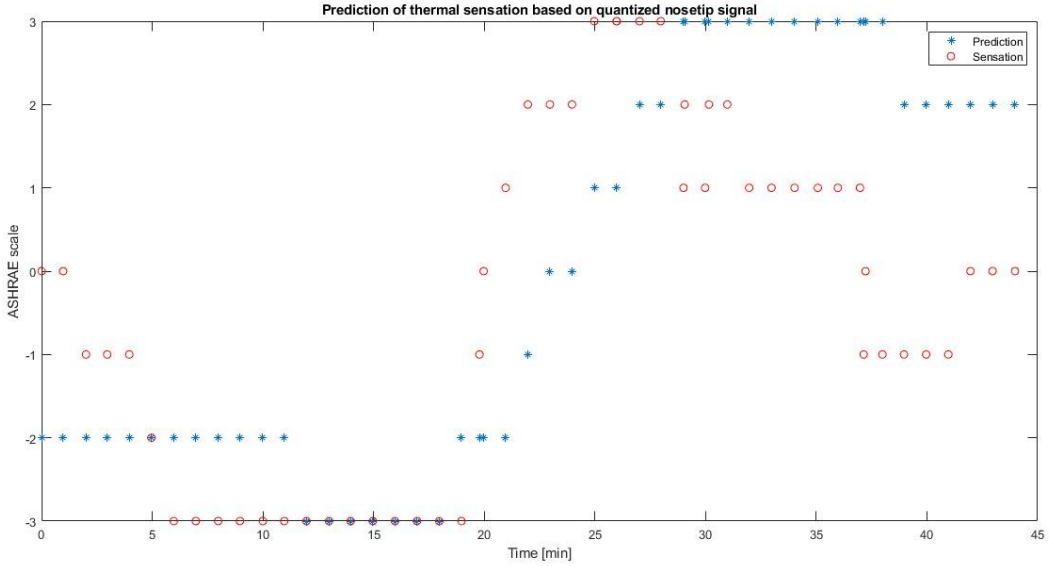

Figure 23. Prediction of thermal sensations of test 1.

6.1.1.2. TEST 2

The second test, represented in Figure 24, which relies its prediction on the derivative of nose tip signal, has provided a normal and significative level of correlation (R=0,57), a percentage of error of 74,50% and a maximum error value recorded of 6.

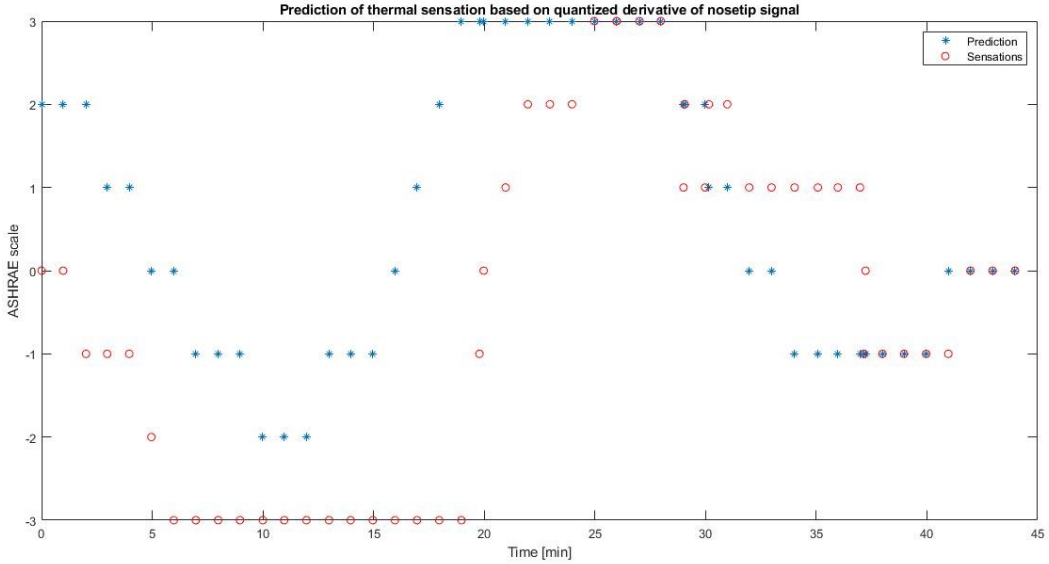

Figure 24. Prediction of thermal sensations of test 2.

6.1.1.3. TEST 3

The third test, which relies thermal sensations' prediction on a corrective quantized derivative, has provided, as shown in the following Figure 25, a good and significative correlation, a percentage of error of 66,66% and a maximum error value of 4.

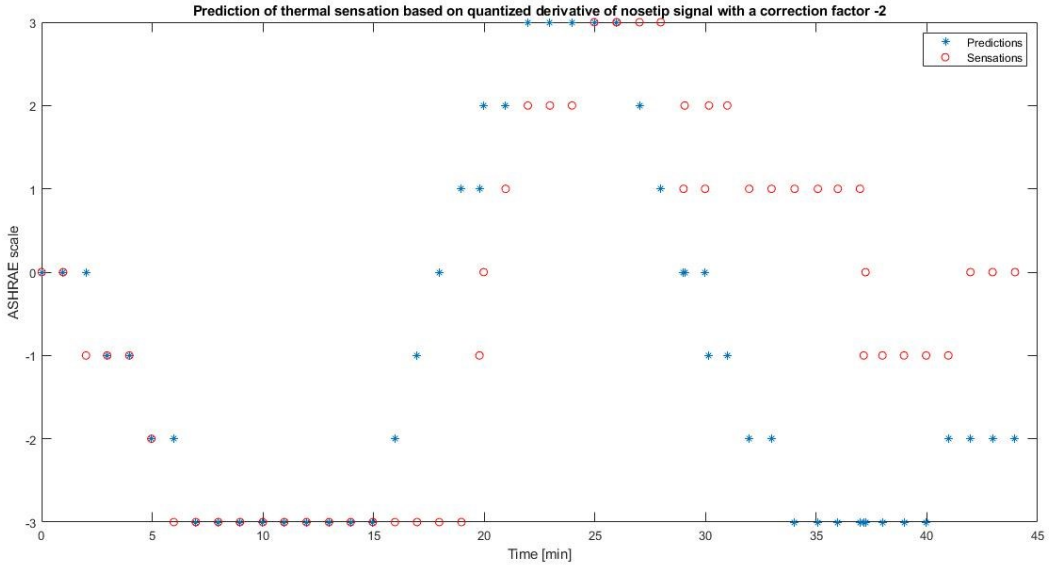

Figure 25. Prediction of thermal sensations of test 3.

6.1.1.4. TEST 4

The fourth test, represented in Figure 26, based on range and slope assumptions over the derivative of nose tip signal, has provided a very good and significative correlation (R = 0,74), a percentage of error of 70,58% and a maximum error value of 3.

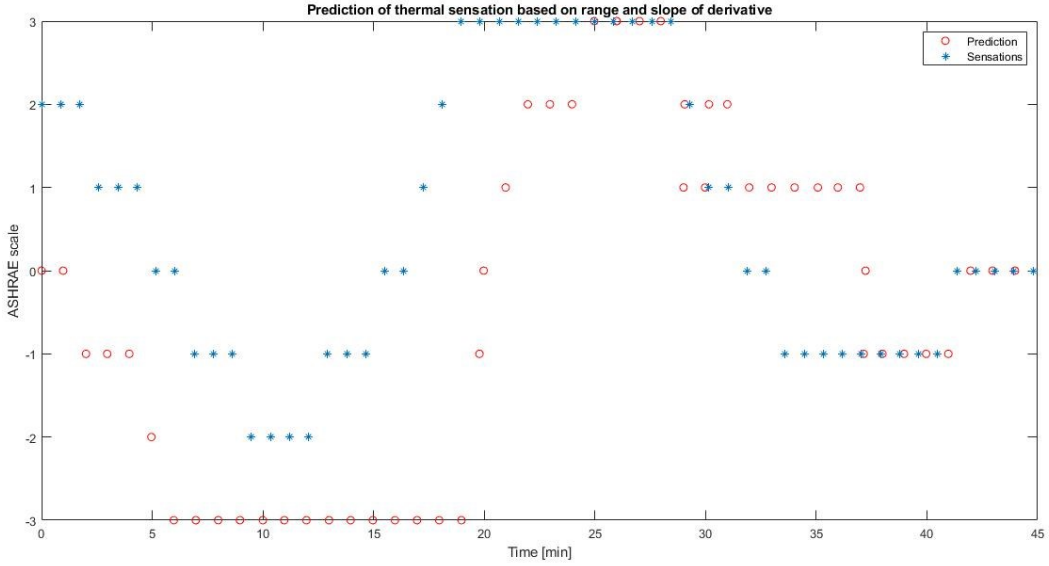

Figure 26. Prediction of thermal sensation of test 4 based on the derivative of the nose tip signal.

The same test, depicted in Figure 27, was performed also on the corrective derivative of nose tip signal (with a correction factor -2), and has provided a similar result for what concern the correlation coefficient (R=0,75). Percentage of error of 50,98% and the max error value is 4.

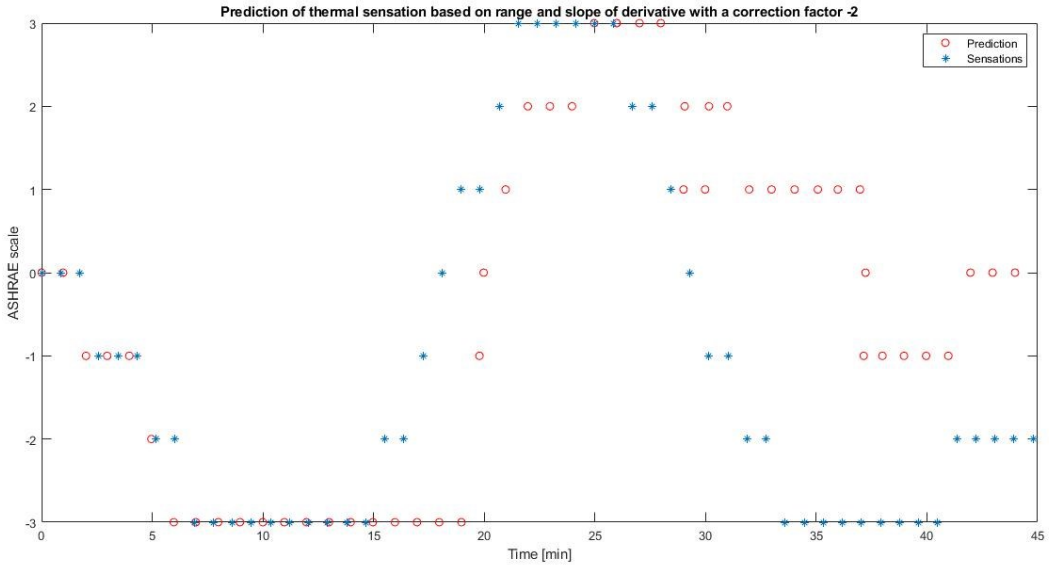

Figure 27. Prediction of thermal sensation of test 4 based on the corrective derivative of the nose tip signal.

6.1.1.5. TEST 5

The fifth test, based on the mean value of windows of the derivative of nose tip signal, has provided a good and significative correlation (R = 0,73), a percentage of error of 72,54% and a maximum error value of 4. Its prediction performance is shown in Figure 28.

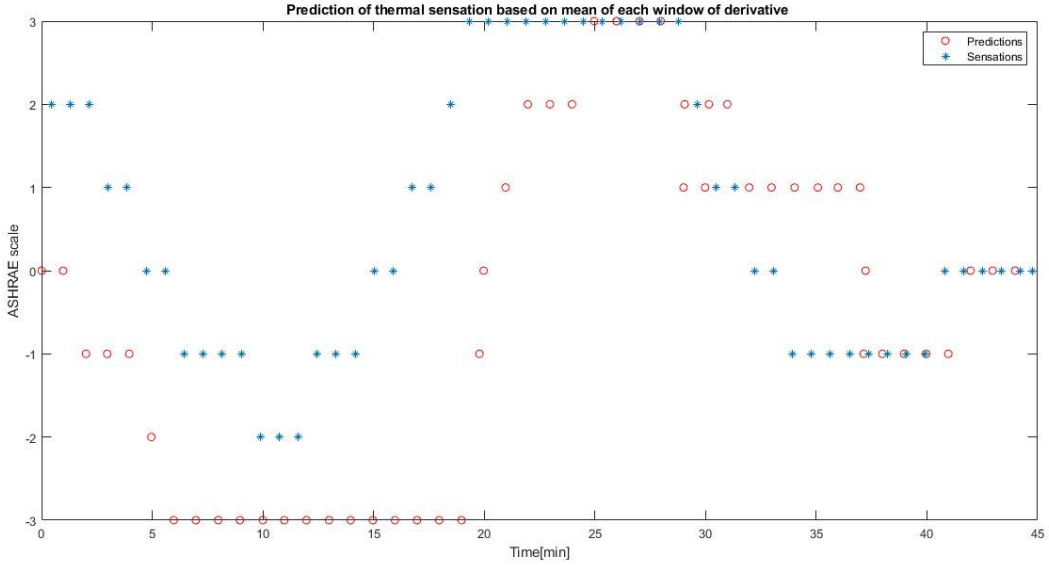

Figure 28. Prediction of thermal sensations of test 5 based on the derivative of the nose tip signal.

The same test was performed also on the corrective derivative of nose tip signal, depicted in Figure 29, and has provided a good and significative correlation coefficient (R=0,75), a percentage of error of 49,01% and the max error value is 4.

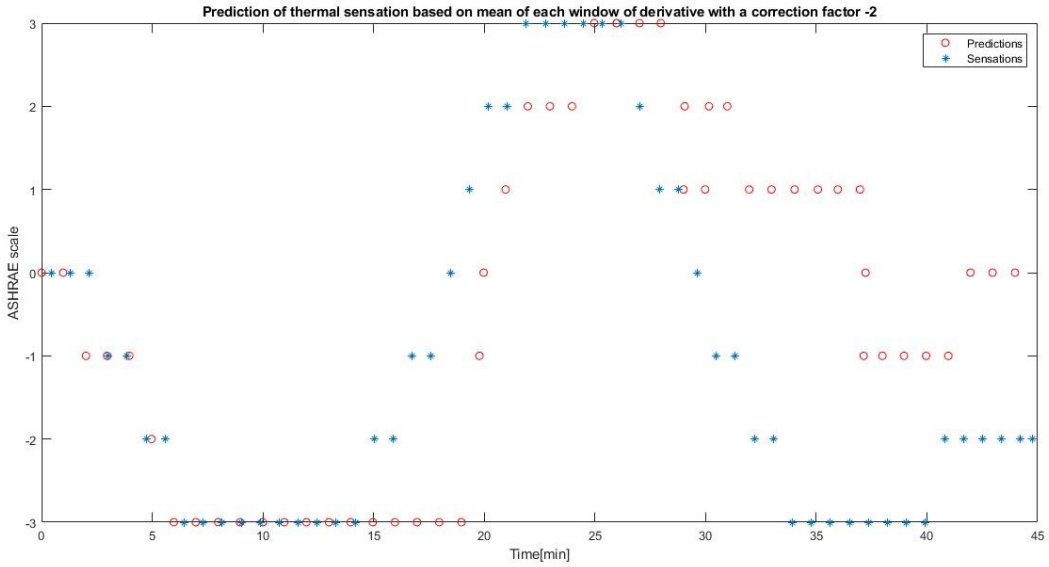

Figure 29. Prediction of thermal sensations of test 5 based on corrective derivative of the nose tip signal.

6.1.1.6. TEST 6

The sixth test, depicted in Figure 30, which relies its prediction on both the nose tip signal and its derivative, has provided a very high and significative correlation coefficient, (R = 0,93), a percentage of error of 64,70% and a maximum error value of 2.

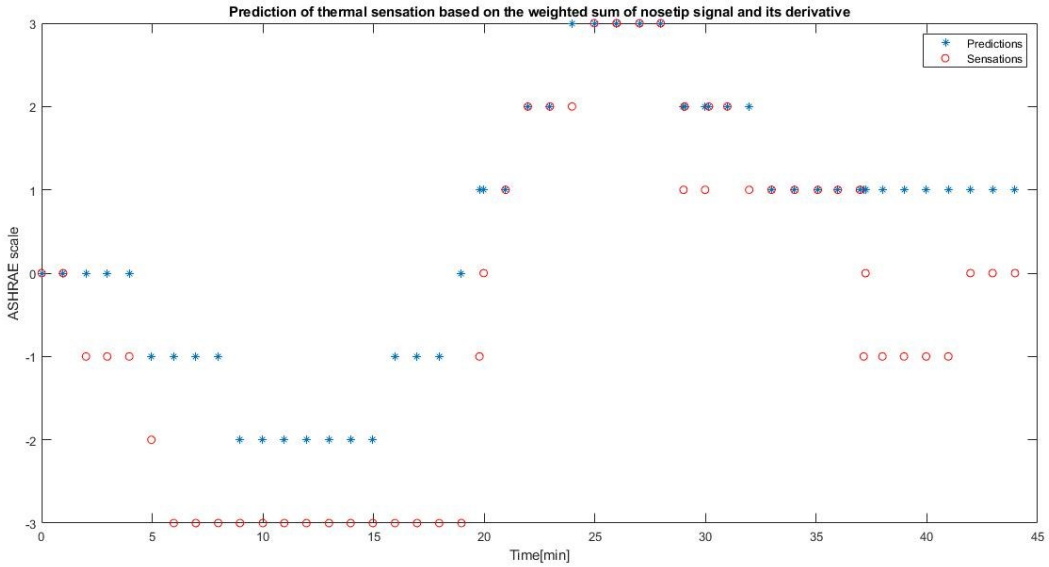

Figure 30. Prediction of thermal sensations of test 6 based on derivative of nose tip signal.

The same test was performed also considering the corrective derivative of nose tip signal and has provided a similar optimum correlation coefficient (R=0,93), a percentage of error of 60,78% and the max error value is 2. In the following Figure 31, its performance is depicted.

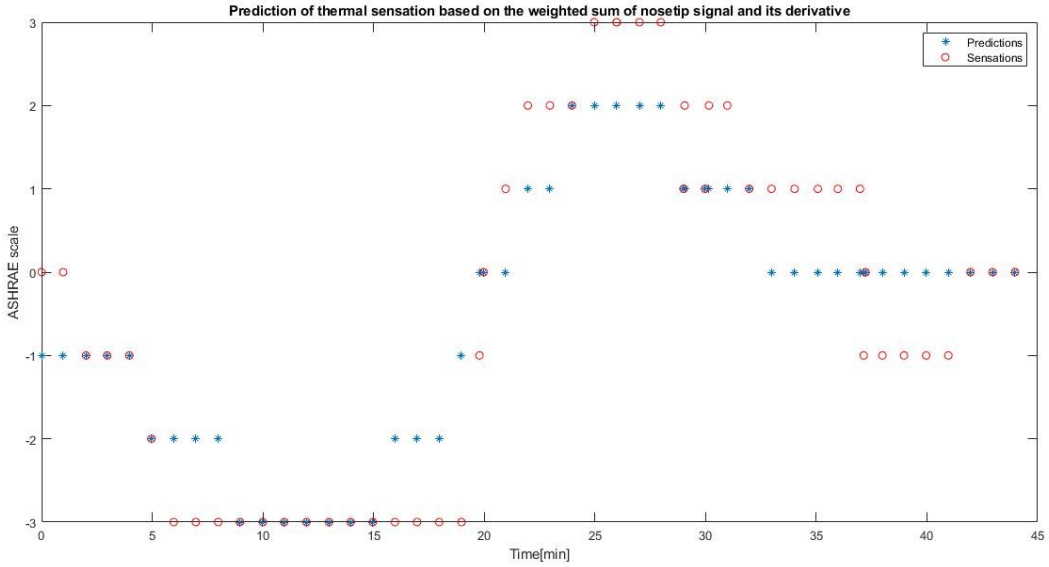

Figure 31. Prediction of thermal sensations of test 6 based on the corrective derivative of nose tip signal.

6.1.1.7. TEST 7

The seventh test, based on the delay of nose tip signal, whose performance is depicted in Figure 32, has provided a normal and significative correlation (R = 0,57), and a percentage of error of 74,50% and a maximum error value of 4.

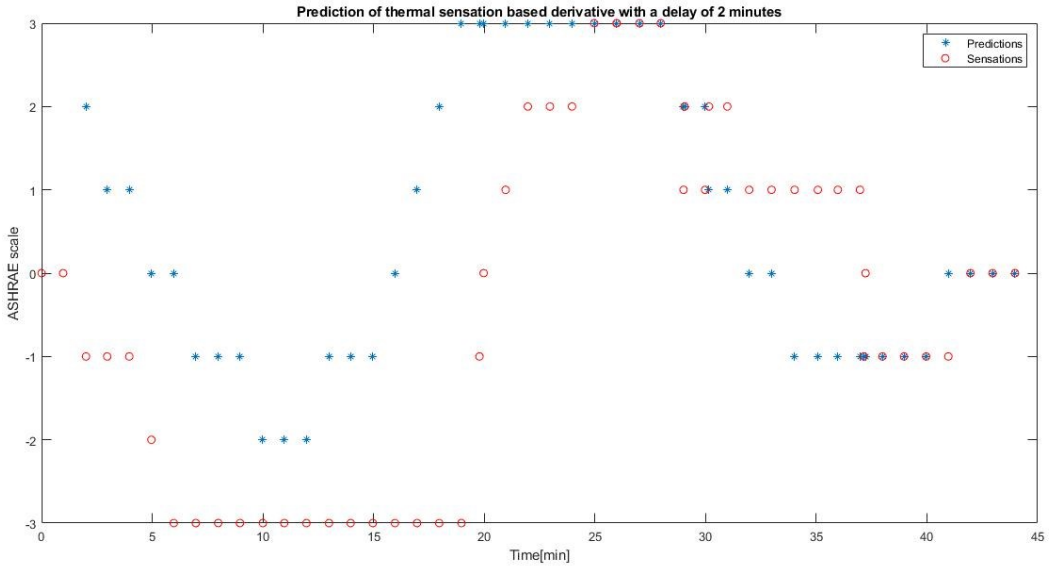

Figure 32. Prediction of thermal sensations of test 7 based on derivative of nose tip signal.

The same test was performed also considering the corrective derivative of nose tip signal, depicted in Figure 33, and has provided a good and significative correlation coefficient (R = 0,60), a percentage of error of 66,67% and the max error value is 4.

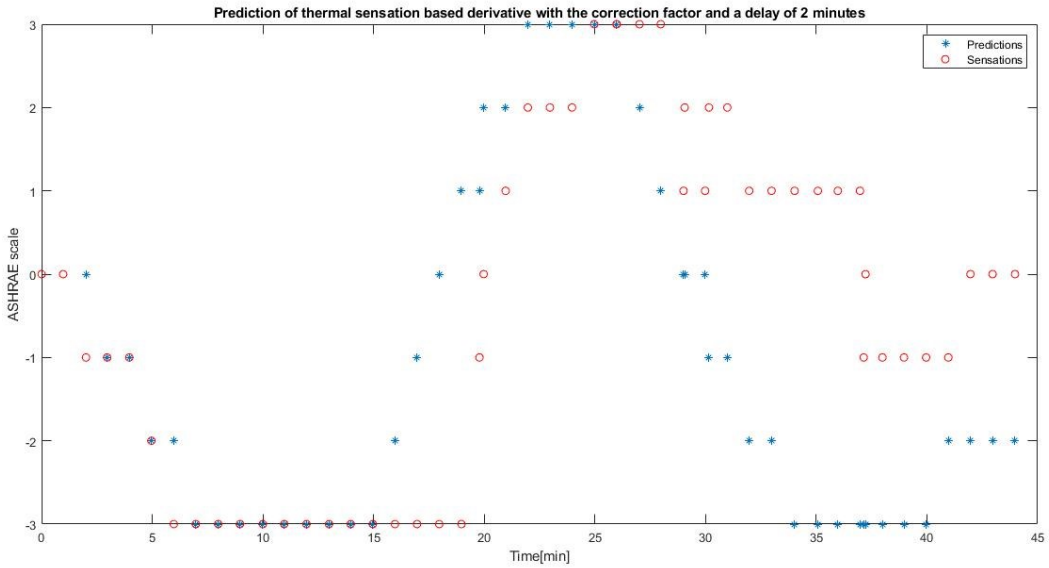

Figure 33. Prediction of thermal sensations of test 7 based on the corrective derivative of nose tip signal.

6.1.1.8. TEST 8

The eighth test, relied on the derivative of the nose tip signal with a scrolling delay, has provided a good and significative index of correlation (R = 0,73), a percentage of error of 78,43 and a maximum error value of 5. Its performance can be showed in the following Figure 34.

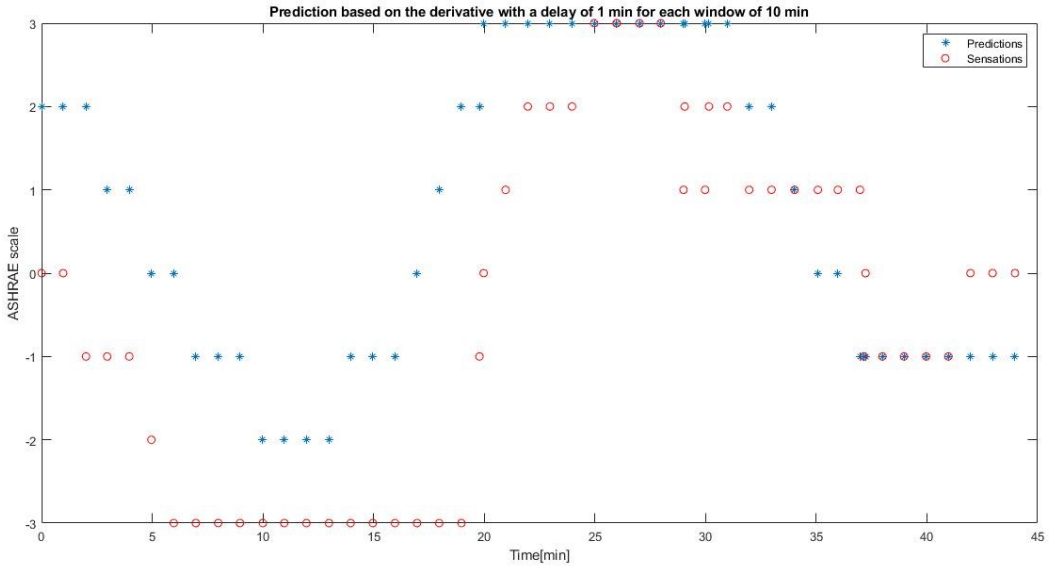

Figure 34. Prediction of thermal sensations of test 8 based on derivative of nose tip signal.

The same test was performed also considering the corrective derivative of nose tip signal, depicted in Figure 35, and has provided a good and significative correlation coefficient (R = 0,77), a percentage of error of 49,01% and the max error value is 4.

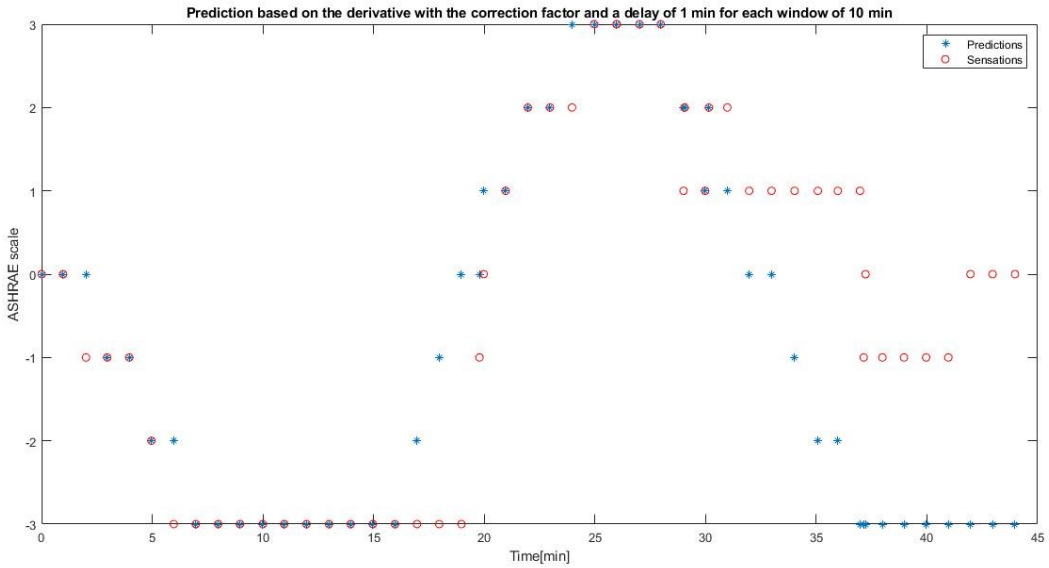

Figure 35. Prediction of thermal sensations of test 8 based on corrective derivative of nose tip signal.

6.1.1.9. TEST 9

The nineth test, based on a delay that increases progressively on the derivative of nose tip signal, has provided a great and significative correlation index, (R = 0,89), a percentage of error of 76,47% and a maximum error value of 2. Its performance can be showed in the following Figure 36.

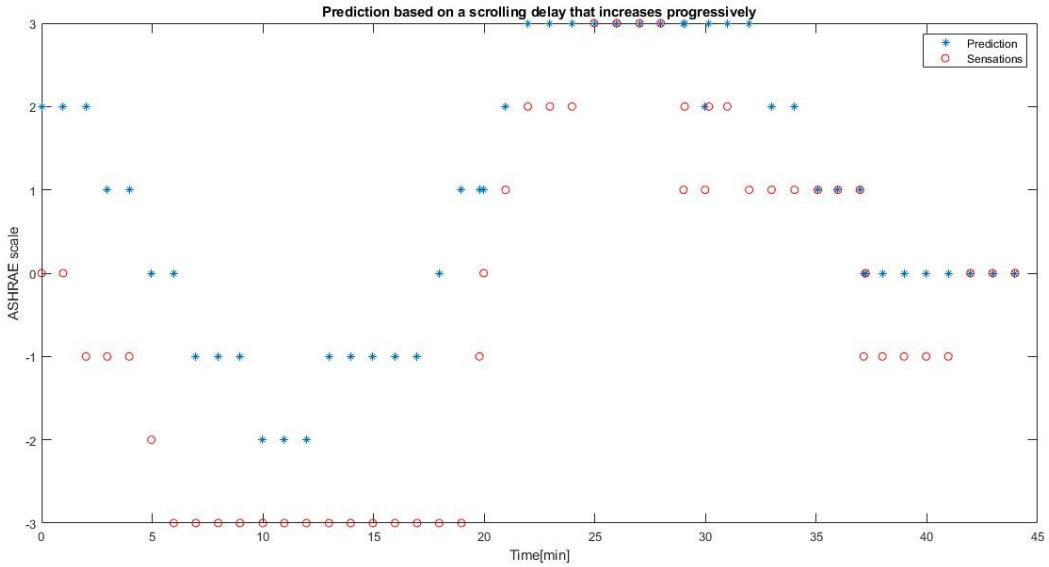

Figure 36. Prediction of thermal sensations of test 9 based on derivative of nose tip signal.

The same test was performed also considering the corrective derivative of nose tip signal, depicted in Figure 37, and has provided a similar great and significative correlation coefficient (R = 0,91), a percentage of error of 49,01% and the max error value is 4.

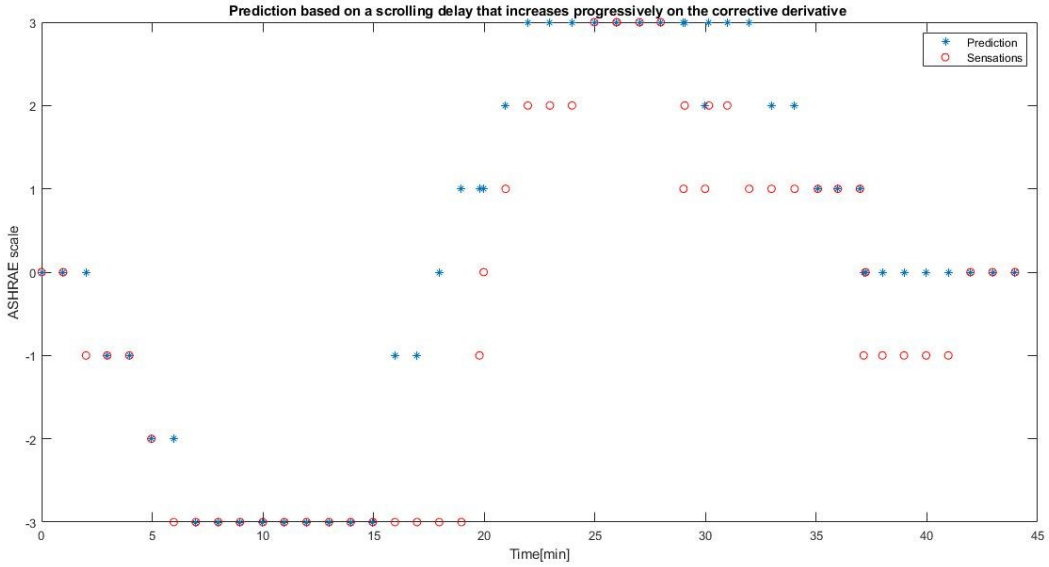

Figure 37. Prediction of thermal sensations of test 6 based on corrective derivative of nose tip signal.

6.1.1.10. TEST 10

The tenth test, based on considerations on the range and slope of consecutive windows of both the nose tip signal and its derivative, has provided, as shown in Figure 38, a very good and significative correlation index (R = 0,93), a percentage of error of 54,90% and a maximum error value of 2.

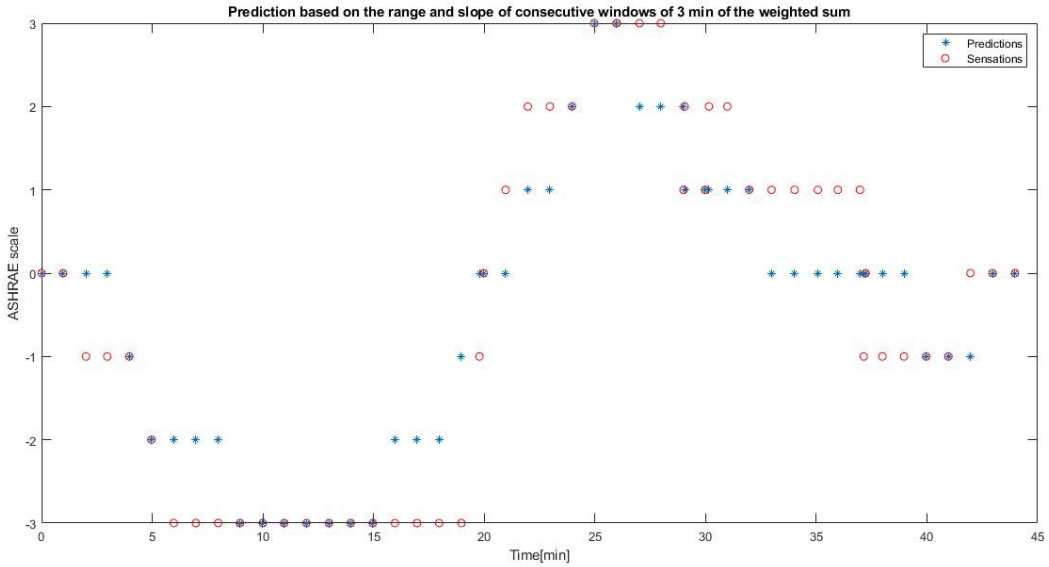

Figure 38. Prediction of thermal sensation of test 10.

In the following Table 6 are summarized all the indexes of the performance of each prediction test on the experiment 4.

Table 6. Performance level of the 10 tests performed on data relative to experiment 4.

		R	p-value	% error	Max error
TEST 1	**Nose tip signal**	0.67	5.85e-08	84.31	4
TEST 2	**Derivative**	0.57	1.13e-05	74.50	6
TEST 3	**Corrective derivative**	0.60	2.56e-06	66.66	4
TEST 4	**Derivative**	0.74	4.21e-10	70.58	3
	Corrective derivative	0.75	1.30e-10	50.98	4
TEST 5	**Derivative**	0.73	8.43e-10	72.54	4
	Corrective derivative	0.75	1.65e-10	49.01	4
TEST 6	**Weighted sum derivative**	0.93	1.37e-23	64.70	2
	Weighted sum corrective derivative	0.93	1.37e-23	60.78	2
TEST 7	**Derivative**	0.57	1.13e-05	74.50	4
	Corrective derivative	0.60	2.56e-06	66.67	4
TEST 8	**Derivative**	0.73	8.11e-10	78.43	5
	Corrective derivative	0.77	2.70e-11	49.01	4
TEST 9	**Derivative**	0.89	1.61e-18	76.47	2
	Corrective derivative	0.91	1.62e-20	49.01	4
TEST 10	**Weighted sum derivative**	0.93	4.31e-23	54.90	2

Specifically, the best performance related to the lowest percentage of error refers to test 5, 8, and 9, both based on the corrective derivative.

6.1.2. SYSTEMS CONTROL THEORY

In this section are reported the results relative to the computation of the transfer function for each experiment, after applying the normalization and resampling of the data into a common sampling frequency, 6 Hz. Specifically, Figure 39 shows a zoom of all the module, that refers to the real part of the FDT, for each experiment in such a way to be compared. While Figure 40 represents all the phases of the FDT for each experiment, that are related to the imaginary part of the function.

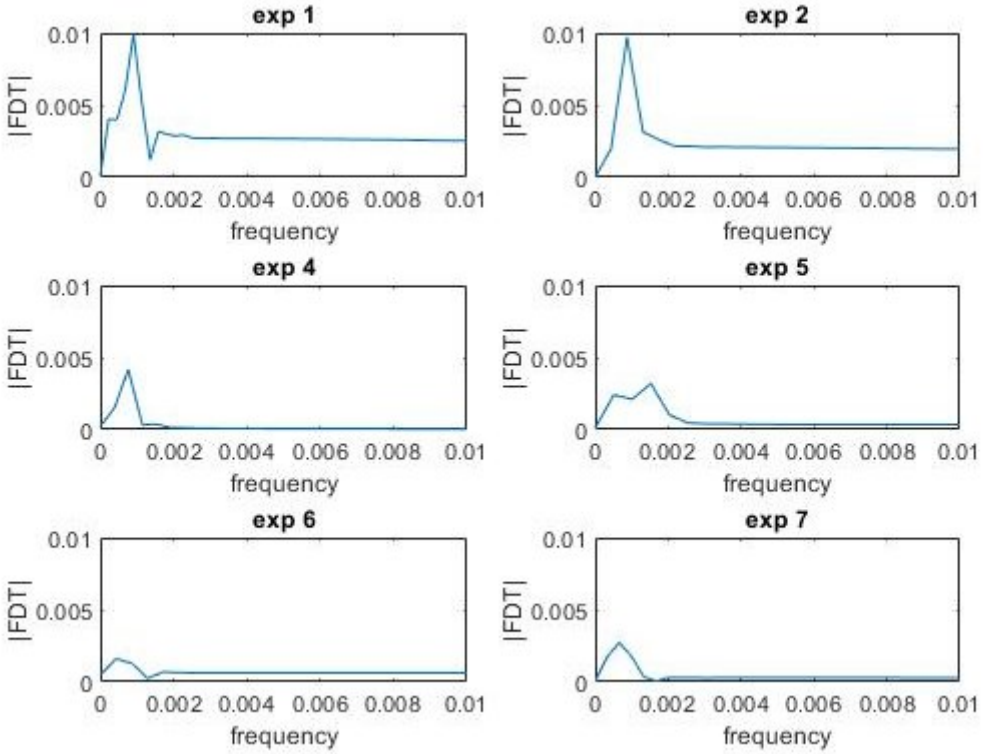

Figure 39. Modules of the FDT relative to all the experiments.

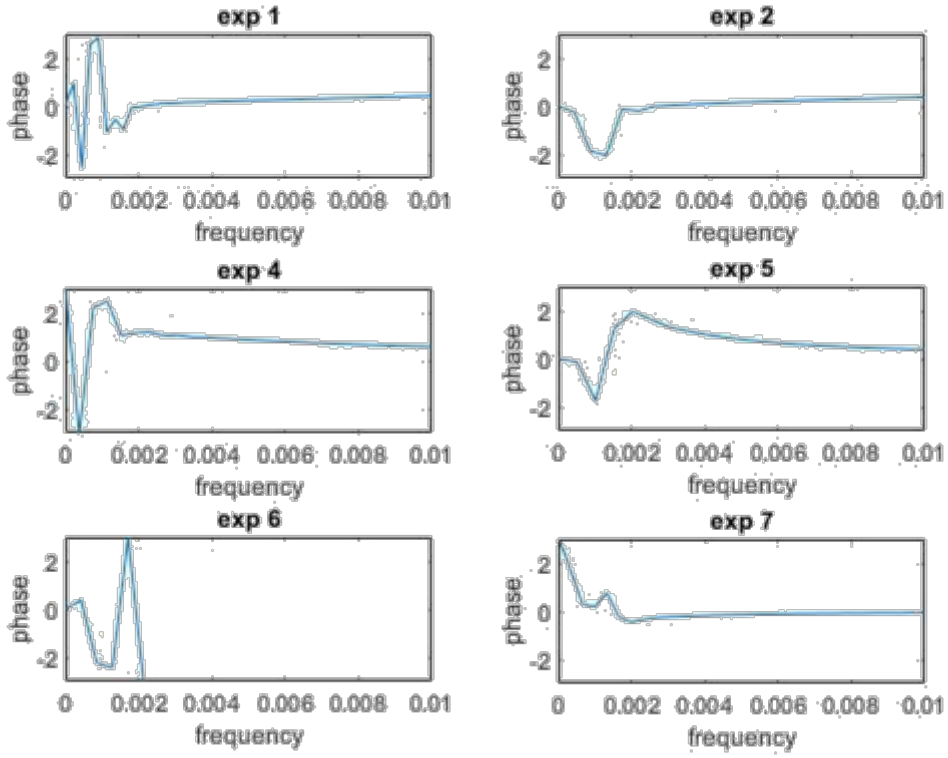

Figure 40. Phases of the FDT relative to all the experiments.

6.1.3. LINEAR REGRESSION MODEL

In this section the results to the linear regression model are reported.

Specifically, the following set of three figures for each experiment show the derivative of the nose tip signal and the relative answers filtered, before and after the shift of the signals around 7 minutes on the right or on the left in order to reach the maximum correlation coefficient, R. The third figure represents the two signals from which have been cut the part in excess after the shift.

Figure 41, Figure 42 and Figure 43 refer to the experiment 1. Correlation among the two signals before the shift results 0,51 and it has been improved and increased to 0,67 after the application of a derivative of nose tip shift on the right of 6,99 minutes.

Figure 44 Figure 45 and Figure 46 refer to the experiment 2. Correlation among the two signals before the shift results 0,66 and it has been improved and increased to 0,94 after the application of the answers shift on the right of 3,22 minutes.

Figure 47, Figure 48 and Figure 49 refer to the experiment 4. Correlation among the two signals before the shift results 0,67 and it has been improved and increased to 0,81 after the application of a derivative of nose tip shift on the right of 3,12 minutes.

Figure 50, Figure 51 and Figure 52 refer to the experiment 5. Correlation among the two signals before the shift results 0,26 and it has been improved and increased to 0,94 after the application of a derivative of nose tip shift on the right of 6,99 minutes.

Figure 53, Figure 54 and Figure 55 refer to the experiment 6. Correlation among the two signals before the shift results 0,10 and it has been improved and increased to 0,87 after the application of a derivative of nose tip shift on the right of 6,99 minutes.

Figure 56, Figure 57 and Figure 58 refer to the experiment 7. Correlation among the two signals before the shift results 0,75 and it has been improved and increased to 0,95 after the application of a derivative of nose tip shift on the right of 2,67 minutes.

Experiment 1

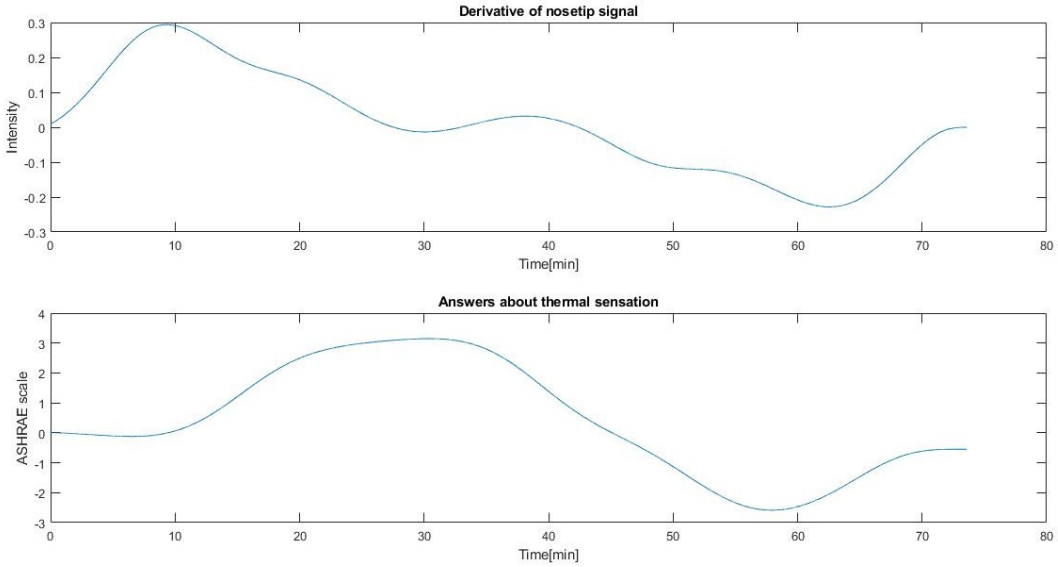

Figure 41. Filtered derivative of nose tip signal and relative answers of experiment 1.

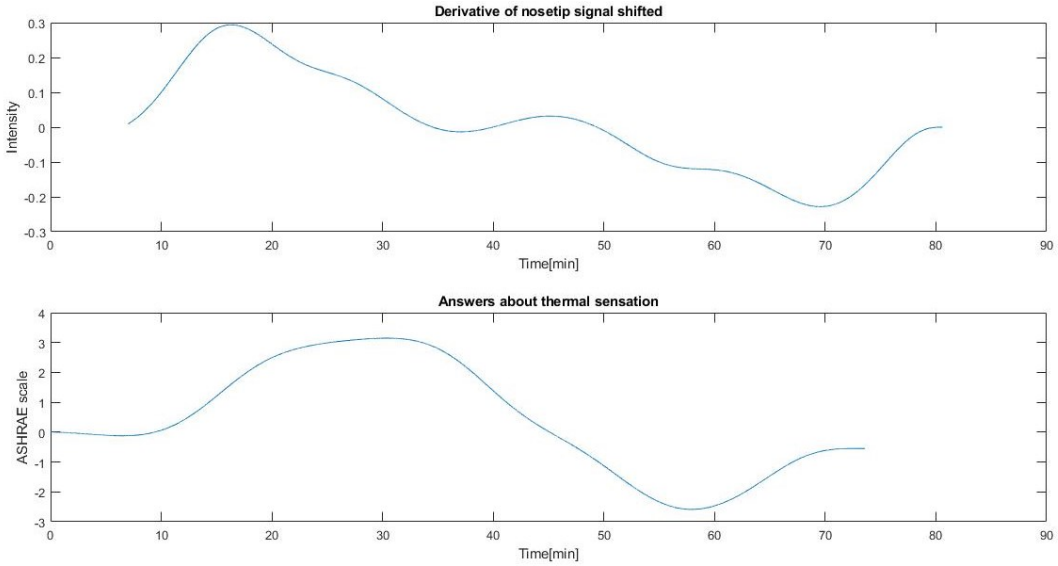

Figure 42. Shifted filtered nose tip signal and relative answers of experiment 1.

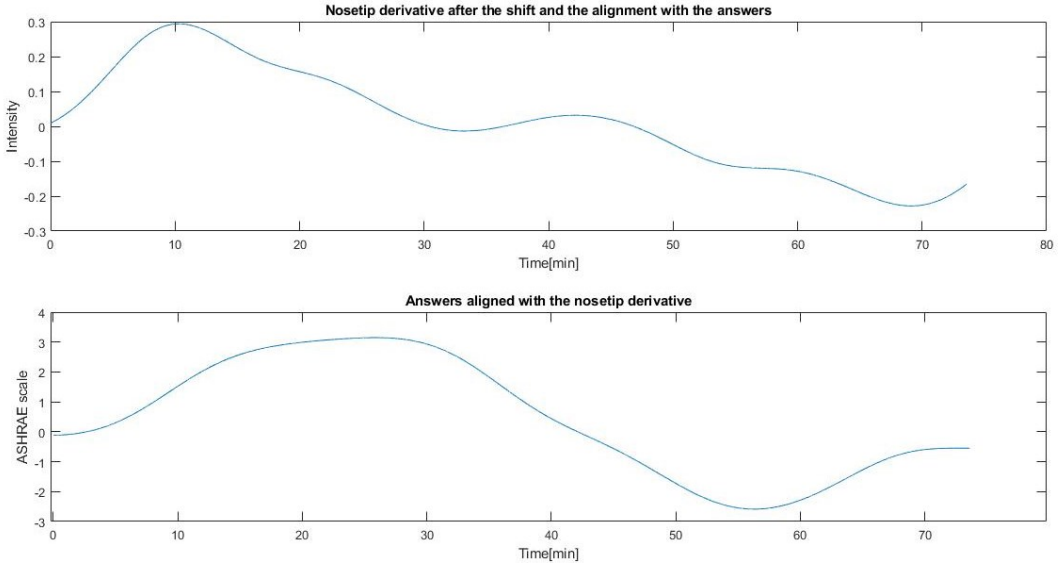

Figure 43. Cut nose tip signal and relative answers after the shift of experiment 1.

Experiment 2

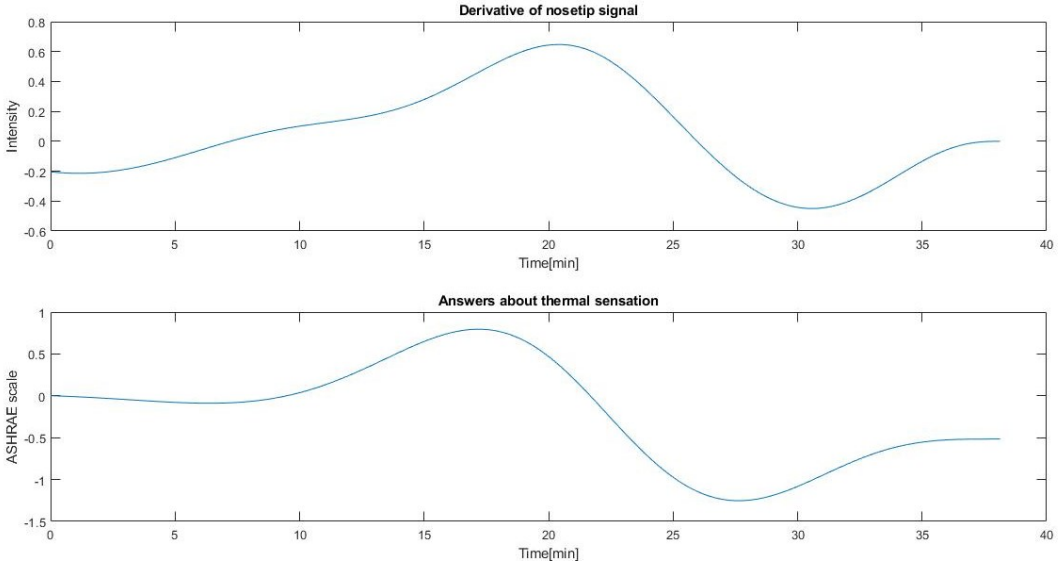

Figure 44. Filtered derivative of nose tip signal and relative answers of experiment 2.

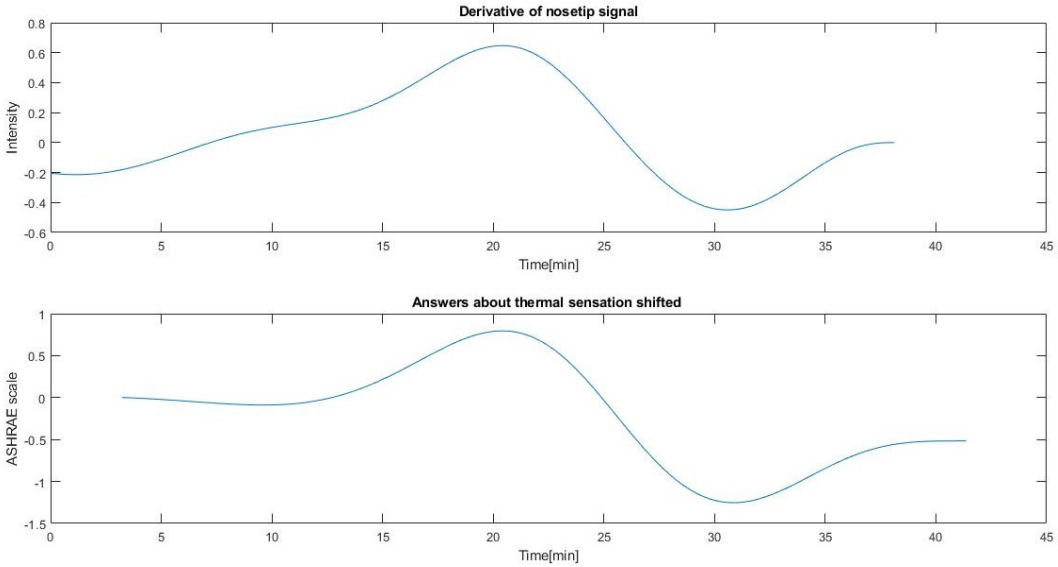

Figure 45. Shifted filtered nose tip signal and relative answers of experiment 2.

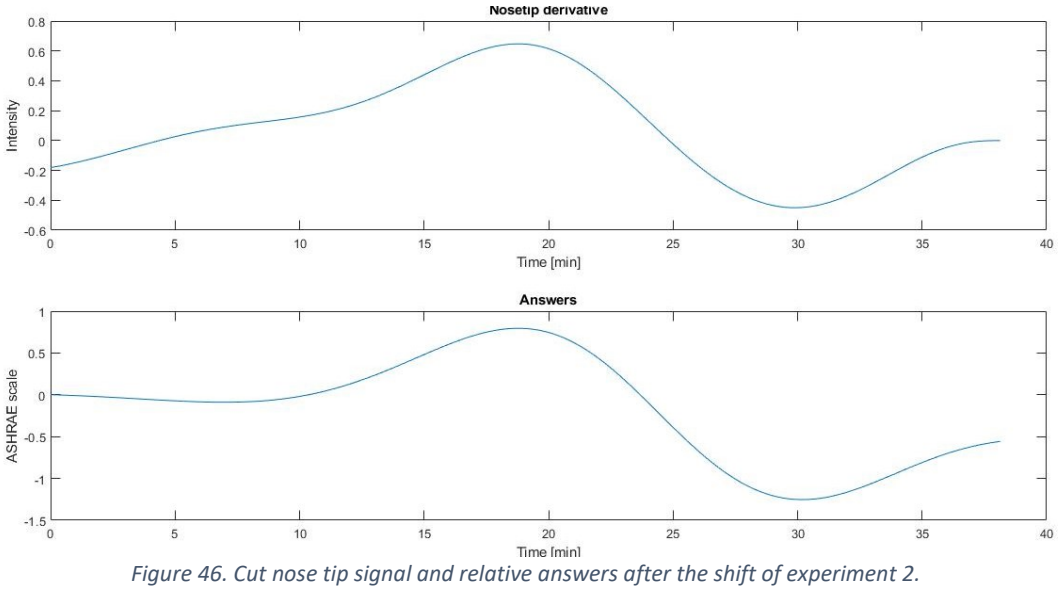

Figure 46. Cut nose tip signal and relative answers after the shift of experiment 2.

Experiment 4

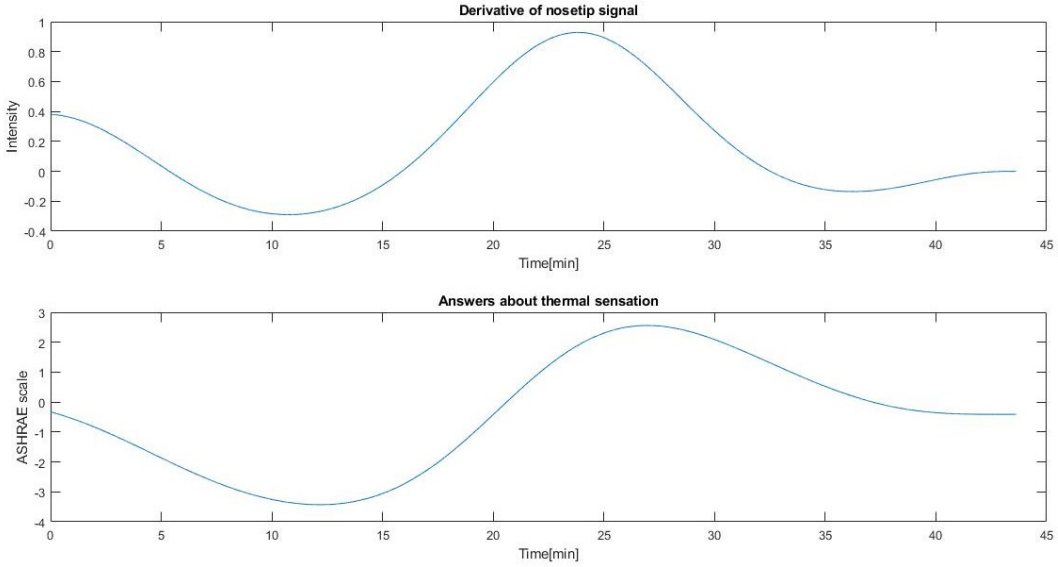

Figure 47. Filtered derivative of nose tip signal and relative answers of experiment 4.

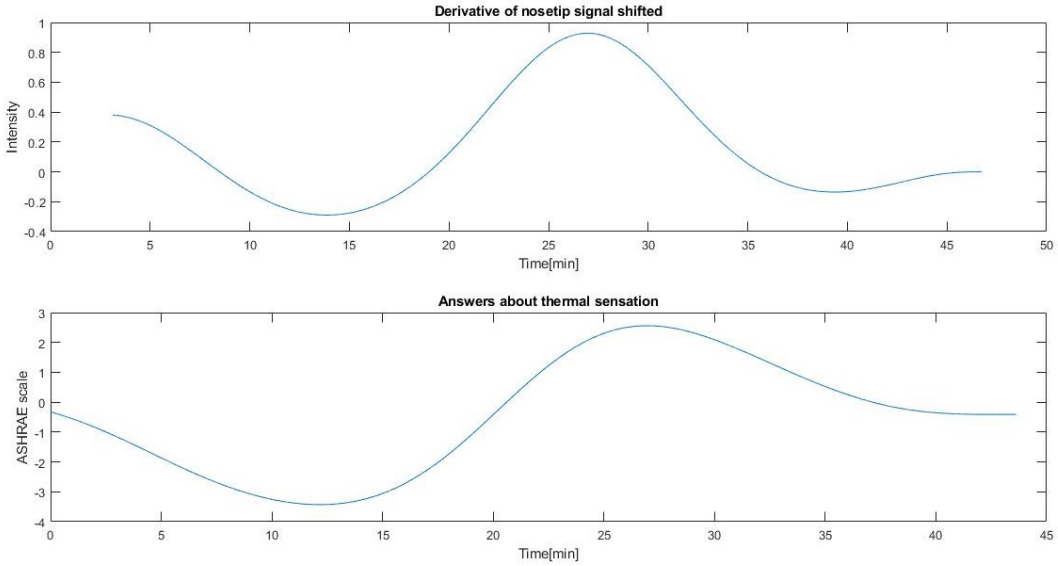

Figure 48. Shifted filtered nose tip signal and relative answers of experiment 4.

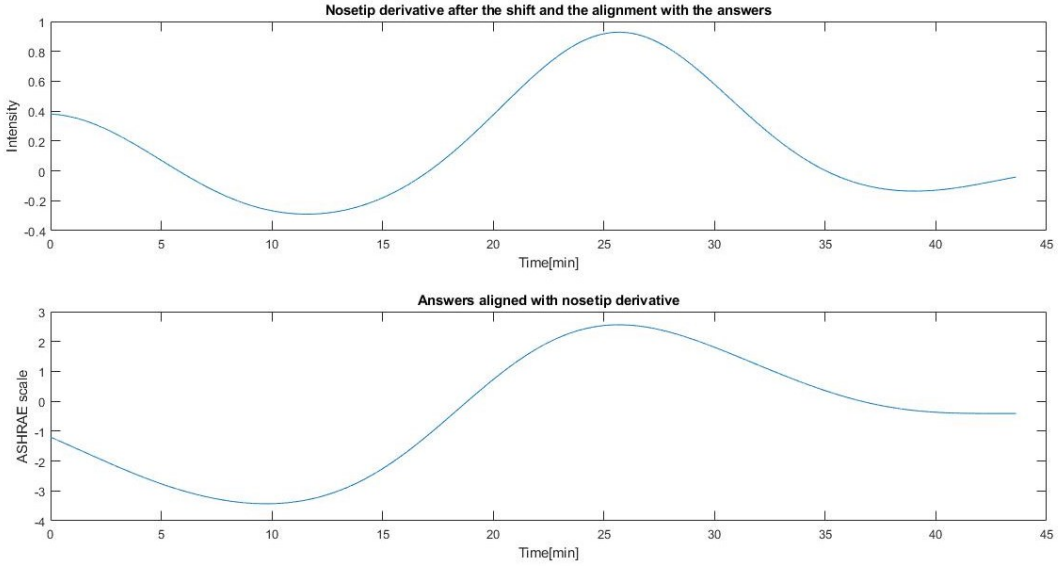

Figure 49. Cut nose tip signal and relative answers after the shift of experiment 4.

Experiment 5

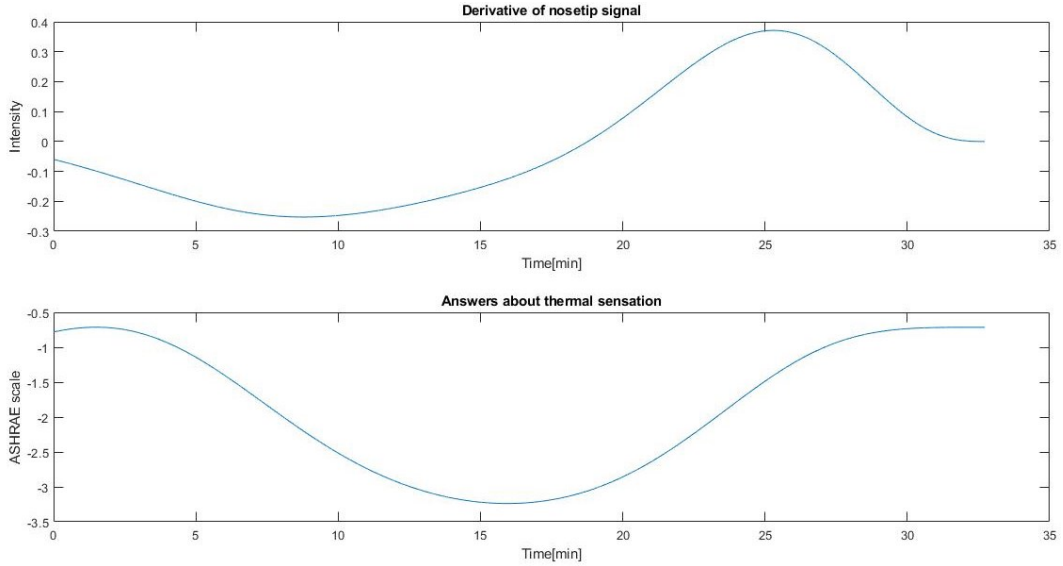

Figure 50. Filtered derivative of nose tip signal and relative answers of experiment 5.

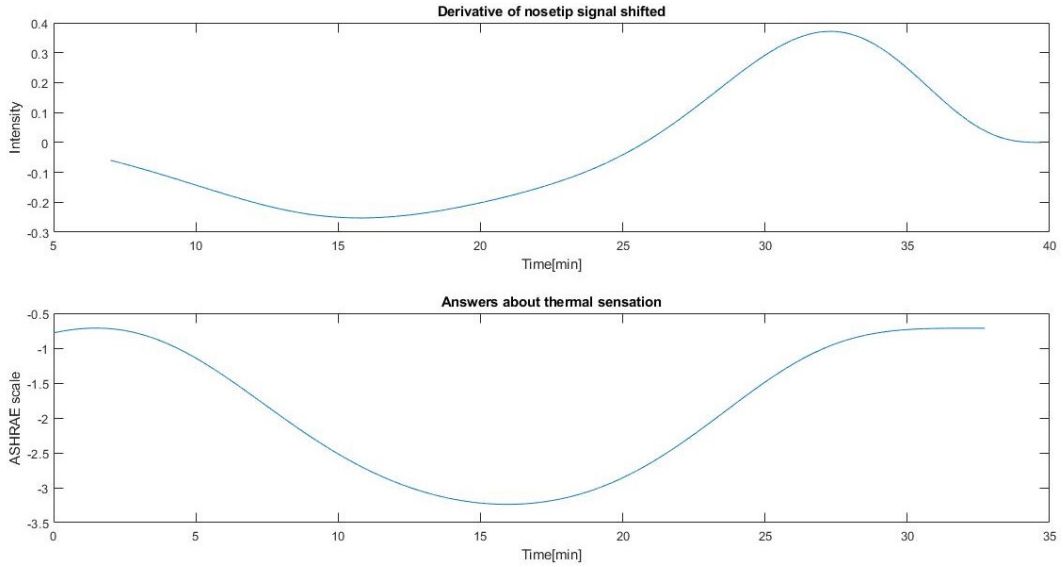

Figure 51. Shifted filtered nose tip signal and relative answers of experiment 5.

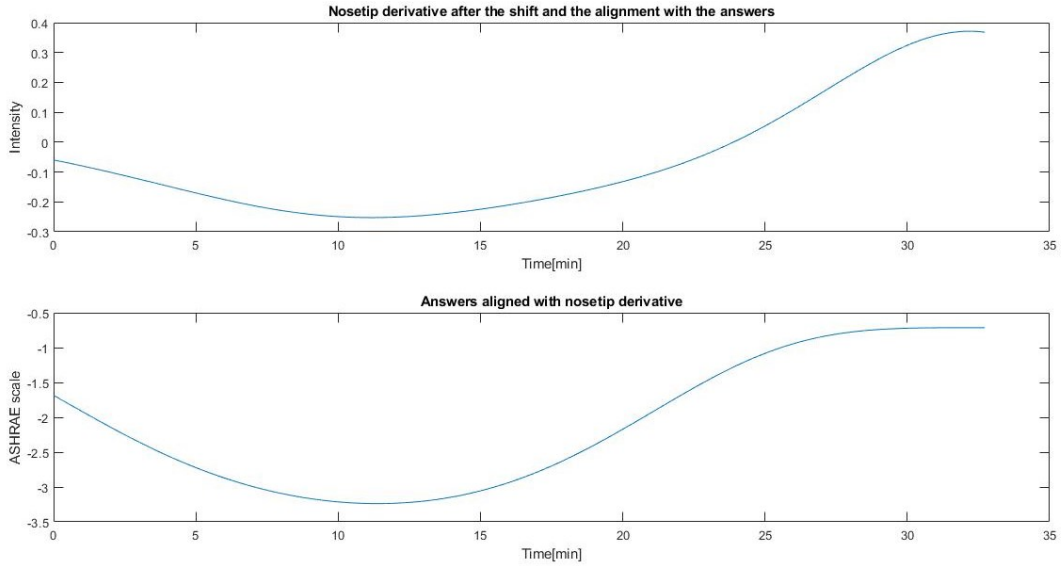

Figure 52. Cut nose tip signal and relative answers after the shift of experiment 5.

Experiment 6

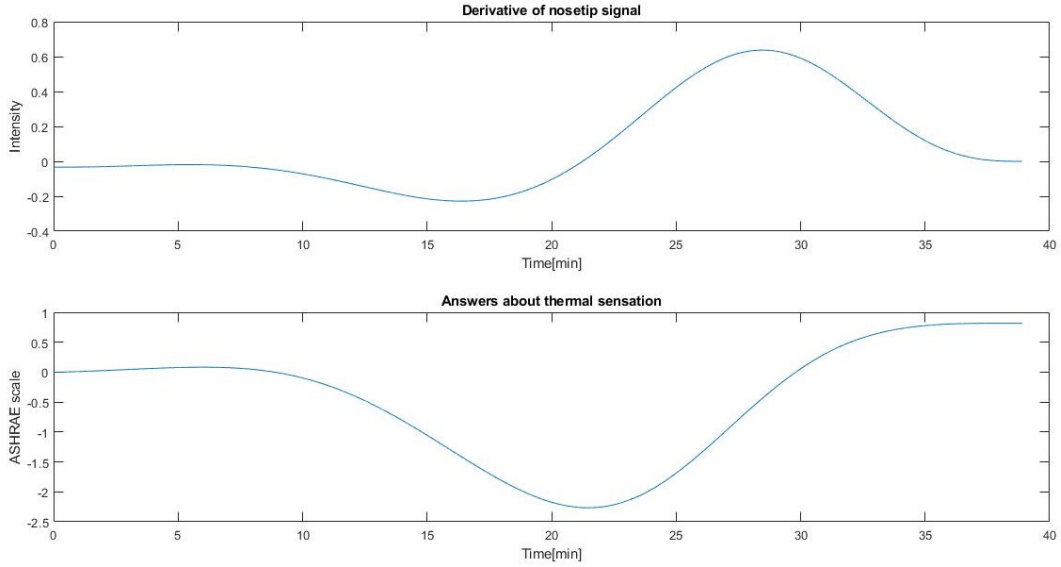

Figure 53. Filtered derivative of nose tip signal and relative answers of experiment 6.

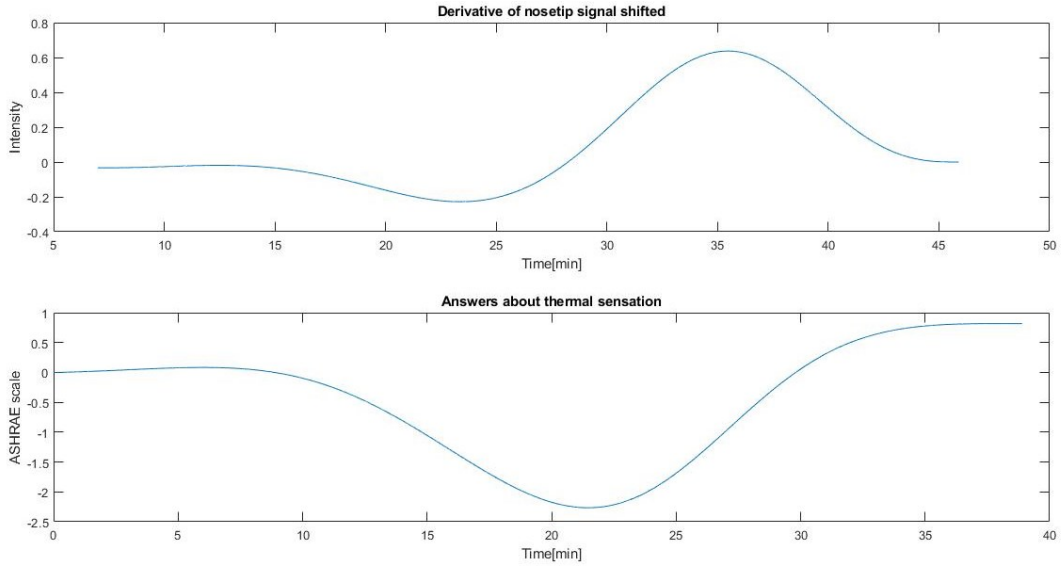

Figure 54. Shifted filtered nose tip signal and relative answers of experiment 6.

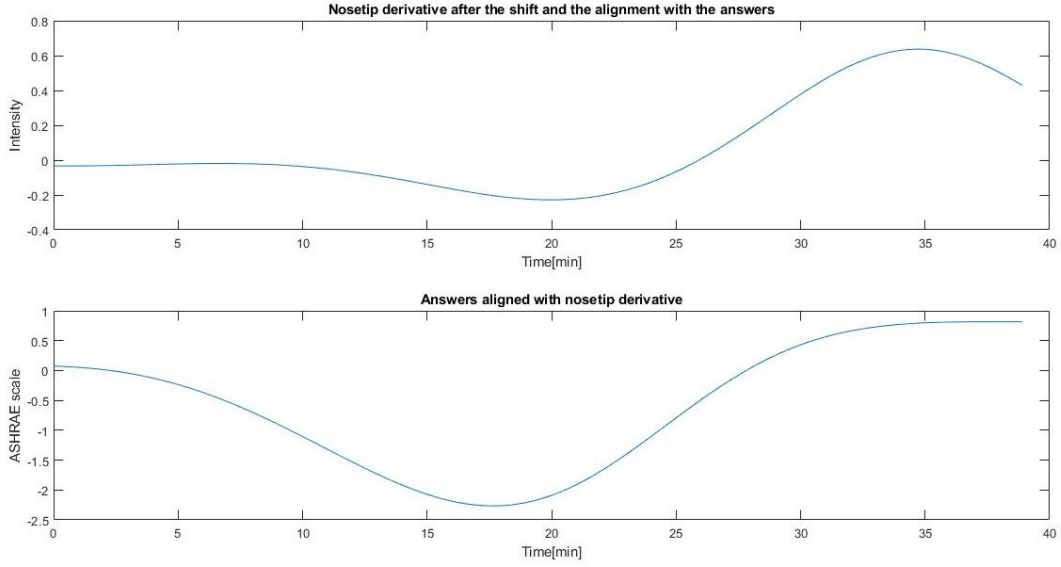

Figure 55. Cut nose tip signal and relative answers after the shift of experiment 6.

Experiment 7

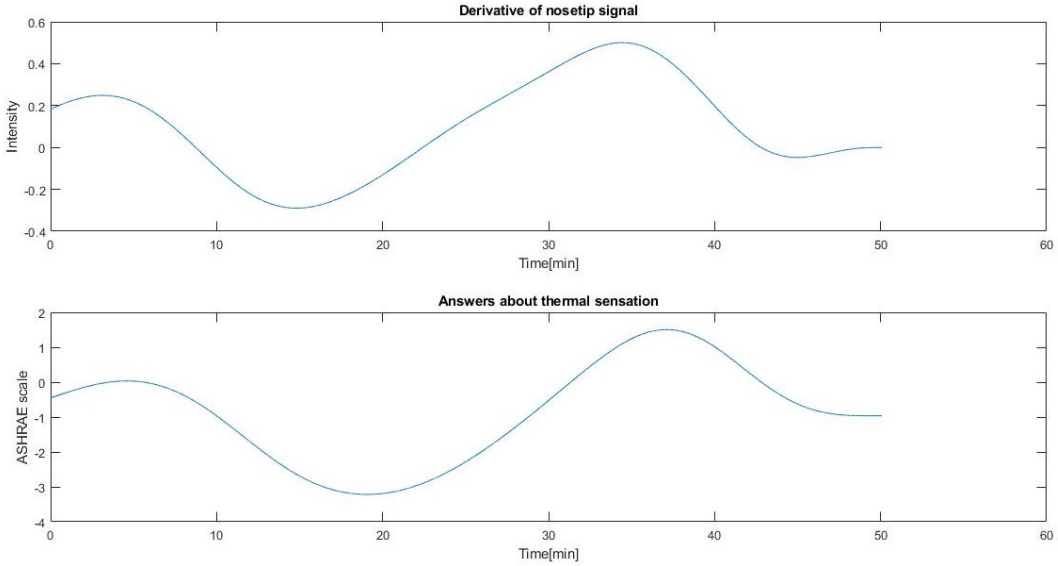

Figure 56. Filtered derivative of nose tip signal and relative answers of experiment 7.

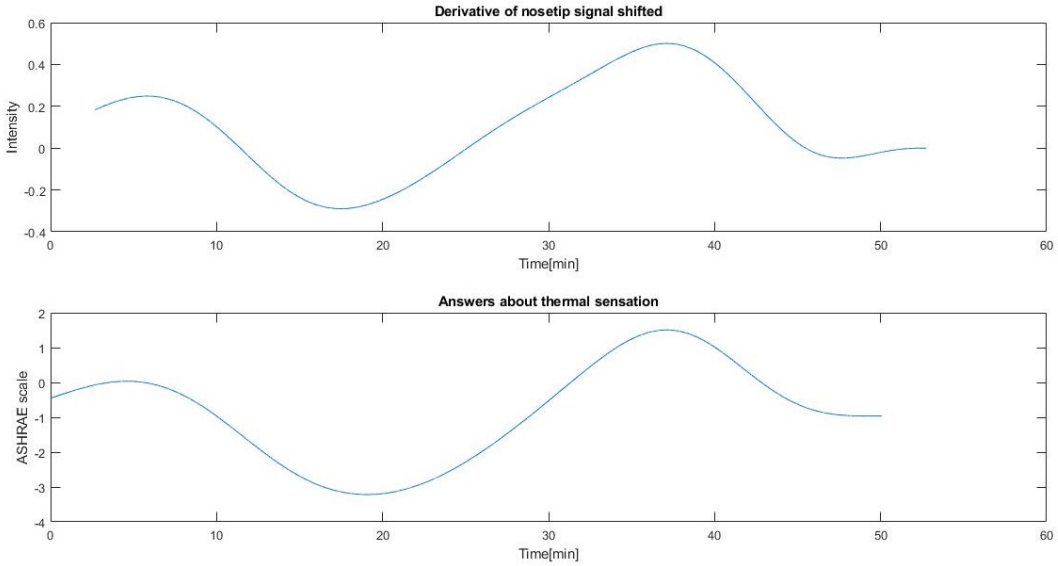

Figure 57. Shifted filtered nose tip signal and relative answers of experiment 7.

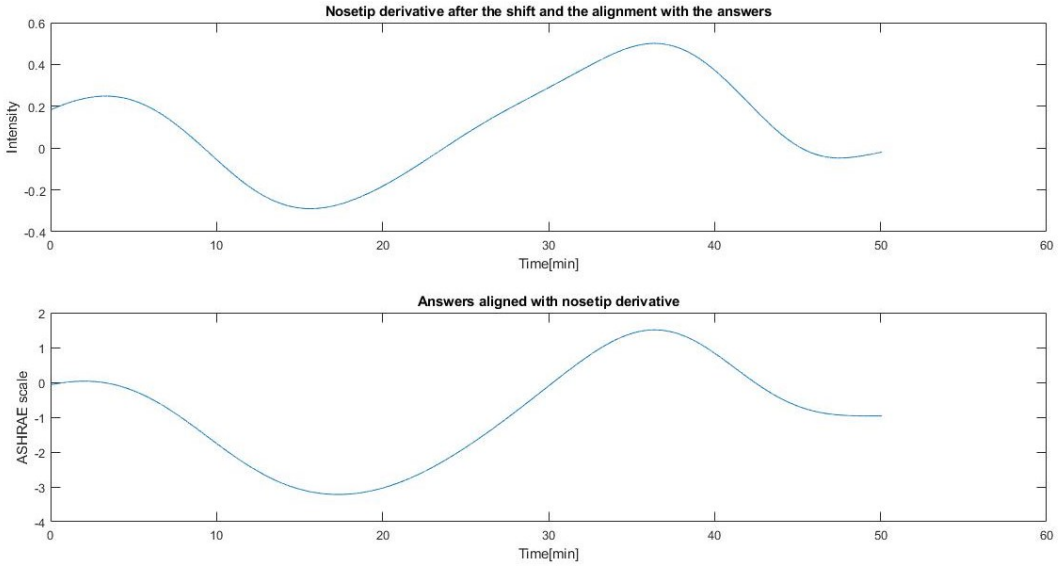

Figure 58. Cut nose tip signal and relative answers after the shift of experiment 7.

In the following Table 7 and Table 8 are summarized all the data relative to the experiments after and before the shift relative to the derivative of nose tip signal and the derivative of glabella signal, respectively.

Table 7. Correlation coefficient before and after the shift between derivative of nose tip signal and answers.

EXP	SHIFT TO THE RIGHT	Lag [min] (max der – max event)	R	R without lag
1	DERIVATIVE	-6,99	0,67	0,51
2	EVENT	3,22	0,94	0,66
4	DERIVATIVE	-3,12	0,81	0,67
5	DERIVATIVE	-6,99	0,94	0,26
6	DERIVATIVE	-6,99	0,87	0,10
7	DERIVATIVE	-2,67	0,95	0,75
		Media lag = -3,92		
		Std lag = 4,04		

Table 8. Correlation coefficient before and after the shift between derivative of glabella signal and answers.

EXP	SHIFT TO THE RIGHT	Lag [min] (max der – max event)	R	R without lag
1	DERIVATIVE	-6,99	0,87	0,83
2	EVENT	1,77	0,94	0,82
4	DERIVATIVE	-3,03	0,93	0,75
5	DERIVATIVE	-6,99	0,93	0,27
6	DERIVATIVE	-6,99	0,88	0,20
7	DERIVATIVE	-4,26	0,91	0,48
		Media lag = -4,42		
		Std lag = 3,47		

Correlation coefficients after the shift of the glabella derivative result more homogeneous and very high indexes for all the experiments among 0,87 and 0,94. Differently, for the derivative of nose tip signals correlation indexes result more heterogeneous among 0,61 to 0,95.

Then, the three regression lines computed on derivative of nose tip signal, derivative of glabella signal, and derivative of both signals, are reported in the following Figure 59, Figure 60 and Figure 61 respectively.

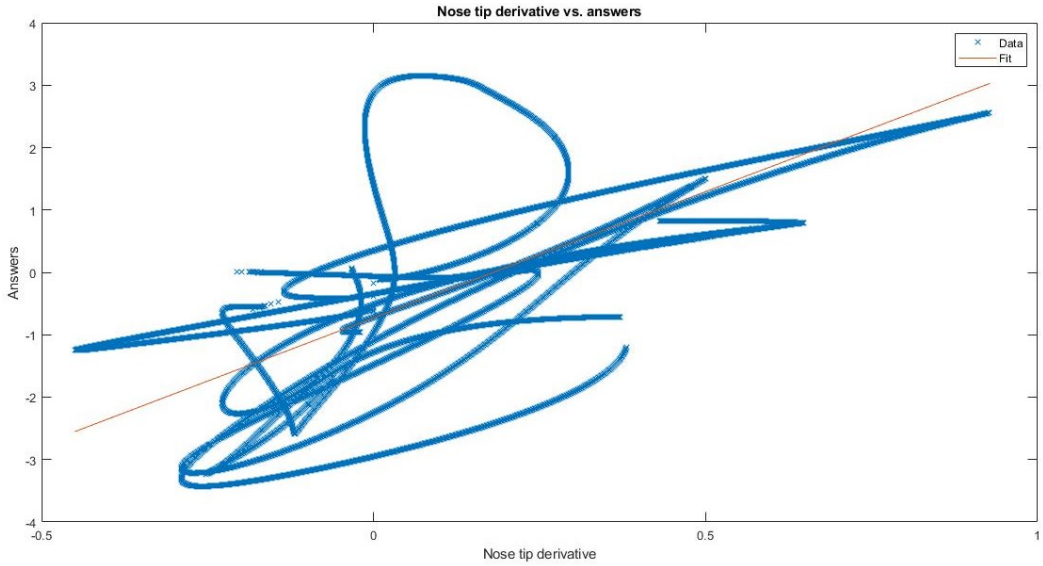

Figure 59. Regression line computed on the derivative of nose tip signal.

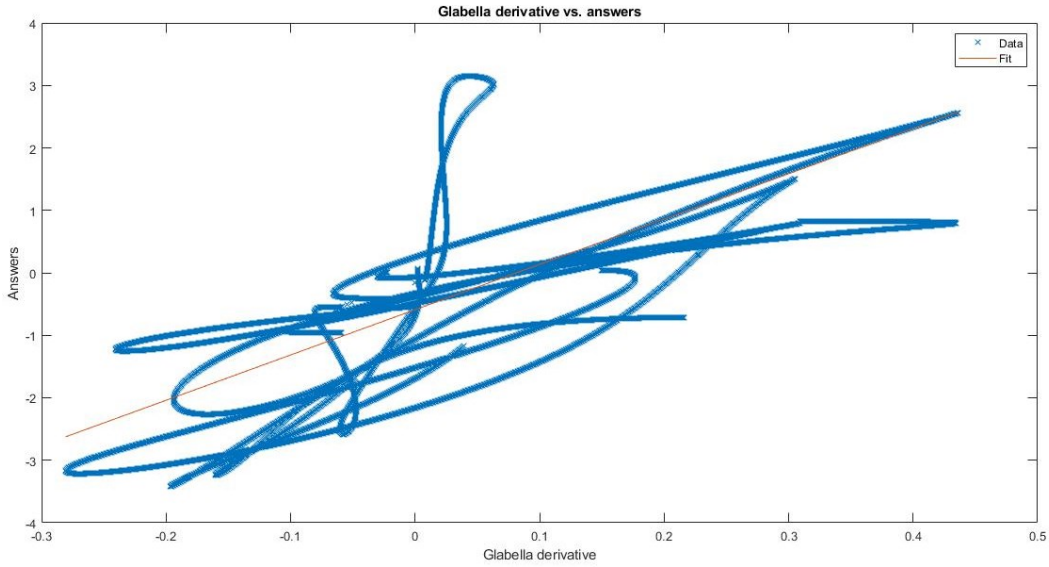

Figure 60. Regression line computed on the derivative of glabella signal.

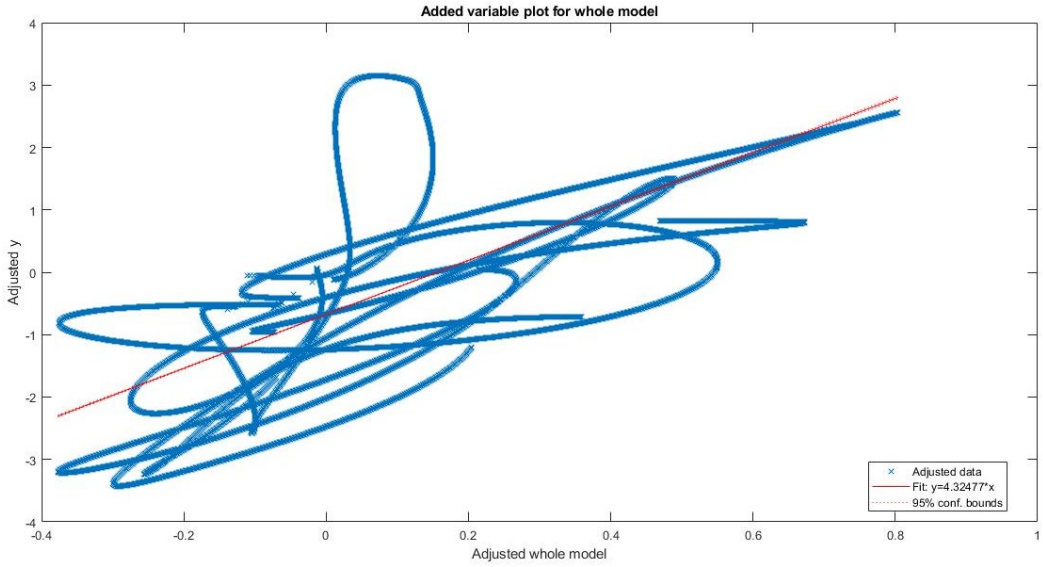

Figure 61. Regression line computed on both the derivative of nose tip and glabella signals.

Thus, the three regression lines have the following structure, expressed in formula (18), (19), and (20):

$$y_1 = -0{,}73 + 4{,}05 \cdot x_1 \tag{18}$$

$$y_2 = -0{,}59 + 7{,}25 \cdot x_2 \tag{19}$$

$$y_3 = -0{,}67 + 1{,}92 \cdot x_1 + 3{,}87 \cdot x_2 \tag{20}$$

Moreover, for what concern the analysis of residuals, errors result to have a normal distribution, as depicted in Figure 62, in that the points of the computed residuals do not lie far from the line proper of the normal distribution.

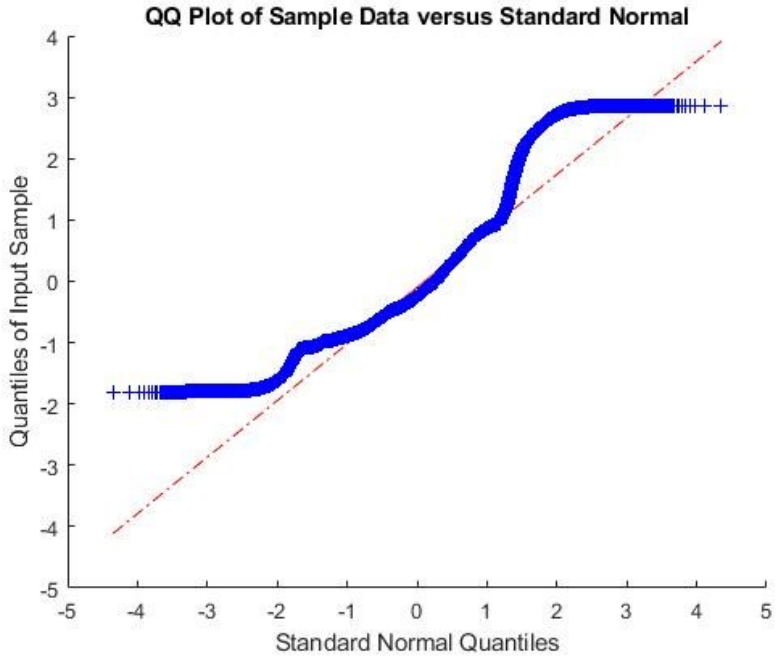

Figure 62. Q-Q plot to verify the normal distribution of the residuals.

Then, the non-correlation of the input independent variables with the error is demonstrated. Indeed, no one relation emerges between the derivative signals and the residuals, as shown in Figure 63.

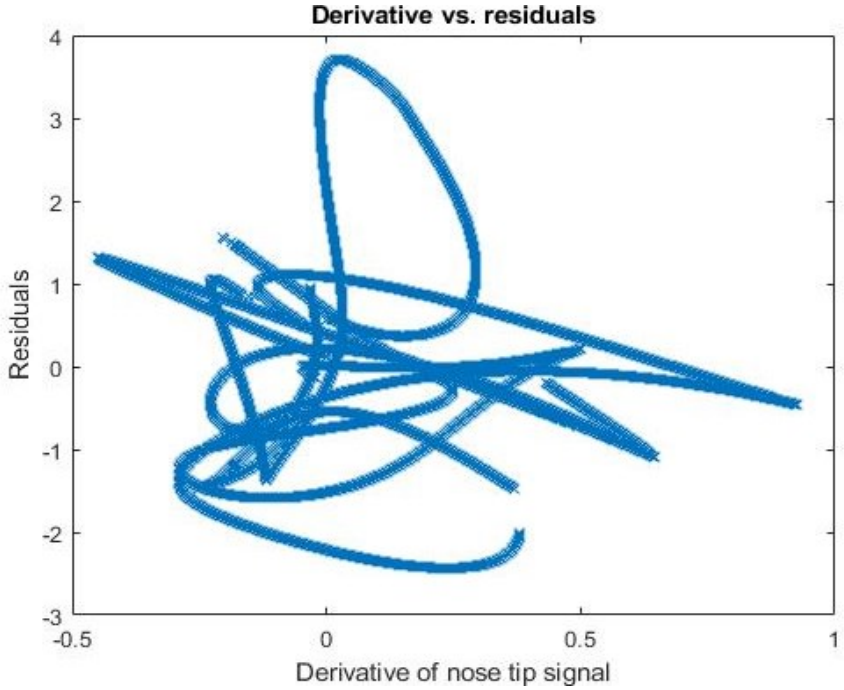

Figure 63. Correlation between input (derivative signals) and residuals.

In the same way, the non-correlation between the output dependent variable and the error has been verified, as depicted in Figure 64. In this case, other than to verify the inexistence of a relation between the two variables, the non-correlation is confirmed by the Breusch–Pagan test, that assumes hypothesis of hetereostadicity.

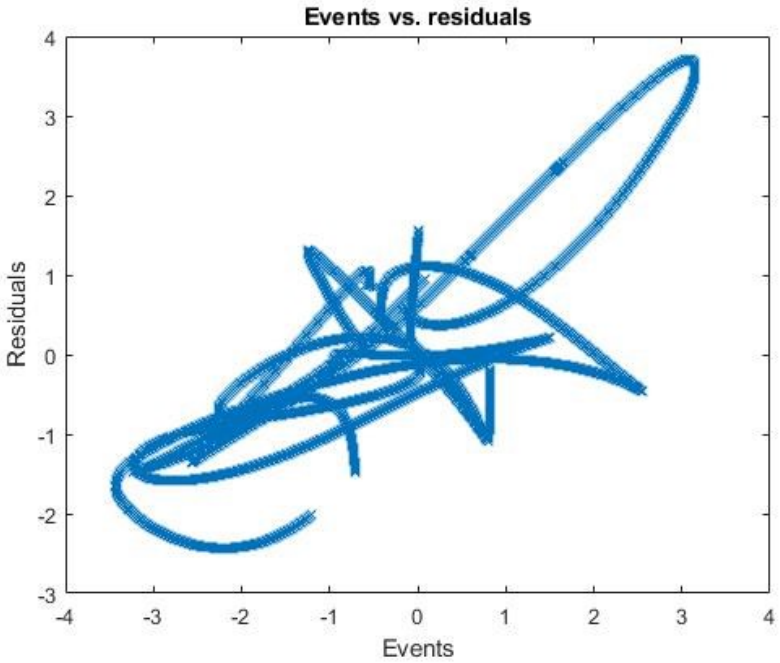

Figure 64. Correlation between output (events) and residuals.

In addition, the linear distribution of residuals has been confirmed, since residuals lie in a casual way around the zero, that refers to the mean of residuals, as shown in Figure 65.

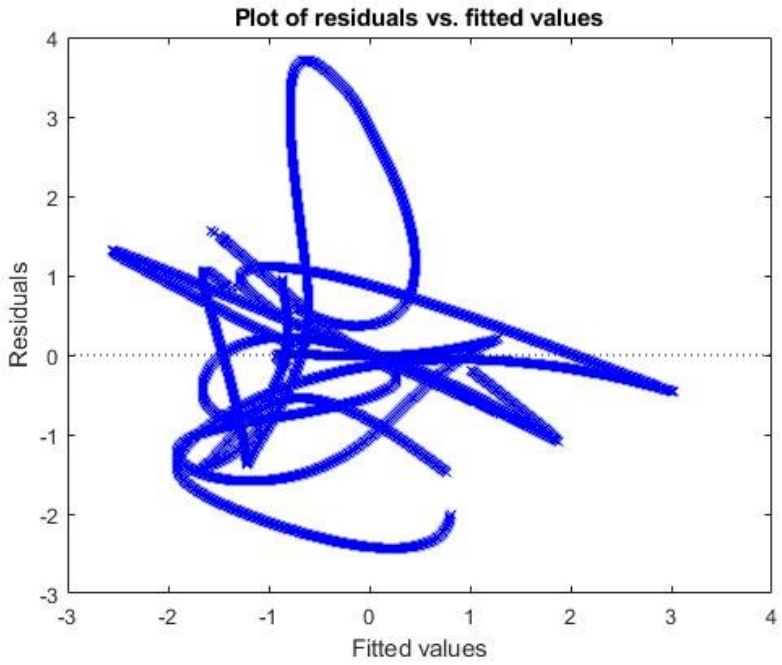

Figure 65. Plot of residuals with respect to the fitted values to verify the linearity of residuals.

The presence of outliers has been verified by three different scores.
The critical value of leverage score is considered as 4.32e-05, computed as the product between 2 by the number of variables (both dependent and independent ones), divided by the number of observations, 369548. Thus, have been found 7699 values over this threshold, that are considered as outliers.
Instead, considering the studentized residuals, were not found any outliers, because there are no residual values greater in absolute value than 3.

Finally, regarding the Cook's distance, and considering a threshold D, defined as the same used for the leverage critical value, have been found 1543 outliers. Instead, considering a threshold of 1, as commonly defined, have no found any outliers.

Since no elevated values were found for all the three measures, no points were considered as outliers.

Lastly, the absence of autocorrelation among residuals has been verified through the Durbin-Watson coefficient, resulted as 2,00 after having created the model on mixed data in a random way.

In the same way, the correctness of the hypothesis has been validated for the other two models.

CHAPTER 7

7.1. DISCUSSION

The aim of this research was to find a method for the evaluation and prediction of the subject's thermal comfort sensations relying on the variation of cutaneous temperature signal.
Indeed, experimental recorded data confirm that people's facial skin temperature, and in particular nose tip and forehead temperature, varies with respect to the change of surrounded environment temperature [54].
In this experiment, performed inside a vehicle, after a brief period (~10 minutes) of acclimatation with the HVAC system off, the ambient temperature has been abruptly changed to extreme stress conditions, varying the settings of the air conditioner. Specifically, for the 1st and 2nd experiments, the first set temperature is the maximum, 27°C, kept on for ~15/20 minutes, and then has been changed to the coolest one, 6 °C, for other ~15/20 minutes. In the other experiments, from 4th to 7th, the phases are reversed: first cold stress phase and then heat stress phase have been applied.
Nose tip and forehead temperature pattern follow the same trend of the ambient temperature due to the thermoregulatory control of human body, resulting into an increase of local temperature under heat stress and into a decrease of local skin temperature under cold stress.
In fact, cutaneous temperature is a good index to obtain information indirectly necessary to interpret comfort conditions and at the same time reducing human participation.
Therefore, skin temperature, and specifically facial cutaneous temperature, is directly affected by changes in blood flow. However, temperature of each facial region varies in magnitude, because for the different thickness of the subcutaneous fat layer, the density of blood vessels, and the amount of skin blood flow, features proper of the facial region and the subject quality. In this study, we are focusing on the nose tip and forehead region, because, although several discrepancies in literature, they result more reliable and reflective of the surrounding temperature due to the highest number of blood capillaries, as well as due to their general non obtrusiveness region from noisy elements, as can be the scarp for the chin region or the glasses for eyes. Thus, real time temperature from nose tip and forehead is used to evaluate human thermal sensation and comfort.

Extraction of cutaneous temperature signal was executed through an IR thermal camera. It is the preferred technology because it results more advantageous for this purpose with respect the other intrusive contact devices, as resistive temperature detectors, thermocouples, thermistors, and thermopiles. Indeed, IR thermal cameras have the capability to non-intrusively capture infrared signals emitted from the human body and allow a real time skin temperature investigation without any contact required with high precision; they have a high level of reliability and above all they allow the preservation of occupants' privacy, a fundamental feature for future installation inside the car.
Therefore, thermography allows to predict subject's thermal state by analyzing the variations of his facial thermal signature.
However, thermal satisfaction is a complex cognitive process strictly dependent from each individual subject and his physical, physiological, psychological condition. For this reason, it cannot be based on a general absolute standard or rules valid for all individuals.
Thermal subjective comfort sensation depends on six different factors, four external factors (radiant temperature, air humidity, air temperature and air speed) and two personal factors that change according to the subject's state and circumstances (metabolic rate and clothing insulation). Even making a big assumption, since the temperature signal can be affected by several factors, all these parameters have been considered constant, and similar for all the subjects under experiments. In order to make this assumption reliable, for all the experiments has been replicated the same situation, inside a steady car, with closed windows, minimizing movements, period of acclimatation, with similar clothing resistance and in a rest condition. By reducing all the possible sources of disturbance, the measured temperature reflects the changes of external temperature, from which, in presence of constant metabolic rate and the other factors that influence the thermal comfort sensation, is possible to estimate the subject's state of comfort or discomfort.

The accurate assessment of thermal comfort inside vehicles is crucial for automated air conditioning systems that can provide a more comfortable environment resulting in a better performance by the driver and improving the safety of all the occupants. In fact, a good thermal ambient reduces stress and fatigue, as well as avoids fogging phenomena that can compromise the good visibility and the driver's reflexes. In addition, as consequence there is also a reduction of energy and a more efficient system that responds to the real instantaneous requirements of the driver [11].
The direct relation between facial local temperature and the relative thermal comfort sensations has been justified and demonstrated by the results obtained in the 3 phases of this study, explained in the following paragraphs.

7.2. EXPLORATIVE PHASE

The explorative phase represents the initial approach to the experimental data. This phase has had the aim to know the data and get familiar with them, then, to analyze their pattern and try to find a possible relationship between variations of thermal nose tip data with the relative subject thermal comfort sensations. Being only a preliminary step, now we have focused only on the nose tip data, and we have ignored those referred to the forehead, because the first ones result greater in magnitude, from which the pattern can be more easily studied and the features, that characterize it, can be more easily extracted.
All the data relative to the 7 experiments are characterized by a great number of NaN values due to the occlusions, rotations and movements of subject's face.
Moreover, this study has been focused on only one experiment.
Experiment 4 has been chosen because it includes an insignificant number of NaN values, which allows us to study the entire pattern and its variations during the overall experiment and because it is characterized by an experiment time duration of about 45.1674 min, as reported in Table 5, considered acceptably long to provide some considerations.
The nose tip signal was preprocessed in order to obtain a smooth cleared signal without the noise that can alter and cover important features.
First of all, the mean removal is applied in order to center the signal on zero.
Then, a strong filtration is applied to obtain a smooth shaped signal, where all the undesired experimental noise components at high frequency represented by rapid oscillations have been removed. Noise components are associated with random uncertainties due to measurement procedure.
Since in real measurements the experimental errors are present as white noise with spectral components distributed uniformly over the entire frequency domain, while the relevant information is usually bandlimited, a suitable filter should be applied in such a way to admit signal only in the low frequency range. Indeed, skin temperature, being a tonic response, depends on very slow variations and produces very slow adaptations. Hence, temperature is a low frequency dependent signal, and a low-pass filter could then be appropriate [75]. As other thermographic applications, to recover useful and informative signal, a 3rd order low pass filter is applied, with a cut-off frequency of 0.001 Hz that does not provoke any lack of relevant frequency component and preserving only very low frequency band information [75].
The 3rd order Butterworth filter can introduce a group delay, since each component crosses the filter with a different velocity, introducing deformations. For this reason, *filtfilt* has been applied in order to remove distortions and delay because it consists of twice application of the filter, compensating for the delay and advance of the components.
Moreover, filtration is essential because without its application, the computed derivative of the signal is characterized by several oscillations, producing a useless and a less informative signal. On the contrary, the strong filtered signal produces a smooth derivative that describes the thermal nose tip variability with respect to the time.
Finally, the choice to scaling data into the range [-3 3] proper of the ASHRAE scale results useful to compare measured data with the sensations felt by the subject and the successive quantization allowed to predict the thermal sensations.

After the preprocessing is applied, 10 tests are performed to verify the relation that exists among the perceived thermal sensation and the recorded signal, and its transformations.

The first test based on the nose tip signal showed that the nose tip temperature signal has been affected by the change of the cabin temperature, but, although has a positive and moderately high correlation coefficient of 0.67 with the recorded sensations, it presents a smoother pattern. Its pattern, in fact, does not allow a faithful prediction above all in the region of a more comfortable state, among -1 +1 range, while it results more reliable in more extreme uncomfortable conditions. Moreover, it presents the highest percentage of error, 84.31%, that has suggested us to exclude the direct relation between temperature of nose tip and the perceived thermal sensations.

The second test instead, is based on the derivative of the nose tip temperature signal. In this situation, the prediction reveals a similar pattern during the total experiment with the recorded sensation, above all in the slope of the two curves. However, it also shows a narrower amplitude of the oscillations, reflection that a quicker change of local temperature responds to a slower change in temperature perception, producing a delay and an anticipation between the 2 signals. This delay is the cause of the lower, but always significative value of the correlation coefficient R, 0.57, and of the greatest maximum error value 6.

With the third test, based on the derivative of nose tip signal, as the previous one, with a correction factor – 2, all the indexes' values have been improved. Indeed, the correlation coefficient is increased to 0.60, the percentage of error was decreased from 74.50% of the previous test to 66.66%, as well as the maximum error value is decreased to 4. The application of the correction factor, has only translated below the signal, improving the level of reliability affecting the intensity of the signal and shifting it almost near to the respective range of the measured sensations. On the contrary, this application has not any effects on the anticipation and delay of the temperature.

The fourth test relies its predictions on some considerations about the amplitude range for each window and its slope. Specifically, making different assumptions if the range of the window is greater than a fixed threshold 0.1, that means that in that window a significative change of the temperature has been occurred, and if smaller of that threshold means that the temperature variability is almost no significative and almost approximate to constant values. In this last case, slope window is analyzed, and if it results with a decreasing trend, due to a decrease in local temperature, the prediction is based on the quantization with a correction factor -1. On the contrary, a correction factor + 1 is applied. These considerations on the range and slope changes, and the application of the correction factors allowed to represent a drastic change in temperature with a correspondent reflection on the thermal sensations that are extremized.
The application of this test on the derivative nose tip signal showed a good level of correlation, 0.74, and relatively high percentage of error 70.58%, also in this case improved if applied on the derivative with the correction factor -2. This test shows a good index of predictability when the HVAC system was set to lowest temperature and highest one, but it lacks when the system was set off for the re acclimatization. Specifically, the change of temperature from higher to lower one is quicker with respect to the subject's thermal adaptations.

The fifth test is based on the mean value of each window of the nose tip signal with the correction factor.
Applying also in this case to both derivative of temperature of nose tip signal and derivative with a correction factor, both show similar results, and specifically, the second one improves the prediction with a less percentage of error, 49.01% against 72.54% of the first case. Also, with this test no improvements are performed when the HVAC system was set off, although is evident the similar trend between the temperature derivative and thermal sensations.

The prediction of the sixth test relies on the equal contribution of both temperature nose tip signal and its derivative. Although they are signals with a different physical meaning, their summation is returned possible thanks to the unit of measure of the constant 0.5 that multiplies them. Another test has been performed replacing the contribution of derivative with the one referred to the derivative with the correction factor. In the first case, it lacks its reliability in correspondence of the very cold discomfort, conversely in the second case, it lacks its reliability in correspondence of discomfort due to very hot stress. However, with this test the correlation coefficient become very high, about 0.93, and the sensations referred to the time duration when the HVAC system was off are predicted more accurately.

The seventh test is based on the derivative and the derivative with the correction factor with a fixed delay of 2-minutes. This delay has been applied, because as revealed by the prior test, between the change of temperature generally precedes the expressed thermal sensations, that is our body does not instantaneously sense the changes in temperature, but it slowly perceives temperature variability, since the

thermoregulatory processes act to maintain thermal homeostasis. Also, in this case the correlation between the two signals is regular that describe a considerable relation among them.

The eighth test consists to apply a delay of 1 minute every 10 minutes window, in such a way to obtain a delay that increases with the time. This can be useful because our body can recover the delay accumulated after a certain period of time. The results shown a high correlation of 0.73 and 0.77 respectively for derivative and the corrective derivative, that is an intense relation between the delayed temperature changes and the relative thermal sensations.

The nineth test is also focused on the delay, but differently from the previous ones it considers a scrolling progressive delay that increases of every 15 minutes. It produces a very high correlation with the thermal sensations of 0,89 and 0,91 respectively for the derivative of nose tip signal and the corrective derivative. This means that the perception of temperature variability, a slow process, suffer a delay that increases with a factor +2 every 15 minutes.

The tenth test allow to extremize the change of the slope of the weighted sum between two consecutive windows of 3 minutes. The extremization applied with the correction factors -1 or +1, allowed to obtain an optimal prediction at every level, both during more comfortable state or during discomfort situations. In this case the correlation coefficient is the highest one, 0,93 with a maximum error value of 2. The so optimum indexes can suggest us that the thermal comfort sensation can be predicted by both the nose tip signal and its derivative. On the same time, they can be the result of an overfitting. However, to confirm their validity, the application of this test on new data must be executed.

Nevertheless, in this study we are no focusing on the validation of the tests, for further application, but they cover a relevant role to understand how local nose tip temperature signal and its derivative varies with respect to external cabin temperature changes. Furthermore, these tests are applied in order to study the temperature changes in relation to the perceived thermal sensations.

All the performed tests showed a good correlation and among these, those with the highest correlation coefficient are those whose prediction is based on the contributions of both nose tip and its derivative, that are test 6 and test 10. Moreover, also the test 9 shows a greatest performance with a correlation factor 0,91. Thus, these results have confirmed the relationship between the temperature signal, its variation represented by the derivative, with the thermal sensations recorded during the experiments. In particular, a greatest correlation with the derivative was emerged, that is the perceived sensation follows the similar trend of the changes of temperature with respect to the time.

Moreover, from these tests it was found the presence of a delay between the variation of temperature on nose tip and the relative perceptions of temperature variations expressed by the thermal sensations in the ASHRAE scale.

7.3. SYSTEMS CONTROL THEORY

In order to find a possible function that relates the output, expressed by the subject's thermal sensations during the entire duration of the experiment, and the input, that is the temperature pattern of the nose tip, during the change of the HVAC system's settings inside the car, the system control theory has been applied. Indeed, the purpose of the system control theory approach was to test whether it is possible to model our data with a transfer function model, in such a way that it can be further applied with new temperature data in order to obtain a prediction of the thermal sensation, and consequently, the thermal requirements of the subject.
Before to apply the definition of the transfer function to each experiment, all the data have been preprocessed, with a common resampling, a data standardization, and a mean removal. This data preprocessing is essential to obtain significative and comparable results, that must be analyzed to discover the underlying relationship between the data.
As shown in figure 37 and 38, it is difficult to quantify the similar patterns of module and phase of all the experiments because they show a different frequency content.
The frequency content of the signals is very low because of the strong filtration applied with the 3rd order Butterworth low filter. However, since the cutaneous temperature is affected by a very slow response adaptation to external climate changes, mediated by tonic thermoreceptors, there is not any lack of relevant information with a high frequency content.
Therefore, even if in all the experiments we are dealing with a very low frequency content, is not possible to find a common interrelationship among all the subjects, and an intrarelationship, i.e., a common FDT pattern referred to different experiments that involve the same subject.

For what concern the module trend, it is possible to note a common interrelationship for all the experiments, identified by the constant presence of a peak around 0.001 Hz. Nevertheless, this peak results with a different amplitude in each experiment, bringing to a demarcation for each situation. Moreover, also among the same individuals, the trend of module differs so much, as demonstrated by the different amplitude of the peak of the experiments relative to the same subject. For example, the FDT of experiment 1 and 4 referred to the same subject, are characterized by a peak with an amplitude of 0.01 and 0.005, respectively. On the same manner the FDT of experiment 2 and 6, relative to the same subject, are characterized by a peak amplitude of 0.01 and 0.002, respectively. Finally, also the FDT of experiments 5 and 7 relative to the same subject are characterized by a peak amplitude of 0.004 and 0.003, respectively.

Differently from the module graphs, that are characterized by a similar trend, the graphs relative to the phase of the transfer function result very different among them. In fact, these graphs do not reveal any similar pattern. These differences refer to the different delay with which each subject in each case study perceives the external temperature variations and becomes aware of them.

Consequently, we can state that it is not possible to find a common relevant pattern that can characterize a unique transfer function, that can be valid for all the experiments, for all the situations, and for all the subjects.

7.4. LINEAR REGRESSION MODEL

Data of nose tip derivative and glabella derivative have been shifted around 7 minutes to the right or to the left in order to reach the maximum correlation with the relative answers.
Generally, it has been noticed that the personal perception about thermal variations suffered of a variable delay with respect to the variation of thermal facial signature, expressed by the derivative, in correspondence of nose tip and glabella.
Nevertheless, in the experiment 2, it has been recorded an anticipation of the personal sensations with respect to the changes of thermal signals in correspondence of both regions analyzed. The explanation of this means that the subject in the experiment 2 has reached its maximum level of discomfort before that the temperature reached the maximum or the minimum level, due to his personal factor, as metabolic rate, or due to his greatest sensibility.
However, a mean value of this shift for all the experiments results in a delay for both the nose tip and glabella, respectively about of 3,92 and 4,42 minutes.
Thus, after the shift all these vectors have been used to create the linear regression model.
Specifically, three models have been implemented, the first one trained only on the derivative of nose tip data as independent variable, the second one trained only on the derivative of glabella data as independent variable, and the last one trained on both derivative data.
All the three showed a good level of performance since their relative root mean squared error varies into a small range between 1,25 - 1,29. The low variability among them depends on the different number of observations and on the quality of the data with which the models have been trained.
By comparing the model based on glabella data the model based on nose tip data, the first one can results a bit more reliable with respect to the other one because in some situations the nose tip temperature variations result more distant from relative sensation pattern and because it is characterized by a lower root mean square error (1,25).
At the same time, it is difficult to rely the model only on the thermal data relative to the glabella region because they have been resulted lower in intensity with respect to the nose tip thermal data. Indeed, the thermal data relative to nose tip are characterized by a highest intensity during the overall experiments, both at lowest and highest thermal stress.
For this reason, it is recommended to train the model on both data of nose tip and glabella temperature variation, because in this way it can improve its effectiveness, exploiting the advantages of both set of data. In this way, the model will be able to predict almost accurately the thermal sensations even when one region is occluded, relying on the thermal pattern of the other facial region. So, data about glabella and nose tip region, applied in concert, can compensate any lack each other, maintaining a high level of reliability.

However, it is difficult to assert and declare which is the best linear regression model among those implemented, that better fits the data, due to their similar performance, and similar root mean square error value.

In addition, before to define the best model it is necessary to record a new set of data with which the model will be tested and validated with a new set of data, in order to assume their correctness.

Moreover, the analysis of residuals has further confirmed the validity of the models, because it has tested that the required assumptions by this type of models have been satisfied: the normal distribution of errors, the independence of errors from the values of the independent variable, the homogeneity of the error variances and the absence of leverage values that can drive the regression.
In particular, to demonstrate the non-correlation among the residuals it has been necessary to mix the data into a random way in order to avoid that the measurements repeated over time on the same individuals can affect the reliability of the indexes' computation.
Thus, all these tests have confirmed the assumption to model thermal facial data and the relative thermal sensations into a linear way, after they are being realigned in correspondence of the maximum correlation.

CHAPTER 8

8.1. CONCLUSIONS

In order to reduce the biggest number of road accidents, that every year occurs, caused by the driver's distraction and drowsiness, this research has the aim to find a facial thermographic marker able to predict the level of individual thermal comfort sensations.
In fact, the facial thermal signature has been continuously extracted by means of a thermo camera, that allowed the preservation of individual's privacy.
In particular, an analysis of thermal facial data, focalized on nose tip and glabella regions, was performed in order to see how signals of cutaneous intensities change in response to temperature variations inside a vehicle. Three different analysis approaches have been implemented and reviewed: an explorative phase, a control theory approach and a linear regression model method.

From the explorative phase, a good relation between the derivative of nose tip signal and the perceived thermal sensations was noticed. Thus, the gradient of the thermal signal, its slope, represents an interesting concept because it allows us to know that thermal sensations are strictly related with the facial thermal signal variations.
Then, it was also noted the presence of a delay between the cutaneous temperature variations on nose tip and the perception of these temperature variations inside the vehicular compartment, that are expressed by the subject's vote about their thermal sensations. Specifically, the delay depends both on the activation of physiological mechanisms in response to thermal variations, and on the individual thermal perception.

The second phase about the application of control system theory did not lead positive results, since it was emerged that all the experiments both those performed on the same and different individuals, cannot be summarized into a unique transfer function. In fact, each different experiment was characterized by a different pattern. For this reason, we can assert that for each different acquisition based on the different subject's conditions exists a different transfer function that relates the temperature pattern with the relative thermal sensations. In fact, also for the experiments related to the same subject, a different pattern has been registered. Therefore, these results underline that thermal comfort sensations are subjected to a different intra and interpersonal variability, that suggests creating subject-specific models.

Finally, the last phase, related to the linear regression method, allowed to quantify the existing delay between the derivative of thermal data and the thermal sensations. The application of this delay allowed to reach very high correlation coefficients, that confirmed the assumption to model the data into a linear way.
Thus, individuals became awareness about their thermal state only after that the variation of cutaneous temperature occurs, specifically after about 4 minutes medially, as demonstrated by the experiments. The similar delay, among the different experiments, highlights that the physiological phenomena of thermoregulation follow a similar timing for all the different subjects. However, the subjects perceive with different intensity the thermal variations.
Then, three linear models have been implemented. One based on the derivative of nose tip data, another one on the derivative of glabella data, and the last one based on both of them.
All the three linear models implemented showed a good and similar performance, nevertheless they will have to be tested and validated with a new set of data, to verify and confirm their correctness.

To conclude, driver's thermal comfort can be correctly predicted exploiting his facial thermal signature. This signal must be calibrated personally because thermal sensations are characterized by an interpersonal variability. The most correct and valid method to predict the driver's thermal comfort state results the linear regression model based on the derivative of the temperature value of nose tip and forehead region shifted with a certain delay.

Thus, in this study the correlation among the thermal sensations and the thermal data has been investigated in static conditions when the vehicle is stationary. Indeed, all the external and personal sources that would interfere with the temperature measurements and with the personal temperature perception have been neglected, as the frequency fluctuations, the solar radiation intensity, the radiative heat exchange from the interior surfaces, the angles of incidence of the solar radiation and the physiological differences between the passengers in terms of age, sex, state of health for instance.

The results of the implemented models are very promising for the necessity to develop a HVAC system that autonomously adapts its functioning to the thermal requirements of the subject, reducing the energy consumption and ensuring a better driving experience.
However, it is necessary to perform further investigations because the implemented models rely on data acquired during experiments which lack a great amount of thermal information because the instability of the acquisition system above all in the most stressful conditions. Indeed, during too high or too cold stress conditions, due to the lowest difference of contrast the system lacks its functionality.

8.2. FUTURE WORKS

In future developments these results can be improved by providing a larger and heterogeneous dataset on which the models implemented in this project, will be trained and tested. Moreover, it is necessary to record new thermal data by means of a more stable system, capable to maintain the signal also in more stressful thermal states, in such a way to treat and overcome the issues about the lack of a great amount of thermal information.
Specifically, with a larger dataset it would be advisable to carry out a survey aimed at confirming the results found in this research, so that, over time, it would be possible to develop thermal comfort management systems that reduce consumption and ensure thermal comfort continuously to the subject.
In addition, in future works, facial temperature patterns could be investigated also during driving, in such a way to exceed the limitation of the current study in which temperature pattern have been analyzed during a stationary steady state. In fact, analyzing facial temperature variations during a driving simulation could include all the external conditions proper of the real performance that can influence the physiological state of the driver, as stress, anger, anxiety states due to traffic, climate conditions, and fatigue. Moreover, it would also be advisable to start considering other variables that influence the determination the state of comfort in order to be able to find a "law" that describes the functioning of air conditioning systems. Examples of variables that would be useful monitor in order to estimate driver's thermal comfort are the HR and RR.
Finally, the reflections due to the geometry of the internal vehicle and their influence in the IR thermal measurement could be considered.

REFERENCES

[1] N. Djongyang, R. Tchinda, and D. Njomo, “Thermal comfort: A review paper,” *Renewable and Sustainable Energy Reviews*, vol. 14, no. 9, pp. 2626–2640, 2010.

[2] P. Danca, A. Vartires, and A. Dogeanu, “An Overview of Current Methods for Thermal Comfort Assessment in Vehicle Cabin,” *Energy Procedia*, vol. 85, no. November 2015, pp. 162–169, 2016.

[3] A. Alahmer, A. Mayyas, A. A. Mayyas, M. A. Omar, and D. Shan, “Vehicular thermal comfort models; A comprehensive review,” *Applied Thermal Engineering*, vol. 31, no. 6–7, pp. 995–1002, 2011.

[4] CSA Research, “OUR LIVES INSIDE OUR CARS,” *CSA Research, European Survey*, no. August, 2016.

[5] M. Lohani, B. R. Payne, and D. L. Strayer, “A review of psychophysiological measures to assess cognitive states in real-world driving,” *Frontiers in Human Neuroscience*, vol. 13, no. March, pp. 1–27, 2019.

[6] D. Cardone *et al.*, “Driver stress state evaluation by means of thermal imaging: A supervised machine learning approach based on ECG signal,” *Applied Sciences (Switzerland)*, vol. 10, no. 16, 2020.

[7] M. Tashakori, A. Nahvi, A. Shahidian, S. E. Hadikiashari, and H. Bakhoda, “Estimation of Driver Drowsiness Using Blood Perfusion Analysis of Facial Thermal Images in a Driving Simulator,” *Journal of Sleep Sciences*, vol. 3, no. 3, pp. 45–52, 2018.

[8] M. Gonçalves *et al.*, “Sleepiness at the wheel across Europe: A survey of 19 countries,” *Journal of Sleep Research*, vol. 24, no. 3, pp. 242–253, 2015.

[9] Y. Sun and X. Yu, “An innovative nonintrusive driver assistance system for vital signal monitoring,” *IEEE Journal of Biomedical and Health Informatics*, vol. 18, no. 6, pp. 1932–1939, 2014.

[10] A. C. I. ACI, “http://www.aci.it/.”

[11] H. Metzmacher, D. Wölki, C. Schmidt, J. Frisch, and C. van Treeck, “Real-time human skin temperature analysis using thermal image recognition for thermal comfort assessment,” *Energy and Buildings*, vol. 158, pp. 1063–1078, 2018.

[12] A. Rogalski, "*Infrared detectors" 2nd edition*, vol. 66. 2012.

[13] N. Zaproudina, "*Methodological Aspects of Use of Individuals and Patients with Non-specific Musculoskeletal Disorders", Publications of the University of Eastern Finland Dissertations in Health Sciences,* 2012.

[14] O. Faust, U. R. Acharya, E. Y. K. Ng, T. Jen, and W. Yu, “Application of infrared thermography in computer aided diagnosis,” *Infrared Physics & Technology*, vol. 66, pp. 160–175, 2014.

[15] D. Cardone and A. Merla, “New frontiers for applications of thermal infrared imaging devices: Computational psychopshysiology in the neurosciences,” *Sensors (Switzerland)*, vol. 17, no. 5, 2017.

[16] I. Fernández-Cuevas *et al.*, “Classification of factors influencing the use of infrared thermography in humans: A review,” Infrared Physics & Technology, vol. 71, no. October 2017, pp. 28–55, 2015.

[17] R. Usamentiaga, P. Venegas, J. Guerediaga, L. Vega, J. Molleda, and F. G. Bulnes, “Infrared thermography for temperature measurement and non-destructive testing,” *Sensors (Switzerland)*, vol. 14, no. 7, pp. 12305–12348, 2014.

[18] A. Rogalski, “History of infrared detectors,” *Opto-electronics Rev.*, vol. 20, no. 3, pp. 279–308, 2012.

[19] G. J. Tattersall, “Infrared thermography: A non-invasive window into thermal physiology,” *Comparative Biochemistry and Physiology -Part A : Molecular and Integrative Physiology*, vol. 202, pp. 78–98, 2016.

[20] M. M. Soares, D. F. Vitorino, and M. A. Marçal, “Application of digital infrared thermography for emotional evaluation: A study of the gestural interface applied to 3d modeling software,” *Advances in Intelligent Systems and Computing*, vol. 777, pp. 201–212, 2019.

[21] P. P. B.F. Jones, “Digital Infrared Thermal imaging of human skin,” *IEEE Engineering in Medicine and Biology*, vol. 17, pp. 7–17, 2002.

[22] D. Industry, “The Ultimate Infrared Handbook for R & D Professionals,” pp. 0–44, 2010.

[23] A. Scarano, F. Inchingolo, and F. Lorusso, “Facial skin temperature and discomfort when wearing protective face masks: Thermal infrared imaging evaluation and hands moving the mask,” *International Journal of Environmental Research and Public Health,* vol. 17, no. 13, pp. 1–9, 2020.

[24] F. De Oliveira, S. Moreau, C. Gehin, and A. Dittmar, “Infrared imaging analysis for thermal comfort

assessment," *Annual International Conference of the IEEE Engineering in Medicine and Biology - Proceedings*, pp. 3373–3376, 2007.
[25] P. Ghassemi, T. Joshua Pfefer, J. P. Casamento, R. Simpson, and Q. Wang, "Best practices for standardized performance testing of infrared thermographs intended for fever screening," *PLoS One*, vol. 13, no. 9, pp. 1–24, 2018.
[26] A. Rogalski, M. Kopytko, and P. Martyniuk, "Antimonide-based Infrared Detectors: A New Perspective," *Chapter 1*, 2018.
[27] S. Zhang, Y. Hu, and Q. Hao, "Advances of sensitive infrared detectors with HgTe colloidal quantum dots," *Coatings*, vol. 10, no. 8, 2020.
[28] A. Rogalski, "Next decade in infrared detectors,", *PROCEEDINGS of SPIE,* no. October 2017, p. 100, 2017.
[29] E. Y. K. Ng and R. U. Acharya, "Remote-Sensing Infrared Thermography: Reviewing the Applications of Indoor Infrared Fever-Screening Systems," *IEEE Engineering in Medicine and Biology*, vol. 28, no. 1, pp. 76–83, 2009.
[30] Z. Qu, P. Jiang, and W. Zhang, "Development and application of infrared thermography non-destructive testing techniques," *Sensors (Switzerland)*, vol. 20, no. 14, pp. 1–27, 2020.
[31] J. Christiansen and W. Dudley, "International Academy of Clinical Thermology Quality Assurance Guidelines Standards and Protocols in Clinical Thermographic Imaging," *INTERNATIONAL Academy of Clinical Thermology*, no. January, pp. 1–35, 2015.
[32] H. Zhang, R. Yang, Y. He, A. Foudazi, L. Cheng, and G. Tian, "A review of microwave thermography nondestructive testing and evaluation," *Sensors (Switzerland)* vol. 17, no. 5. 2017.
[33] D. S. Haddad, M. L. Brioschi, M. G. Baladi, and E. S. Arita, "A new evaluation of heat distribution on facial skin surface by infrared thermography," *Dentomaxillofacial Radiology*, vol. 45, no. 4, pp. 1–10, 2016.
[34] E. F. J. Ring, "History of thermology and thermography: Pioneers and progress," *Thermology International.*, vol. 22, no. 3, pp. 3–7, 2012.
[35] M. Kopaczka, L. Breuer, J. Schock, and D. Merhof, "A modular system for detection, tracking and analysis of human faces in thermal infrared recordings," *Sensors (Switzerland)*, vol. 19, no. 19, 2019.
[36] S. Sonkusare *et al.*, "Detecting changes in facial temperature induced by a sudden auditory stimulus based on deep learning-assisted face tracking," *Scientific Reports*, vol. 9, no. 1, pp. 1–11, 2019.
[37] M. Kopaczka, J. Nestler, and D. Merhof, "Face detection in thermal infrared images: A comparison of algorithm- and machine-learning-based approaches," *Lecture Notes in Computer Science (including subseries Lecture Notes in Artificial Intelligence and Lecture Notes in Bioinformatics),* vol. 10617 LNCS, pp. 518–529, 2017.
[38] M. Kopaczka, J. Schock, J. Nestler, K. Kielholz, and D. Merhof, "A combined modular system for face detection, head pose estimation, face tracking and emotion recognition in thermal infrared images," *IST 2018 - IEEE International Conference on Imaging Systems and Techniques, Proceedings*, 2018.
[39] M. Kopaczka, R. Kolk, J. Schock, F. Burkhard, and D. Merhof, "A Thermal Infrared Face Database with Facial Landmarks and Emotion Labels," *IEEE Transactions on Instrumentation and Measurement*, vol. 68, no. 5, pp. 1389–1401, 2019.
[40] T. Baltrušaitis, P. Robinson, and L. P. Morency, "Constrained local neural fields for robust facial landmark detection in the wild," *Proceedings of the IEEE International Conference on Computer Vision*, no. December, pp. 354–361, 2013.
[41] D. Cardone, P. Pinti, and A. Merla, "Thermal Infrared Imaging-Based Computational Psychophysiology for Psychometrics," *Computational and Mathematical Methods in Medicine*, vol. 2015, 2015.
[42] I. Znamenskaya, E. Koroteeva, A. Isaychev, and A. Chernorizov, "Thermography-based remote detection of psycho-emotional states," pp. 2–7.
[43] S. Ebrahimian, H. Kiashari, A. Nahvi, A. Homayounfard, and H. Bakhoda, "Monitoring the Variation in Driver Respiration Rate from Wakefulness to Drowsiness: A Non-Intrusive Method for Drowsiness Detection Using Thermal Imaging," *Journal Sleep Science*, vol. 3, no. 2, pp. 1–9, 2018.
[44] S. Ioannou, V. Gallese, and A. Merla, "Thermal infrared imaging in psychophysiology: Potentialities and limits," *Psychophysiology*, vol. 51, no. 10, pp. 951–963, 2014.

[45] C. H. O. Youngjun and N. Bianchi-Berthouze, “Physiological and Affective Computing through Thermal Imaging: A Survey,” *arXiv*, pp. 1–32, 2019.
[46] M. Kopaczka, R. Kolk, and D. Merhof, “A fully annotated thermal face database and its application for thermal facial expression recognition,” *I2MTC 2018 - 2018 IEEE International Instrumentation and Measurement Technology Conference: Discovering New Horizons in Instrumentation and Measurement, Proceedings*, pp. 1–6, 2018.
[47] V. Kosonogov *et al.*, “Facial thermal variations: A new marker of emotional arousal,” *PLoS One*, vol. 12, no. 9, pp. 1–15, 2017.
[48] B. Lecorps, H. G. Rödel, and C. Féron, “Assessment of anxiety in open field and elevated plus maze using infrared thermography,” *Physiology and Behavior*, vol. 157, pp. 209–216, 2016.
[49] Gregory F. Lewis, Rodolfo G. Gatto, Stephen W. Porges, “A Novel Method for Extracting Respiration Rate and Relative Tidal Volume from Infrared Thermography,” *Psychophysiology*, vol. 23, no. 1, pp. 1–7, 2012.
[50] M. Czaplik, N. Hochhausen, H. Dohmeier, C. B. Pereira, and R. Rossaint, “Development of a ‘Thermal-Associated Pain Index’ score using infrared-thermography for objective pain assessment,” *Proceedings of the Annual International Conference of the IEEE Engineering in Medicine and Biology Society, EMBS*, pp. 3831–3834, 2017.
[51] B. R. Nhan and T. Chau, “Classifying affective states using thermal infrared imaging of the human face,” *IEEE Transactions on Biomedical Engineering*, vol. 57, no. 4, pp. 979–987, 2010.
[52] C. Filippini *et al.*, “Facilitating the Child–Robot Interaction by Endowing the Robot with the Capability of Understanding the Child Engagement: The Case of Mio Amico Robot,” *International Journal of Social Robotics*, 2020.
[53] J. Jorge *et al.*, “Non-contact assessment of peripheral artery haemodynamics using video infrared thermography,” *IEEE Transactions on Biomedical Engineering*, vol. X, pp. 1–11, 2020.
[54] D. Li, C. C. Menassa, and V. R. Kamat, “Non-intrusive interpretation of human thermal comfort through analysis of facial infrared thermography,” *Energy and Buildings*, vol. 176, pp. 246–261, 2018.
[55] D. Purves, G. J. Augustine, W. C. Ha, J. O. Mc, L. E. White, and F. Edition, “Neuroscience,” vol. 4th edition.
[56] A. Ghahramani, G. Castro, S. A. Karvigh, and B. Becerik-Gerber, “Towards unsupervised learning of thermal comfort using infrared thermography,” *Applied Energy*, vol. 211, pp. 41–49, 2018.
[57] C. L. Lim, “Fundamental concepts of human thermoregulation and adaptation to heat: A review in the context of global warming,” *International Journal of Environmental Research and Public Health*, vol. 17, no. 21, pp. 1–33, 2020.
[58] H. Genno *et al.*, “Using facial skin temperature to objectively evaluate sensations,” *International Journal of Industrial Ergonomics*, vol. 19, no. 2, pp. 161–171, 1997.
[59] C. C. Cheng and D. Lee, “Enabling smart air conditioning by sensor development: A review,” *Sensors (Switzerland)*, vol. 16, no. 12, 2016.
[60] A. C. Cosma and R. Simha, “Thermal comfort modeling in transient conditions using real-time local body temperature extraction with a thermographic camera,” *Building and Environment*, vol. 143, no. June, pp. 36–47, 2018.
[61] B. Pavlin, G. Pernigotto, F. Cappelletti, P. Bison, R. Vidoni, and A. Gasparella, “Real-time monitoring of occupants’ thermal comfort through infrared imaging: A preliminary study,” *Buildings*, vol. 7, no. 1, 2017.
[62] M. L. Reyes, J. D. Lee, Y. Liang, J. D. Hoffman, and R. W. Huang, “Capturing Driver Response to In-Vehicle Human-Machine Interface Technologies Using Facial Thermography,” *PROCEEDINGS of the Fifth International Driving Symposium on Human Factors in Driver Assessment, Training and Vehicle Design affective*, pp. 536–542, 2009.
[63] H. Zhang, L. Dai, G. Xu, Y. Li, W. Chen, and W. Q. Tao, “Studies of air-flow and temperature fields inside a passenger compartment for improving thermal comfort and saving energy. Part I: Test/numerical model and validation,” *Applied Thermal Engineering*, vol. 29, no. 10, pp. 2022–2027, 2009.
[64] “https://www.flir.it/products/a615/.”
[65] “https://www.intelrealsense.com/depth-camera-d415/.”

[66] “https://buy.mi.com/it/item/3205000015.”
[67] D. A. Socolinsky and A. Selinger, “Thermal face recognition in an operational Scenario,” *Proceedings of the IEEE Computer Society Conference on Computer Vision and Pattern Recognition*, vol. 2, 2004.
[68] A. Kwasniewska and J. Ruminski, “Real-time facial feature tracking in poor quality thermal imagery,” *Proceedings - 2016 9th International Conference on Human System Interactions, HSI 2016*, pp. 504–510, 2016.
[69] A. Kwaśniewska and J. Rumiński, “Face detection in image sequences using a portable thermal camera,” pp. 493–499, 2016.
[70] M. Kopaczka, K. Acar, and D. Merhof, “Robust Facial Landmark Detection and Face Tracking in Thermal Infrared Images using Active Appearance Models,” *Proceedings of the 11th Joint Conference on Computer Vision, Imaging and Computer Graphics Theory and Applications (VISIGRAPP 2016*), vol. 4, no. Visigrapp, pp. 150–158, 2016.
[71] M. Kristo and M. Ivasic-Kos, “An overview of thermal face recognition methods,” *2018 41st International Convention on Information and Communication Technology, Electronics and Microelectronics, MIPRO 2018 - Proceedings*, pp. 1098–1103, 2018.
[72] Y. K. Cheong, V. V. Yap, and H. Nisar, “A novel face detection algorithm using thermal imaging,” *ISCAIE 2014 - 2014 IEEE Symposium on Computer Applications and Industrial Electronics*, pp. 208–213, 2015.
[73] P. M. Corcoran, "*Reviews, Refinements and New Ideas in Face Recognition,*" 2012.
[74] C. Filippini, D. Perpetuini, D. Cardone, A. M. Chiarelli, and A. Merla, “Thermal infrared imaging-based affective computing and its application to facilitate human robot interaction: A review,” *Applied Sciences (Switzerland)*, vol. 10, no. 8, 2020.
[75] S. Rainieri and G. Pagliarini, “Data filtering applied to infrared thermographic measurements intended for the estimation of local heat transfer coefficient,” *Experimental Thermal and Fluid Science*, vol. 26, no. 2–4, pp. 109–114, 2002.